University of Utah

Department of Chemical Engineering

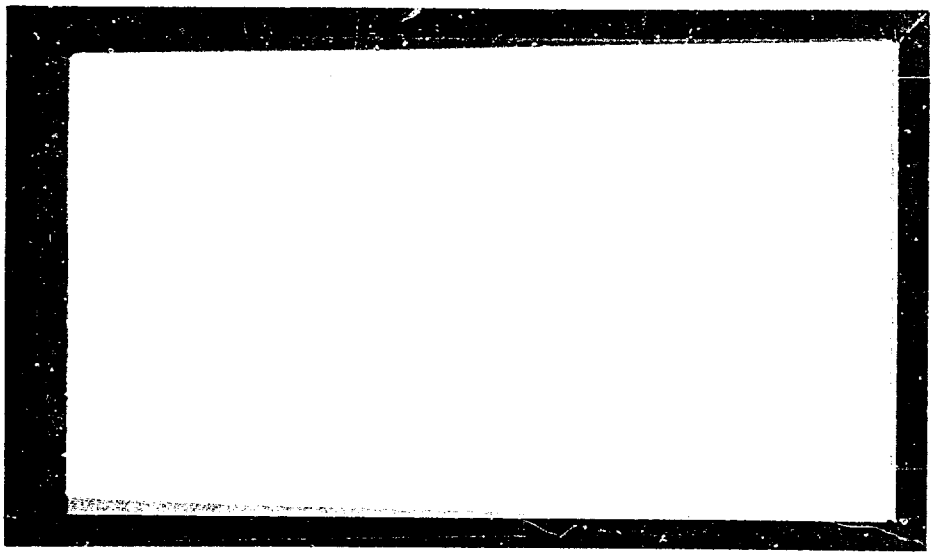

Salt Lake City, Utah

AFOSR 66-1764

TECHNICAL REPORT

ACOUSTIC INSTABILITY IN COMBUSTION

UNDER GRANT AF AFOSR 446-63

August 1, 1966

Report prepared by: Carl L. Oberg

Report approved by: Norman W. Ryan

Norman W. Ryan
Principal Investigator

PREFACE

This report is taken from the thesis of C. L. Oberg (Ph.D., University of Utah, 1965). The work was performed under sponsorship of the Air Force Office of Scientific Research, Grant AF-AFOSR 446-63.

TABLE OF CONTENTS

LIST OF FIGURES

LIST OF TABLES

ABSTRACT

Acoustic instability in solid propellant rockets is observed as a high-amplitude oscillation in the acoustic modes of the gas cavity, the combustion processes providing the driving energy. In general, the solid phase, i.e., the propellant, participates in the wave behavior. In this work, the behavior of both the gas phase and the solid phase were experimentally studied in a small rocket motor.

The motor used in this study is known as a T-burner and is, basically, a centrally-vented cylindrical cavity with propellant being burned at one or both ends. In such a motor the longitudinal modes of oscillation are excited. The T-burner has been fairly widely used to estimate the amplifying characteristics, in the form of acoustic admittances, of the burning surface. In the gas-phase portion of the author's work, pressure measurements were made at both ends of a T-burner while a thin sample of propellant was burned in one end. In the solid-phase work, similar measurements were made but a long cylinder of propellant was burned, the propellant being advanced as it burned to maintain the burning interface at a fixed position. The propellant used was composed principally of ammonium perchlorate and polybutadiene-acrylic acid copolymer.

The data from the gas-phase study showed evidence of unusual acoustic behavior, unusual in the sense that it was considerably different from previous descriptions. In the past the acoustic behavior in the gas cavity has been thought to closely approximate the behavior

that would be present in the absence of gains, losses, or mean flow. Such behavior requires the pressure amplitudes to be nearly equal at both ends of the motor. The data obtained showed the amplitude at the burning end of the motor to be lower by a factor of .45, nominally. A careful evaluation of the experimental system verified the observation. Subsequent consideration led to the conclusion that an asymmetric reflection was occurring in the vicinity of the vent, the reflection being such that a portion of the wave traveling toward the propellant was reflected so as to reinforce the wave traveling in the opposite direction. There appears to be no other way of explaining the data.

The usual method of using the T-burner is to measure rates of growth and decay of oscillations and subsequently infer values for the acoustic admittance from these rates. Such measurements were also made in the author's work. In addition, a technique was devised to extend the method in the low frequency region where the oscillations would not grow, i.e., the motor was stable. Firings were made with a nominal frequency of 200 cps using a T-burner. It was found that the pressure pulse from the igniter system excited oscillations, but the combustion provided insufficient energy to maintain the oscillations. Decay rates were measured with propellant burning in one, both, or neither end of the motor. These decay rates were used to estimate the acoustic admittance of the burning surface.

In the study of solid phase participation in the oscillations, the pressure measurement at the non-burning end of the motor was used to infer the pressure at the burning surface. The inferred value and

the measurement under the propellant were subsequently used to infer the acoustic behavior of the propellant. Initially, the data appeared to indicate a degradation of the propellant with burning time. However, further examination showed that the apparent changes could equally well be due to wall effects or changes in the amount of asymmetric reflection during the burning. The results were rather inconclusive because of the inability to separate the various effects.

CHAPTER I

INTRODUCTION

It seems appropriate to begin with a description of what is meant by acoustic instability. If a rocket motor is exhibiting acoustic instability, it is observed that the acoustic modes of oscillation for the gas cavity are excited to a high amplitude. More specifically, if one were to make multiple pressure measurements in the gas cavity of a motor during a period of unstable but steady operation, one would measure a pressure of the type

$$p = p_0 + p_1 \tag{1.1}$$

where p_1 is of the type

$$p_1 = f(x,y,z) \cos \left[\omega t + \theta(x,y,z)\right] \tag{1.2}$$

The nomenclature may be found in Appendix O. The observed variation of the oscillating pressure, p_1, with position and the observed variation of frequency with the dimensions of the cavity would be well described by the corresponding solutions of the acoustic wave equation for the particular geometry [e.g., 17,21]. Apparently Smith and Sprenger were among the first to observe this relationship [52]. Because of the ever-present damping in all real systems, the pressure oscillations in an unstable motor would decay out if no acoustic energy source were present. The combustion process provides a source. The combustion of solid propellants at normal operating pressures takes place in a very

thin zone, the solid being heated sufficiently for gasification and burned within a region about 100 microns in thickness [e.g., 21,56]. Leaving this region are gaseous products which are very nearly in chemical equilibrium. It is this region, the flame or combustion zone, that appears to provide the most likely source of acoustic energy; and in fact, it is believed to be the primary source [e.g., 5,21,22, 23,36]. The only other possible sources are expected to be unimportant, being due vortex generation or reactions in the main body of the gas.

In a practical motor acoustic instability may lead to many undesirable effects [e.g., 1,21,43]. At times the pressure amplitude may become very large. Amplitudes of the same order of magnitude as the mean pressure, with mean pressure levels of 70 or 100 atm., have been reported. Occasionally the propellant breaks up due to very large stresses, and excessive mean pressures result. Burning rate changes frequently occur. Large roll torques have resulted. Heat transfer to the hardware is enhanced. Even at low amplitudes, vibrations are transmitted throughout the motor. Obviously these phemomena can lead to inefficient operation and even disastrous results.

Acoustic instability has been an ever-increasing problem since about 1942. As the propellants have become more energetic, so too have the instances of instability. In earlier years, and in some engines even today, such things as inert baffles or rods, and holes in the propellant were used as remedies for the problem [e.g., 1,30]. In every case the remedy was obtained by a trial-and-error process because so little was known about the mechanism of the instability. More recently, adding powdered metals to the propellant has proven very effective in

preventing or reducing the level of instability. There is no assurance, however, that powdered metals will be adequate with new and exotic propellants of the future. The instability problem has proven so troublesome that there are many laboratories devoting considerable effort to various aspects of the problem.

Other Research: Current and Past

A number of theoretical analyses of the combustion zone during acoustic instability have been presented. Because of the extreme complexity of the behavior in the combustion zone, each theory has treated a simplified model. The first theory put forth was by Grad in 1948 [19]. His theory included a kind of relaxation time or time lag that was to be associated with finite reaction rates. Also the later theories of Cheng [8] and Green [20] included time lags. Each of these models predicted a very peaked frequency response and thus indicated instability in selected frequency ranges. Experimental data which are now available show clearly that this is not the case, oscillations being observed over wide ranges of frequency.

Other models have been analyzed and presented more recently which do not incorporate a time lag, for example the theories of Smith [51], of Shinnar and Dishon [50], and of McClure, Hart, and Bird [2,24,36].

The most prominent and complete theory is that of McClure, Hart, and Bird. They have treated a simplified model also; however, they have gone to considerable lengths to retain as much realism as possible and still have a tractable analysis. Their model for the burning zone

was one dimensional and all reactions were assumed to be localized at two planes, the surface and the flame. Diffusion effects were neglected, as were momentum effects. Even with a model this restricted, the solutions to the pertinent equations became very complex. The final solutions contain a good many (seventeen) physical parameters which are, for the most part, unknown for most propellants. By means of what is hoped to be judicious guessing at the values of these parameters, they predict instability over a broad range of frequencies. This is held to be a reasonable degree of success for the model.

Also McClure and associates demonstrated that one should expect the solid propellant to participate in the acoustic behavior [2]. Angelus was able to experimentally verify this kind of behavior [1]. The participation of the solid phase was also dramatically demonstrated by Ryan et al. [47].

Experimentally, there has been considerable effort expended in recent years in attempting to measure various contributions to the overall instability picture. This is demonstrated by the large number of people engaged in instability research [see for instance, references 31,57,58, also the June and July, 1964, issues of the AIAA Journal].

There are many review articles available which discuss the current status of both theoretical and experimental research. The most current are those by Hart and McClure [21] on theory and Price [44] on experimental research which were presented at the Tenth Symposium on Combustion. Also references [2,43] are good review articles.

The theory of the unstable behavior in the flame zone has advanced to such a stage that many of the general features of experimental findings

may be explained [37]. On the other hand, it is at a stage where little more can be learned without detailed and reasonably accurate experimental information. The experimental information has been slow in becoming available and is currently rather limited. The reason for the lack of adequate experimental information is the great difficulty in making the necessary measurements.

Both theory and experiment have indicated that the acoustic behavior of the flame zone may be treated as a boundary condition for the acoustic problem in the gas cavity [e.g., 2,21]. Theoretical models may be related to this boundary condition in order to evaluate their success. From the practical standpoint, the boundary condition must be used to assess the stability of a practical motor [21]. In acoustic terms the boundary condition may be characterized by the acoustic admittance, y, which is defined as

$$y = \pm \frac{\tilde{u}}{\tilde{p}} \tag{1.3}$$

Consequently it would be desirable to directly measure the acoustic velocity and acoustic pressure in the flame zone so as to directly obtain the admittance. Unfortunately the flame zone is hostile and resists such measurements because of the small thickness ($\simeq$ 100 microns), and the high mean temperature ($\simeq$2500°K) and pressure($\geq$15 atm.). The acoustic behavior of the flame is not easily measured either, as the amplification that an impinging wave receives upon reflection is of the order of one per cent [2,21]. Consequently, the appropriate measurements are very difficult and the ingenuity of the experimentalist is greatly taxed.

Several kinds of experiments have been tried in order to measure the admittance. For instance, several attempts have been made to measure the effect of the combustion on a single reflected pulse [32, 40,41]. The idea is to compare the shape of a pulse or weak shock wave as it impinges on the burning surface with the shape of the same pulse after reflection. To date, no positive results have been produced although great care and diligence have been exhibited by the experimentalists. Similarly, no results have been published from attempts which involved passing a wave through the flame from the propellant side [4]. Sirens have been used to create an oscillating environment, but here again, no admittance values were produced. Similarly, a modification of a conventional acoustic approach, the Mawardt Method, has failed [33,34]. Only a device known as a T-burner has had a reasonable degree of success. A T-burner was used in this investigation.

T-Burners

A typical T-burner is depicted in Figure 1. Basically it is a cylindrical rocket motor in which propellant samples may be burned in one or both ends. The combustion products are allowed to escape through a centrally located vent. For convenience we shall describe the burner as a "single-" or "double-ended" burner when propellant is burned in one or both ends, respectively. Horton, while at the University of Utah, showed that such a motor would exhibit instability for sufficiently unstable propellants [26]. In this configuration the longitudinal modes of oscillation are excited, and for the most part, only the fundamental mode is observed. Following ignition of the

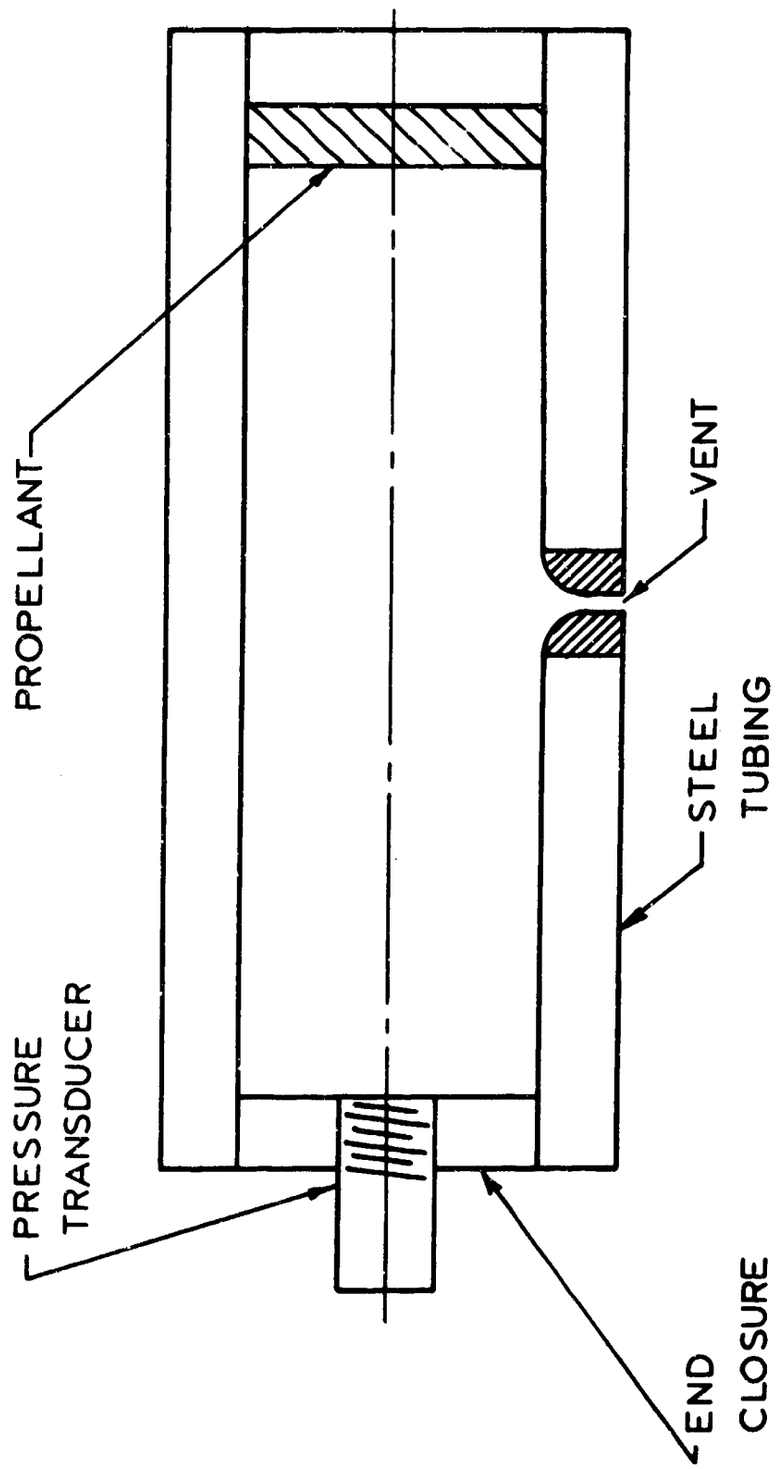

Figure 1. Sketch of T-burner configuration.

propellant the oscillatory pressure grows in an exponential fashion, i.e.,

$$p_1 = A\, e^{\alpha t} \cos \omega t \qquad (1.4)$$

The quantity α is known as the growth constant. It is experimentally determined by plotting the logarithm of the oscillatory pressure amplitude against time and measuring the slope. After the propellant is consumed the oscillatory pressure decays in a similar exponential fashion. The corresponding α is known as the decay constant. These growth and decay constants have been used to infer values of the acoustic admittance. The usual methods for using these data are described by Coates et al. [10, also Appendix E].

In Figure 2 are shown oscilloscope traces which typify the kinds of pressure records obtained from a T-burner. The upper trace is the oscillating component of pressure and the lower trace is the total pressure. This particular record was obtained from a T-burner whose exhaust vent was a sonic nozzle; the equilibrium mean pressure was, therefore, determined by the nozzle size. Frequently T-burners are vented into a pre-pressurized surge tank so that there is little change in mean pressure during ignition and burning. In Figure 3 is shown a typical oscillatory growth transient.

Introduction to this Investigation

This investigation is divided into two rather distinct parts, the first concerned with the solid phase and the second with the gas phase. The solid phase work developed from experimental work by Coates [11] and an analysis of his data by Ryan and Coates [49, also see Appendix L].

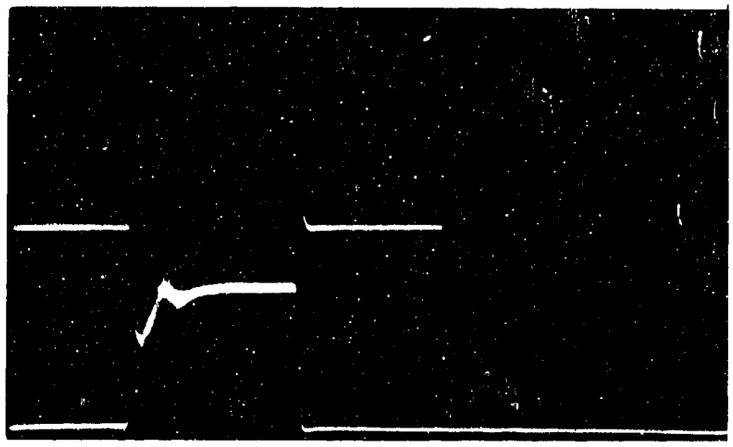

Figure 2. Typical trace from a single-ended T-burner firing, Run No. 0-255. Top trace is oscillatory pressure followed by reference at .27 atm/cm. Bottom trace is total pressure at 6.8 atm/cm. Sweep rate is .5 sec/cm. from left.

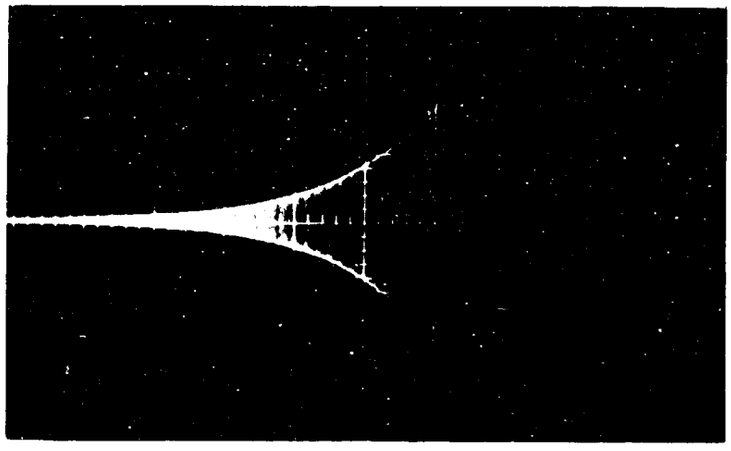

Figure 3. Typical oscillatory growth transient. Run No. 0-251. Sweep rate 100 msec/cm. from left. No vertical scale.

Coates' experiment made use of a variation of the T-burner in which one fairly long grain of propellant was burned. This grain was advanced during burning at a rate commensurate with its burning rate so that the burning interface remained at a nearly fixed position. Coates' data showed rather dramatic evidence of the participation of the propellant in the oscillatory behavior [47]. In addition the analysis of his data suggested that the viscoelastic properties of propellant were drastically deteriorating while the propellant oscillated. Coates' experiment was repeated in this investigation in order to study the apparent degradation in viscoelastic properties. Further discussion of this part of the work will be deferred until later.

The second part of this work developed quite naturally from the first. In order to understand the behavior of the solid propellant it was necessary to know the oscillating pressure at both ends of the propellant. The pressure at the burning surface had been inferred from pressure measurements at the non-burning end of the motor through acoustic theory. However, an experimental check of the approach showed the pressure inferred was greatly in error. The second part of this work became one of trying to ascertain why the oscillating pressure distribution was much different than expected on the basis of previously reported information. The experimental data suggested that the acoustic behavior of the burning surface was possibly quite different from anything previously report The implications were sufficiently important to warrant a thorough investigation. In addition a portion of the gas-phase work was concerned with obtaining the acoustic admittance values for several propellants.

CHAPTER II

GAS PHASE THEORY

The acoustic behavior in the gas cavity of a T-burner is usually thought to approximate the acoustic behavior of a rigid, closed tube which contains an inviscid, non-reacting gas with the same velocity of sound as the combusion products. For convenience we shall describe this no-loss-no-gain acoustic field as the "zero-order" acoustic field. The fundamental, longitudinal mode of oscillation of the gas cavity in a T-burner is thus expected to be approximated by

$$p = A\, e^{j\omega t} \cos \frac{\omega x}{c} \qquad (2.1)$$

where the origin of coordinates has been taken at one end of the motor and the radial dependence has been neglected. In particular if one were to measure the acoustic pressure at both ends of a T-burner, he would expect to find equal amplitudes and a phase difference of π radians. In this work preliminary experiments had shown the pressure amplitudes at the two ends of a single-ended T-burner to be substantially different rather than nearly equal. The primary concern of this study was to ascertain why the amplitudes were unequal. If it was due to the combustion processes, then it would be of great importance since previous estimates of the acoustic admittance for the burning surface could be in considerable error. If it was due to other acoustic phenomena, it would at least be valuable information. Rather fortunately, the latter will be shown to be the case.

The approach used in this work was to develop an analytical description of the acoustic behavior in terms of several parameters. These parameters were then evaluated from experimental data. The analysis was sufficient to describe the effects of combustion, if these were the source of the unequal amplitudes, but was insufficient to describe strong reflection phenomena. The acoustic field defined by the experimentally-determined parameters was then tested for its ability to describe the real behavior. In so doing, sufficient information was obtained to determine that the deviations from an approximately zero-order field were, in all likelihood, caused by an asymmetric reflection in the vicinity of the nozzle.

We shall proceed to develop a theoretical analysis of the acoustic behavior in the gas cavity as well as other needed relationships. Although the analytical description will actually prove inadequate to describe the real behavior, the analysis will prove useful in elucidating the situation.

Qualitative Description of Motor Behavior

Before embarking on an analytical description of the acoustic behavior in a T-burner, the complexity of the system will be noted in a qualitative manner. Although the T-burner was originally conceived as a system which would be relatively simple to describe analytically, the system is nevertheless still very complex. In Figure 4 is a sketch of a T-burner; the dashed lines are meant to depict the mean flow. Gas is generated by the burning propellant and subsequently flows out through a sonic nozzle. In the vicinity of the nozzle the mean velocity must be

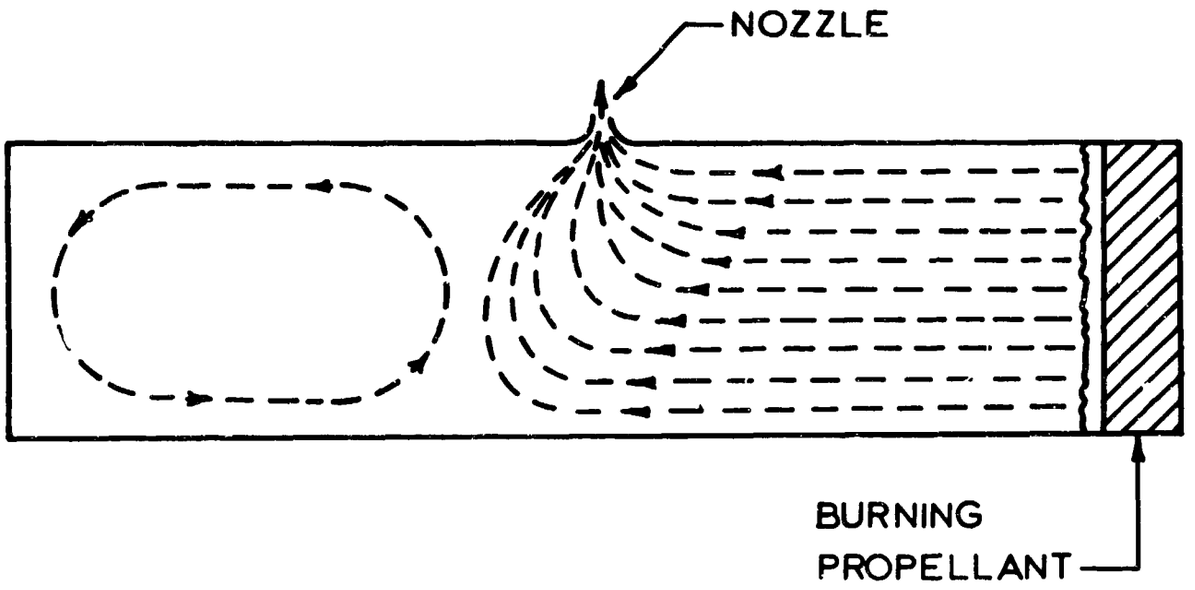

Figure 4. Sketch of T-burner configuration showing (expected) lines of mean flow.

large. At the non-burning or "cold" end the gas is expected to be relatively stagnant except for some circulation due to the mean flow near the nozzle. This circulation should be adequate to maintain the mean gas temperature nearly uniform throughout the motor. Following ignition there may be some cold gas trapped in the non-burning end, but it is eventually swept out by the circulation. At the other end there will be a boundary layer at the curved walls which will build up from the burning surface in a manner similar to the entrance region in a tube. The wall temperature near the propellant will be greater than farther down the cylinder. There is possibly a considerable degree of small-scale turbulence in the vicinity of the burning surface because of the heterogeneous nature of the propellant.

It is readily seen that a detailed mechanistic description is impossible; simplifying assumptions will be required. In the past it has frequently been assumed that the acoustic behavior in the gas cavity of a rocket motor deviates only slightly from the behavior that would occur in the absence of combustion and transpiration [e.g., 38]. Similarly, it has been assumed that the acoustic behavior in a T-burner is very nearly the same as that of a closed cylinder [e.g., 10, 55]. The effects of the mean flow have either been neglected entirely or have been assumed to modify only the boundary conditions [e.g., 39]. At times, the one-dimensional damped-wave equation has been applied, with the effects of mean flow being neglected [e.g., 10,55]. Thus, it may be observed that previous theoretical descriptions assume that the behavior in the main body of the gas is reasonably well described by simple acoustics.

We will now consider some of the regions of particular analytical difficulty.

1. The nozzle is particularly difficult to handle. There has been some theoretical and experimental work done on acoustic losses associated with vents. Hart [25] and McClure [39] have concluded from their theoretical studies that the losses are negligible for a subsonic orifice. Cold-flow experiments carried out at Bolt, Beranek, and Newman, Inc. [18] indicate that the losses are approximately proportional to the vent cross-sectional area and inversely proportional to the Mach Number in the vent, at least for low velocities (subsonic) in the vent. Also it is strongly dependent upon displacement from the nodal position, i.e., the position of the pressure node. These studies are inadequate for the problem at hand but they do permit some hope that the nozzle may be neglected without serious error. In the literature there appears to be no consideration of major distortion of the acoustic field attributable to the nozzle. Experimentally the overall losses in the T-burner used in this study have not been found to be highly sensitive to nozzle location so that these effects would appear to be reasonably small. In any case the specific effects of the nozzle will be neglected in this analysis.
2. The mean flow can usually be neglected in acoustic analyses as long as the Mach Number is small. The average Mach Number

for the system used was about .01 and should be negligible. The effects of mean flow will be estimated.

3. The damping due to the walls is dependent upon the wall temperature so that the damping should be position dependent. However, the wall damping with a steep thermal gradient and uniform wall temperature is very difficult to treat analytically [6] and, therefore, one can only hope that an average value for the damping is adequate.
4. The effect of the turbulence is unknown; however, it is presumed that it may be neglected because the scale of turbulence is much smaller than the acoustic wave length.
5. The effect of a mean temperature variation along the axis of the motor could be significant, but the gradient is thought to be negligible for a motor less than 30 or 40 cm. in length. This effect is expected to increase with the length of the motor. In Appendix F analyses are made of several simple systems with mean temperature variations.

It is in this setting then that an approximate theoretical description will be developed.

Acoustic Relationships

We wish to use acoustic theory to infer the nature of the acoustic field from measurements in the motor. There are two classes of measurements which can be made, those made before or after the firing and those made during the firing. Those made during the firing will be restricted to dynamic pressure measurements since it is very difficult to measure

anything else. However, the dynamic pressure data will provide frequency and amplitude information throughout the firing for a particular location and phase differences between locations. Before or after a firing it is possible to measure various dimensions in the motor. Also the properties of the propellant such as density and burning rate may be obtained in supplemental tests. Now we shall proceed with the theoretical description, recognizing that it must be expressed in terms which may be obtained from these kinds of information.

In order to develop an analysis, the following simplifications will be made:

1. The main body of the gas will be assumed to be homogeneous, i.e., there are no variations in properties or mean temperature.
2. The gas will be assumed to behave as a non-reactive ideal gas.
3. Initially the effects of mean flow will be neglected and later estimated.
4. The effects of the nozzle will be neglected.
5. The oscillations will be assumed to be sufficiently small to allow application of the conservation equations in linear perturbation form. (See Appendix C for a discussion of the limitations of this assumption.)
6. The dissipation function will be neglected, in accord with Rayleigh [45].
7. Finally, cylindrical symmetry will be assumed.

Under these restrictions the conservation equations may be written as

motion--x direction

$$\rho_0 \frac{\partial \tilde{u}}{\partial t} + \frac{\partial \tilde{p}}{\partial x} = \mu \nabla^2 \tilde{u} + \frac{1}{3} \mu \frac{\partial}{\partial x} \nabla \cdot \vec{\tilde{u}} \tag{2.2}$$

continuity

$$\frac{\partial \rho}{\partial t} + \rho_0 \nabla \cdot \vec{\tilde{u}} = 0 \tag{2.3}$$

energy

$$\rho_0 C_v \frac{\partial \tilde{T}}{\partial t} = k \nabla^2 \tilde{T} - \rho_0 \nabla \cdot \vec{\tilde{u}} \tag{2.4}$$

Rayleigh gives the solutions to these equations for which he credits Kirchhoff [45]. These solutions, as modified for the needs of the problem at hand, are obtained in Appendix A. The acoustic pressure and admittance of the burning boundary are found to be

$$\tilde{p} = \gamma_T p_0 A_1 J_0(k_1 r) e^{j\omega t} \cosh j\gamma x \tag{2.5}$$

$$y = - \frac{\gamma}{\rho_0 \omega} \tanh j\gamma x \tag{2.6}$$

The origin of coordinates in these solutions has been taken at the non-burning end of the motor. Also, the acoustic velocity has been set equal to zero at the origin (the rigid, steel flange). In addition, small terms have been neglected. These solutions are expected to be valid everywhere except near the curved boundaries.

Equation (2.5) will form the basis for inferences as to the nature of the acoustic field. It will be possible to determine the parameters in this expression from data. The determined parameters may then be used to calculate the acoustic admittance from Equation (2.6). The radial dependence in Equation (2.5) will never actually be evaluated although it could be calculated, at least in principle. The argument of the Bessel function should be small enough to permit approximation of the function by unity. In any case we shall give only token verbal recognition to the existence of a radial dependence.

An expression for the propagation constant, γ, is also obtained in Appendix A. The expression is necessarily approximate, however, because it is necessary to apply boundary conditions at the curved boundaries in order to obtain the expression. This expression is:

$$\gamma \simeq \frac{\omega}{c}\left\{1 + \frac{(1+j)}{r_w(2\omega)^{1/2}}\left[\upsilon^{1/2}\left(\gamma_T^{1/2} - \frac{1}{\gamma_T^{1/2}}\right) + (\mu')^{1/2}\right]\right\} \tag{2.7}$$

Cantrell [6] has obtained a very similar expression (see Appendix A) for a system in which the steep temperature gradient was retained.

The hyperbolic cosine in Equation (2.5) may be rewritten in exponential form. In that case, each exponential then represents a wave, one traveling in each direction. When a uniform mean flow term is introduced, the effect is to augment or suppress the velocity of wave propagation depending on whether the wave moves with or contrary to the mean flow. The propagation constant in this case becomes approximately,

$$\gamma_{\pm} = \mp (1 \pm M)\, \gamma \tag{2.8}$$

where the plus subscript corresponds to the positive wave, i.e., the wave traveling in the positive direction. The correction is small and will be neglected.

The acoustic admittance given in Equation (2.6) corresponds to the virtual admittance described by McClure [39]. He has pointed out that there is a convection of acoustic energy into the system due to the mean flow. Equation (2.6) gives a virtual admittance rather than an actual admittance because the mean flow was neglected. In Appendix D appear the details of why this arises.

It is noteworthy that the expressions for the acoustic pressure and admittance (Equations (2.5) and (2.6)) are in a sense more general than the analysis used, if the parameters are experimentally determined. The solution is of the form

$$Ae^{j\omega t}\, e^{j\gamma x} \tag{2.9}$$

This is a valid solution (along a linear coordinate) for a great many systems with constant properties. In the section on the analysis of the solid phase, the same solution will be found to satisfy the visco-elastic equations of motion for the solid. Also, as long as the viscous and convective effects are small, the equation of motion (x direction) may be approximated as

$$\rho_0 \frac{\partial \tilde{u}}{\partial t} + \frac{\partial \tilde{p}}{\partial x} = 0 \tag{2.10}$$

or

$$\tilde{u} = \frac{1}{\rho_0 \omega} \frac{\partial \tilde{p}}{\partial x} \tag{2.11}$$

where a harmonic time dependence has been assumed to obtain the latter equation. With the aid of Equations (2.9) and (2.10) it is necessary only to apply the appropriate boundary conditions to obtain Equations (2.5) (except for the small radial dependence) and (2.6). In Appendix F similar solutions are obtained for systems with a mean temperature variation as long as the variations are not too large.

Let us now consider how the parameters in Equation (2.5) may be related to experimental measurements. The product of terms $\gamma_T \rho_0 A_1$ is simply the absolute value of the acoustic pressure at the origin. The length L may be calculated from the length of the motor, the sample length, and the linear burning rate. We are left with the evaluation of γ. The imaginary part of γ ($\gamma \equiv b\text{-}ja$) is related to the damping suffered by the wave and will always be very small. If advantage is taken of this fact, then an excellent approximation is

$$\frac{|\tilde{p}|}{|\tilde{p}_g|} \simeq |\cos bx| \tag{2.12}$$

where both pressures are measured along the axis of the motor. The value of aL may be obtained from a phase-angle measurement of the oscillatory pressure at some point along the axis referred to the origin. Thus

$$\tan \phi = \tanh ax \tan bx \simeq ax \tan bx \tag{2.13}$$

The value of aL may also be approximated from the oscillatory-decay rate after the propellant is consumed. This decay rate may be obtained from the amplitude data. The amplitude of the wave traveling in the positive direction is attenuated as e^{-ax} and, similarly, the

negative wave is attenuated as e^{ax}. If the wave is reflected perfectly from each end of the motor during the decay, then the amplitude at a particular position will decay by an amount e^{-2aL} in one cycle of oscillation. If the rate of decay may be represented as $e^{+\alpha_D t}$, where α_D is negative,

$$aL = -\frac{\alpha_D}{2f} \tag{2.14}$$

Thus the rate of decay is a measure of $\underline{a}$ also. However, α_D is somewhat dependent upon the amplitude and in order to be appropriate, the initial value must be chosen. We shall use α_D to denote the initial decay. Equation (2.13) is obtained analytically in Appendix A.

In addition it is possible to relate the growth constant, α, and the linear decay constant, α_{DL}, to $\underline{a}$. The linear decay constant will be defined in the next section. In Appendix A the relationship is shown to be

$$a = \frac{\alpha - \alpha_{DL}}{c} \tag{2.15}$$

With a knowledge of $\underline{a}$ and $\underline{b}$ the calculation of the acoustic admittance may be essayed. It is convenient to express the admittance in reduced form by multiplying by $\frac{p_0}{u_0}$, the ratio of mean pressure to mean velocity. The steady-state continuity equation requires that

$$\rho_0 u_0 = r_0 \rho_s \tag{2.16}$$

If advantage is taken of the smallness of $\underline{a}$, then the real and imaginary parts of the reduced admittance may be written as

$$\frac{p_0}{u_0} y' = - \frac{p_0}{r_0 \rho_s} \left(\frac{a}{\omega}\right) [bL + \tan bL \, (1 + bL \tan bL)] \qquad (2.17)$$

$$\frac{p_0}{u_0} y'' = \frac{p_0}{r_0 \rho_s} \left(\frac{b}{\omega}\right) \tan bL \qquad (2.18)$$

Growth Constant Considerations

Now consideration will be shifted to the significance of growth and decay constants. It will be presumed that the growth and decay of the acoustic field at a particular position may be described by an exponential in time, e.g.,

$$\tilde{p} = |\tilde{p}| \, e^{\alpha t} \, e^{j\omega t} \qquad (2.19)$$

For a closed system the time average acoustic energy may be written as

$$\langle \mathcal{E} \rangle = \left\langle \int_V \frac{1}{2} \left[\frac{p_1^2}{\rho_0 c^2} + \rho_0 u_1^2 \right] dV \right\rangle \qquad (2.20)$$

where $\langle \; \rangle$ indicates a time average and the subscripts indicate the order of perturbation for real quantities. If $\alpha \ll \omega$, upon insertion of equations of the same type as Equation (2.19),

$$\frac{d \, \ell n \langle \mathcal{E} \rangle}{dt} = 2\alpha \qquad (2.21)$$

Thus, for a closed system, the growth constant is directly related to the rate of energy input. For an open system the result must be modified as shown by Cantrell and Hart [7]. Their treatment is outlined in Appendix B. Their result is

$$2\alpha = \frac{-\left\langle \int_S \vec{n} \cdot \left\{ p_1 \vec{u}_1 + \frac{p_1^2 \vec{u}_0}{\rho_0 c^2} + \rho_0 \vec{u}_1 (\vec{u}_1 \cdot \vec{u}_0) + \rho_1 u_0 (\vec{u}_1 \cdot \vec{u}_0) \right\} dS \right\rangle}{\left\langle \int_V \left\{ \frac{1}{2} \frac{p_1^2}{\rho_0 c^2} + \frac{1}{2} \rho_0 u_1^2 + \rho_1 (\vec{u}_1 \cdot \vec{u}_0) \right\} dV \right\rangle} \qquad (2.22)$$

This equation is for isentropic and irrotational flow and is valid to second order in the perturbed quantities and first order in Mach Number.

Note the implication in the Cantrell result that α is really the sum of several contributions due to the various surfaces. Thus

$$\alpha = \sum_i \alpha_i \qquad (2.23)$$

where the sum is over all surfaces and the α_i's are positive if the contributing surface is supplying acoustic energy. Obviously the growth constants cannot be true constants or the amplitude would grow without bound. The α_i's must be dependent upon amplitude in such a way that the losses balance the gains at steady state. The fact that experimental data may be described by a constant α in the low amplitude range has been taken as an indication that the contribution of the burning surface is independent of amplitude and, similarly, the losses are independent of amplitude [27]. If the value of α_b for the burning surface may be obtained experimentally and the integrals of the Cantrell-Hart expression evaluated, the admittance of the burning surface may be obtained. In order to do this, the surface integrals must be related to the admittance of the burning surface. Coates has given the most frequently used approaches to estimating α_b from experimental data (see Appendix E). Cantrell and Hart have evaluated the integrals

 PAGE 26 OMITTED

in their expression, for the particular case of a T-burner, by neglecting small terms and assuming small deviations from the zero-order field, i.e., the acoustic field for a closed cylinder. They obtained

$$\alpha_b = - \frac{\gamma_T u_0}{L} \left(\frac{p_0}{u_0} y' \right) \tag{2.24}$$

where the relation $\omega = \frac{\pi c}{2L}$, which applies to the zero-order field, has been used.

While considering growth and decay constants, it is interesting to note that at steady state, i.e., when stable oscillations exist,

$$\alpha = \alpha_b + \alpha_D(A) = 0 \tag{2.25}$$

where $\alpha_D(A)$ represents the losses and is such a function of amplitude that

$$\lim_{A \to 0} \alpha_D (A) = \alpha_{DL} \tag{2.26}$$

It is thus observed that if the oscillations decay from a steady value following burn-out (i.e., completion of burning), the initial decay constant will be numerically equal to the growth constant due the burning surface before burn-out. That is

$$\alpha_b = - \alpha_D \tag{2.27}$$

If the zero-order approximation to the acoustic field is assumed and the initial decay constant measured, another estimate of the acoustic admittance is thus obtained.

It is worth noting at this point that the criterion for stability of a practical motor can be obtained from the Cantrell-Hart result.

It is simply required that

$$\alpha = \sum_i \alpha_i \leq 0 \tag{2.28}$$

for stability. With a knowledge of the appropriate boundary conditions and sufficient knowledge of the acoustic field to evaluate the integrals, the degree of stability or instability could be assessed.

The Response Function

Most of the currently available data on instability has been reported in terms of the pressure "response function," $\frac{\tilde{\mu}}{\epsilon}$, which was introduced by Hart and McClure [24]. The response function may be simply related to the acoustic admittance by perturbing the mass-flux definition, i.e., $\dot{m} = \rho u$. When this is done the response function is found to be numerically equivalent to the negative reduced-virtual acoustic admittance, that is,

$$\frac{\tilde{\mu}}{\epsilon} = - \frac{p_0}{u_0} y \tag{2.29}$$

From this result Equation (2.24) may be rewritten as

$$\alpha_b = \frac{\gamma_T u_0}{L} \operatorname{Re}\left[\frac{\tilde{\mu}}{\epsilon}\right] \tag{2.30}$$

Thus as long as a portion of the perturbation in mass flux is in phase with the pressure perturbation and in the same direction, the surface will have amplifying characteristics.

Summary of Equations to be Used

$$\tilde{p} = \gamma_T p_0 A_1 J_0(k_1 r)\, e^{j\omega t} \cosh j\gamma x \tag{2.5}$$

$$\frac{|\tilde{p}|}{|\tilde{p}_g|} \simeq |\cos bx| \tag{2.12}$$

$$\tan \phi \simeq ax \tan bx \tag{2.13}$$

$$aL = \frac{-\alpha_D}{2f} \tag{2.14}$$

$$a = \frac{\alpha - \alpha_{DL}}{c} \tag{2.15}$$

$$\gamma \simeq \frac{\omega}{c}\left\{1 + \frac{1+j}{r_w(2\omega)^{1/2}}\left[\upsilon^{1/2}\left(\gamma_T^{1/2} - \frac{1}{\gamma_T^{1/2}}\right) + (\mu')^{1/2}\right]\right\} \tag{2.7}$$

$$\mathrm{Re}\left[\frac{\tilde{\mu}}{\tilde{\epsilon}}\right] = \frac{p_0}{r_0 \rho_s}\left(\frac{a}{\omega}\right)[bL + \tan bL\,(1 + bL \tan bL)] \tag{2.31}$$

$$\mathrm{Im}\left[\frac{\tilde{\mu}}{\tilde{\epsilon}}\right] = -\frac{p_0}{r_0 \rho_s}\left(\frac{b}{\omega}\right)\tan bL \tag{2.32}$$

$$2\alpha = \frac{-\left\langle \int_S \vec{n} \cdot \left\{ p_1 \vec{u}_1 + \frac{p_1^2}{\rho_0 c^2}\vec{u}_0 + \rho_0 \vec{u}_1 (\vec{u}_1 \cdot \vec{u}_0) + \rho_1 \vec{u}_0 (\vec{u}_1 \cdot \vec{u}_0) \right\} dS \right\rangle}{\left\langle \int_V \left\{ \frac{1}{2}\frac{p_1^2}{\rho_0 c^2} + \frac{1}{2}\rho_0 u_1^2 + \rho_1 (\vec{u}_1 \cdot \vec{u}_0) \right\} dV \right\rangle} \tag{2.22}$$

$$\alpha_b = \frac{\gamma_T u_0}{L}\,\mathrm{Re}\left[\frac{\tilde{\mu}}{\tilde{\epsilon}}\right] \tag{2.30}$$

CHAPTER III

GAS-PHASE EXPERIMENTAL APPROACH

In Chapter II an analytical description of the acoustic behavior was developed. In this chapter we shall describe how experimental measurements were used to determine the parameters in that analysis. The acoustic field which corresponds to these pa ers will subsequently be evaluated.

There are two classes of measurements which can be made in a T-burner: those made during the firing and those made before or after the firing. During a firing only the dynamic pressure can be measured without great difficulty. Before a firing such information as the pertinent dimensions in the motor and physical properties of the propellant may be obtained. Therefore, for the problem at hand one must use such measurements to infer the behavior of the acoustic field.

Consider now the analytical expression for the acoustic pressure, Equation (2.5),

$$p = \gamma_T p_0 A_1 J_0 (k_1 r)\ e^{j\omega t} \cosh j\gamma x \qquad (2.5)$$

It will never actually be necessary to calculate the radial distribution but we must recognize that it exists. The task is to examine Equation (2.5) to ascertain the measurements necessary to determine the parameters. The complication of radial dependence, represented by the Bessel function in the above expression, may be evaded by making

all measurements at equivalent radial positions. With this restriction, measurements as functions of time of the pressure amplitude of two positions, the phase angle between them, and the frequency will provide sufficient information to make the equation useful. One other restriction must be imposed, this being that both measurements cannot be made at pressure antinodes. The last restriction is due to a kind of degeneracy in the equations, i.e., the phase angle is precisely π radians for all values of γ. It may be observed, however, that the phase angle need not be measured if the initial decay rate is measured. The phase angle measurement is more difficult to make, but it has the virtue of providing the necessary information without resorting to measurements made during transient operations.

The pressure transducers in use when this work was begun were of the uncooled variety so that it was necessary to locate them in positions where they would not be overheated. This necessity prohibited any measurements in the curved wall of the motor. However, if the necessary measurements could be made with one transducer at the non-burning end and a second one under the propellant, then the transducers would not be overheated. Consequently, initial firings were made to ascertain whether or not a meaningful measurement could be made through the propellant. It was thought that when the propellant was sufficiently thin the measured pressure would at least asymptotically approach the pressure existing on the gas side of the flame. These firings indicated that the relative amplitude and phase angle between the two measurements did not vary significantly with the thickness of the propellant

when the propellant thickness did not exceed 1 cm. Thereby it was concluded that the burning surface pressure could be measured in this manner.

We shall briefly consider the experimental system at this point. A complete description will be relegated to the Appendix (Appendix G). The T-burner used for this work made use of a centrally located sonic nozzle. The burner was constructed so that the length could be varied and, thereby, the oscillatory frequency. The acoustic cavity was 3.86 cm. in diameter and ranged in length from 10 to 26 cm., nominally. The mean pressure within the cavity was nominally 14.5 atm., being controlled by the nozzle diameter. The propellant chosen for the study was Utah F because of previous experience with this propellant and data available on it. The characteristics of this propellant may be found in Appendix H. Propellant samples were securely bonded into one end of the motor, the initial sample length being 1.27 cm., nominally. Two piezoelectric pressure transducers were located axially, one at each end. During a firing the oscillatory outputs from these two pressure transducers were amplified and recorded on magnetic tape. The two data channels were nominally identical; however, it proved best to record a reference signal through each channel immediately following the data from a firing. These reference signals permitted compensation for differences in circuitry of the channels. The recorded data were later reproduced, filtered, and the needed information extracted. The relative phase angle was measured with an electronic phase meter. The output of the phase meter, the frequency information, and all

amplitude information were obtained by displaying the appropriate electrical signal on an oscilloscope and photographing the trace.

In Figure 5 is shown a typical example of the data reproduced from the magnetic tape. The amplitude data were easily measured from such photographs. On the other hand, the two phase-angle traces exhibit considerable fluctuations. Such fluctuations limited the ability to measure the phase angles with confidence. The fluctuations occurred even though the data were closely filtered. It is most likely that they were due to distortion of the waveform. The growth and decay rates were also much easier to measure than the phase angles.

The experimental reproducibility was quite good. In Figure 6 are shown pressure traces from four consecutive firings. These traces demonstrate the reproducibility attained. The bonding of the samples in place proved to be particularly important.

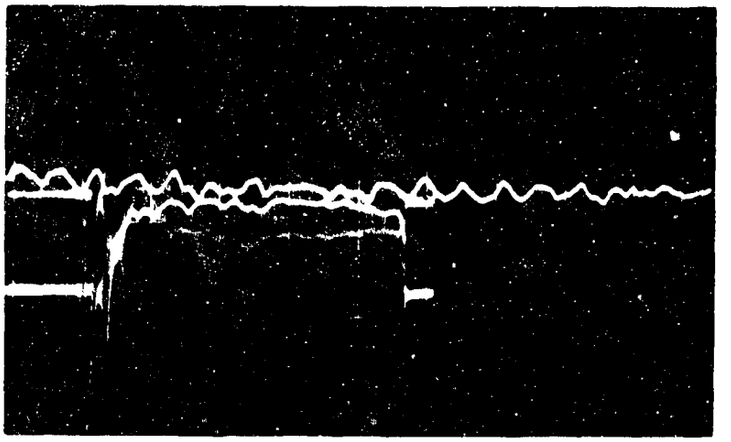

Figure 5. Typical phase-angle and amplitude data. Top and bottom oscillatory envelopes are from cold and burning ends, respectively. Top and bottom irregular traces are phase-angle traces from data and reference, respectively. Distance between these traces represents 180°- ϕ at 4.4°/cm.

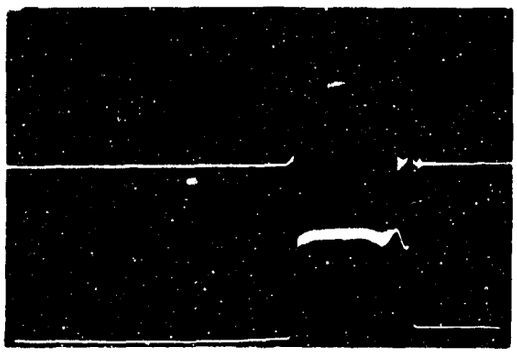

Run No. 0-223
Oscillating pressure .34 atm/cm

Run No. 0-224
Oscillating pressure .23 atm/cm.

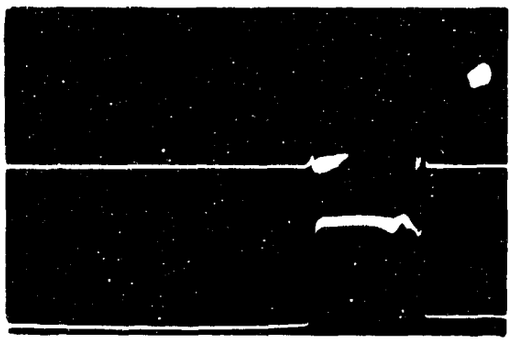

Run No. 0-225
Oscillating pressure .27 atm/cm

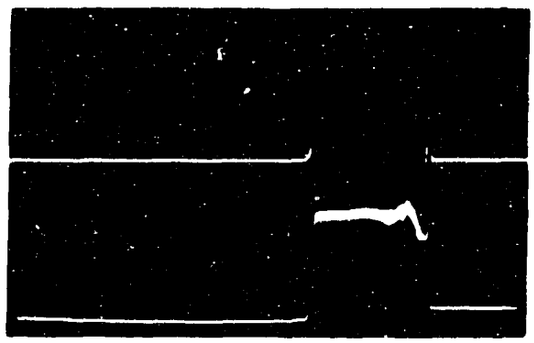

Run No. 0-226
Oscillating pressure .27 atm/cm

Figure 6. Pressure traces from four consecutive firings which are indicative of the reproducibility achieved. For each case, sweep rate is .5 sec/cm. from right and bottom trace is total pressure at 6.8 atm/cm.

CHAPTER IV

GAS-PHASE RESULTS AND DISCUSSION

In this chapter we shall describe the general character of the experimental data. It will be pointed out that the data are incompatible with an acoustic field which approximates the zero-order field. The data will be shown to very strongly indicate that acoustic energy is being trapped at the non-burning end of the motor, apparently due to asymmetric flow conditions in the vicinity of the nozzle. Finally, a few related experimental observations will be discussed.

In Figure 7 are shown pressure traces from two typical single-ended firings; the first typifies the pressure behavior in the 2.5- to 4.5-kilocycle frequency range and the second typifies the behavior in the 1- to 2.5-kilocycle range. In each case the mean pressure is seen to rise rapidly following ignition and remain at a fairly uniform level until burn-out (termination of burning). The level mean pressure trace indicates that the burning area was uniform throughout the firing. The low-frequency mean-pressure trace shown in Figure 7 is somewhat irregular; however, this will be attributed to effects other than mean burning at the end of this chapter. This figure shows the kinds of oscillatory envelopes observed. In all cases the oscillations began within 100 milliseconds after the ignition transient. The waveform during the growth period was sinusoidal while the amplitude was low and became distorted as the amplitude became large. In the high frequency

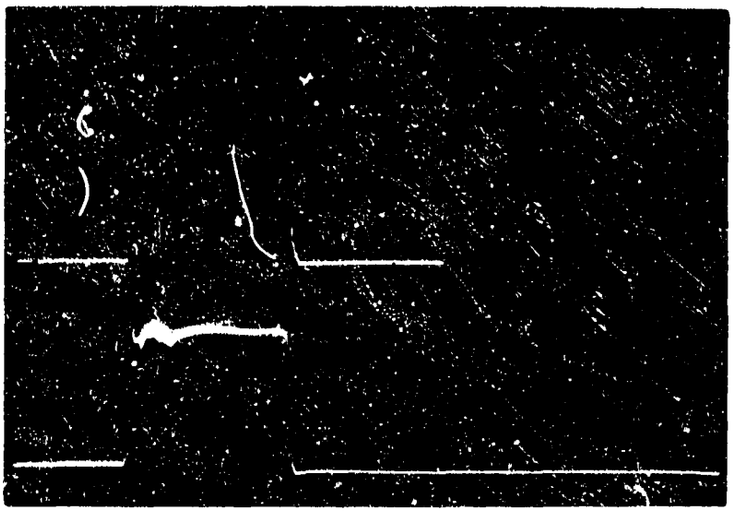

Run No. 0-253. Nominal frequency 4.2 kc.
Oscillating pressure .27 atm/cm.
Total pressure 6.8 atm/cm.
Sweep rate .5 sec/cm. from left.

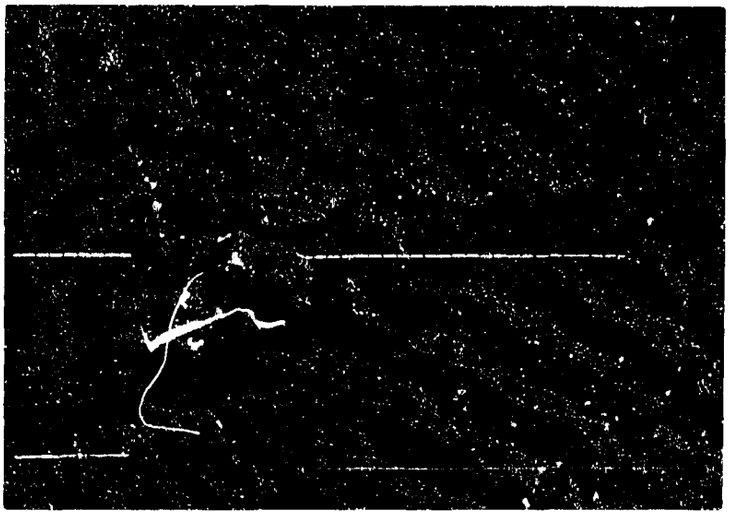

Run No. 234 Nominal frequency 1.9 kc.
Oscillating pressure .27 atm/cm.
Total pressure 6.8 atm/cm.
Sweep rate .5 sec/cm. from left

Figure 7. Typical pressure traces from single-ended firings.

range the waveform typically was distorted during the first one-third of the firing after the growth transient. The amplitude would then drop, frequently to about half of the initial amplitude, and would again become sinusoidal. In Figure 8 are shown waveforms typical of these two regions. On the other hand, in the low frequency range the amplitude would rise during the growth transient to a maximum. The amplitude would then decrease steadily to a minimum and subsequently grow again. The minimum was observed in all firings in the low-frequency range and always occurred when about one-fourth of a 1.27-cm. sample remained. This peculiar amplitude behavior will shortly be associated with the energy trap concept alluded to in the opening paragraph.

Once the data from a firing had been recorded, it was reproduced in order to acquire the desired information. In Figure 9 are shown the data from two typical firings. The relative amplitude measurement was taken from such photographs. We shall define "relative amplitude" as $\left|\tilde{p}_s\right| / \left|\tilde{p}_g\right|$ for convenience. Note in Figure 9 that the oscillatory amplitudes were considerably different at the two ends of the motor. This difference in amplitude was always observed.

The relative amplitudes from a number of firings are plotted in Figure 10. The data shown are from runs whose mean pressure traces indicated that the burning was well behaved. Furthermore, the data were measured near burn-out and during stable oscillations. The effect of poor mean burning in the latter part of a firing was to increase the relative amplitude, which remained, however, significantly less than unit.

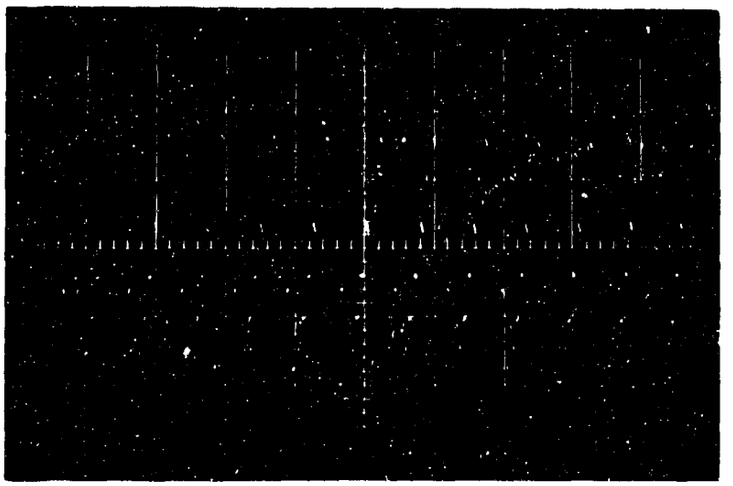

Early portion of run (No. 0-260)
Frequency 5.3 kc.

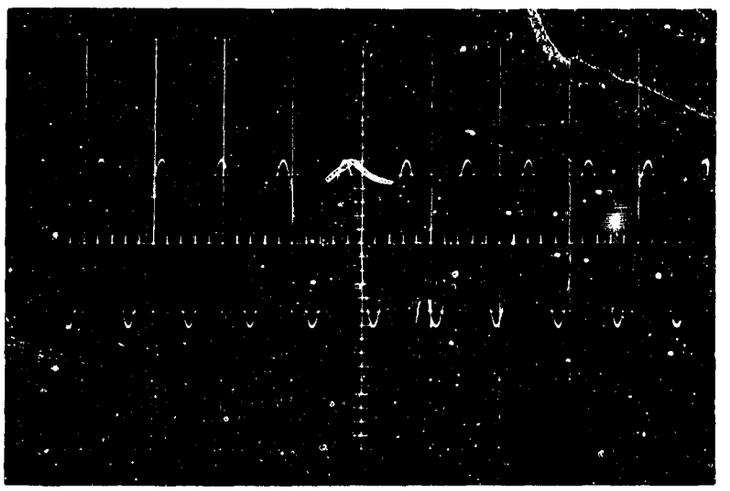

Latter portion of run.
Frequency 4.6 kc.

Figure 8. The change in waveform frequently observed during a firing.

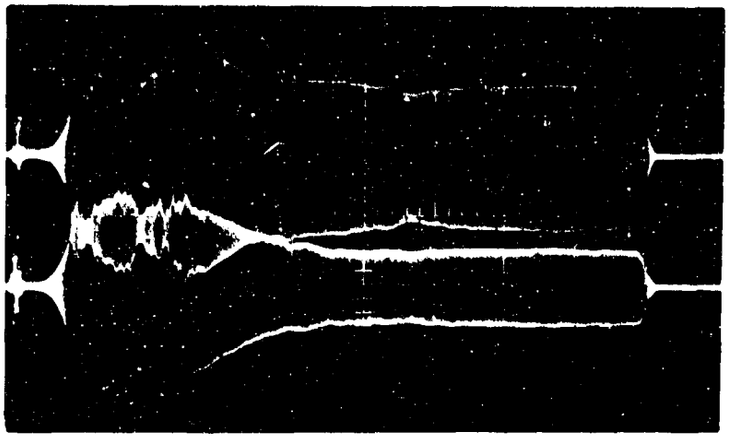

Run No. 0-260.
Nominal frequency 4.1 kc.
Vertical scales are nominally equal sweep from left.

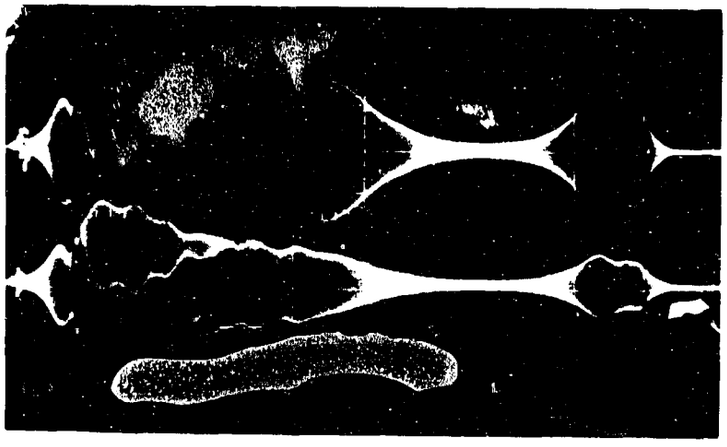

Run No. 0-227.
Nominal frequency 1.4 kc.
Vertical scales are nominally equal, sweep from left.

Figure 9. Typical amplitude data from single-ended firings.

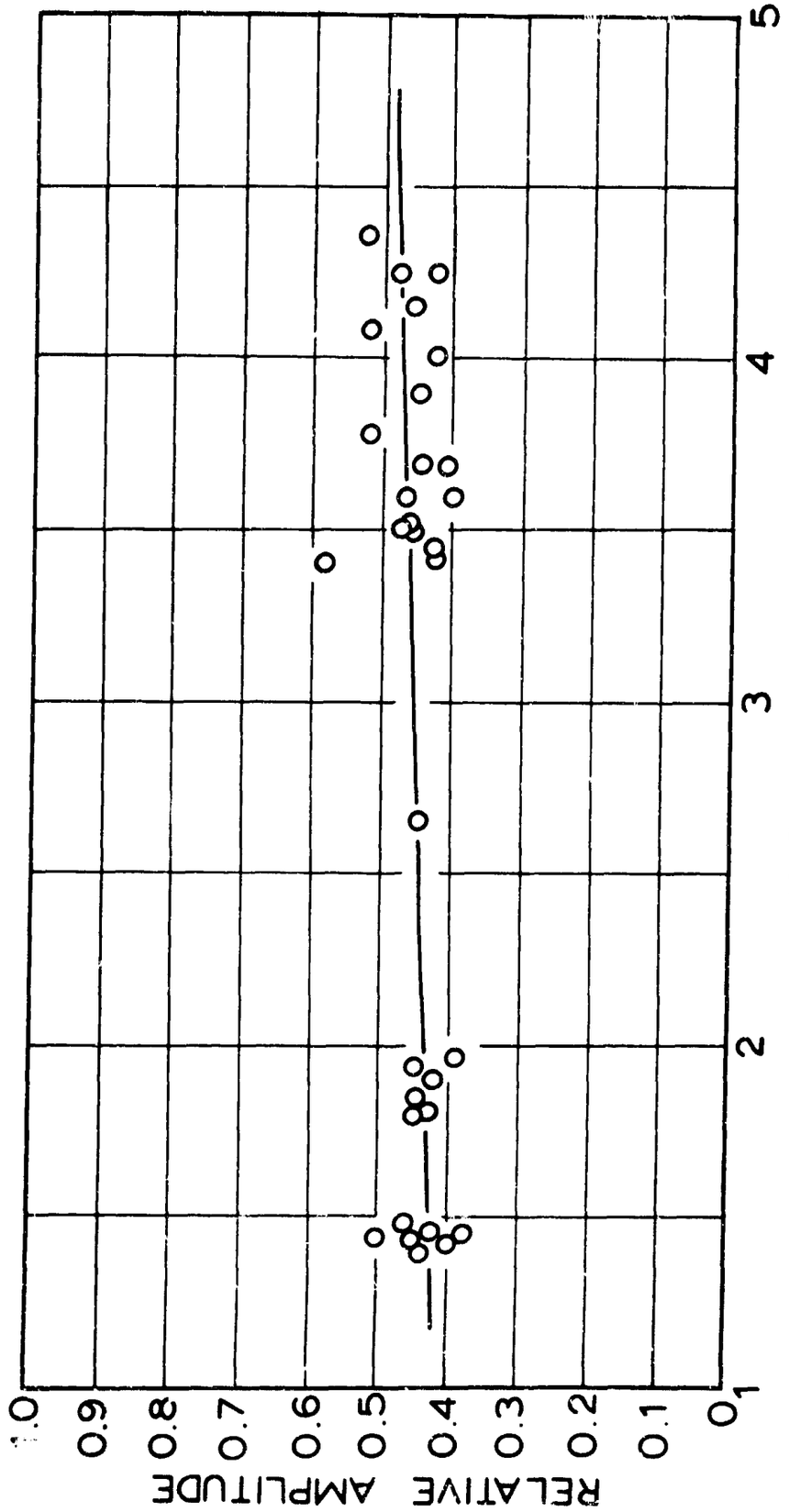

Figure 10. Measured relative amplitude from experimental data.

The experimental observations that (1) the relative amplitude was much less than unity and (2) the measured phase-angle was slightly less than π radians are of substantial importance. In particular, these observations rather conclusively indicate that the zero-order acoustic-field approximation is invalid in these circumstances. In order for the zero-order approximation to hold, the relative amplitude would have to be nearly unity and the phase angle very nearly π radians. These observations were the real incentive for this research work. If the deviation from zero-order was due to the combustion process, then it would be of great importance to assess the implications in terms of the estimated acoustic admittance for the burning surface. Consequently a number of firings were made in order to characterize the behavior.

In the past the zero-order approximation has been frequently used. However, there appear to be few experimental investigations of the validity of the assumption. Strittmater et al. [55] report measuring the frequency before and after burn-out. On the basis of their measurements they conclude that the acoustic field is nearly zero-order. Horton [28,29] reports measuring the pressure amplitude at the burning interface, the cold end, and under a thin sample of propellant. He concludes that the amplitudes are equal within experimental accuracy at all three locations. Thus his results are completely contrary to those obtained in this work. However, if his propellant was considerably different from Utah F, the effects which are quite apparent in this work may not have been evident in his data. Coates [10,11], in his T-burner work, apparently found the zero-order approximation to be valid since he uses this approximation in his analysis of the acoustic

behavior. Therefore, it appears that this work is the first in which substantial deviations from the zero-order field have been observed, or, at any rate, recognized.

In an attempt to ascertain why the low relative amplitude might occur due to other than combustion phenomena, an extensive examination of various aspects of the problem was undertaken. The details of this examination are given in Appendix I. The conclusions reached are as follows:

1. The measured amplitude ratio exists within the motor. In particular, it is not introduced by the instrumentation, it is not introduced by either the thermal boundary layer at the cold end or the boundary layer associated with the flame, and it is not due to the propellant behind which the low amplitude is measured.
2. Although the gas may be cooler at the non-burning end of the motor, the predicted effect is in opposition to that measured.
3. Pressure measurements made in the curved wall of the motor (propellant side of the nozzle) are compatible with the pressure measured under the propellant.
4. Measurements made with the nozzle shifted toward the propellant from the midpoint of the motor indicate that the pressure node is located in the vicinity of the midpoint.
5. The low relative amplitude persists through most of the decay transient after burnout. One can readily see this in Figure 11, in which a typical decay transient is shown.

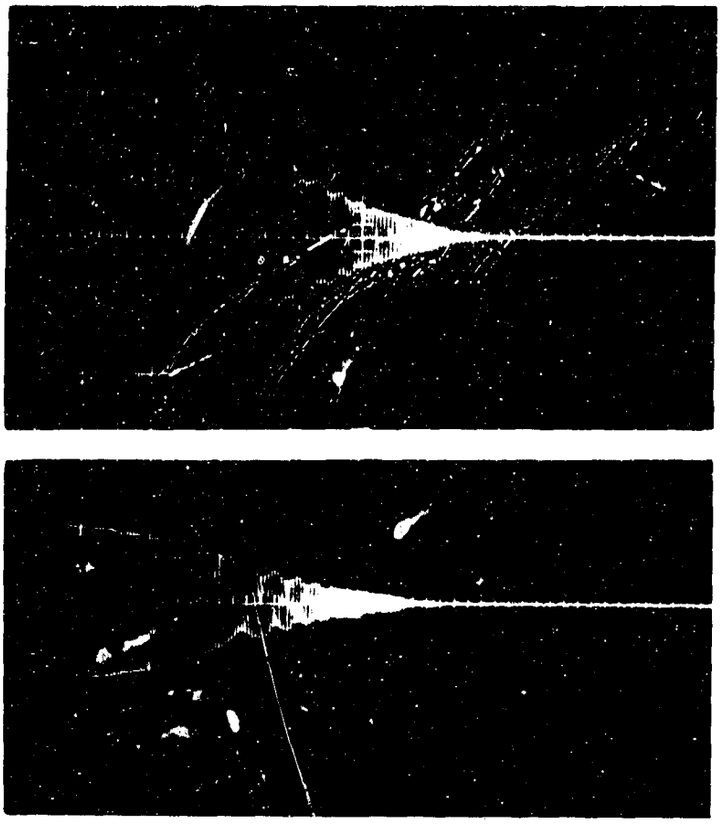

Figure 11. Oscillatory decay transient from each end of the motor. The lower trace should be shifted about .6 cm. to right in order to correspond in time to the top trace. Data from Run No. 0-260, time scale is approximately 6.25 msec/cm.

The latter two of the above conclusions indicate that perhaps the analytical description developed in Chapter II is inadequate.

First consider the fourth conclusion given above. If the analytical description were adequate, the pressure node would be shifted toward the propellant from the midpoint in order to satisfy the measured relative amplitude. More specifically, the analytical description indicates

$$\tilde{p} \simeq \left|\tilde{p}_g\right| e^{j\omega t} \cos bL \left(\frac{x}{L}\right) \qquad (4.1)$$

Accordingly, a low relative amplitude requires that $bL < \pi$ and, therefore, the cosine term will be zero when $\frac{x}{L} > .5$. Since the fourth conclusion indicates that the pressure node is near the midpoint, it is in conflict with the description given by Equation (4.1).

The last conclusion given above seems to be a particularly severe indictment of the analytical description given in Chapter II. In order for the analytical description to be adequate, it must describe the decay transient as well as the steady state behavior. In Appendix A it is shown that, if the reflection is perfect at the propellant end after the propellant is consumed, then necessarily

$$\tan b_D L = 0 \qquad (4.2)$$

$$b_D L = n\pi \qquad n = 1,2,3,\ldots \qquad (4.3)$$

This also necessitates that

$$\cos b_D L = 1.0 \qquad (4.4)$$

for all component frequencies. An analytical solution to the decay

transient problem must satisfy the steady-state burning pressure distribution as an initial condition; therefore, the complete solution would be a series of terms each of which would decay at a different rate. However, the filtering would remove all except the fundamental frequency. Thus, in order to meet the expected boundary condition at the end of the motor after burn-out, the measured relative amplitude should go to unity as the burn-out occurs. Since the relative amplitude does not go to unity, the analytical description does not describe the real behavior.

The fact that the unusual acoustic field persists throughout the decay transient should make it possible to eliminate all chemical reactions as possible sources of the unusual behavior. The combustion processes must cease very soon after burn-out. The cooling that accompanies the mean pressure decay should freeze all chemical equilibria very early in the transient.

On the basis of the information at hand, it appears that a considerable portion of a wave traveling in the positive direction (i.e., away from the cold end) is suffering a distributed reflection such that the wave traveling in the opposite direction is reinforced, only a part of the positive wave reaching the propellant. The reflection must be distributed because essentially one frequency is present. The only likely source of such a reflection is the flow field in the neighborhood of the nozzle. There is some evidence of a similar reflection being observed in a similar configuration [4 3]. The mean flow in this region is sufficiently complicated that no theoretical explanation can be presented at this time; however, we shall present substantial experimental support for the postulated behavior.

The analytical description that has been developed should be sufficiently general to describe most phenomena except a reflection of the type we have described. Consequently, it is felt that the failure of the analytical pressure distribution actually supports the concept of an asymmetric reflection.

In the light of this postulated reflection, some early work Horton [26] did may be significant. He measured a low relative amplitude in single-ended firings. However, he felt that his measured amplitude at the propellant end was low by a factor of .45. This factor was obtained from non-burning viscoelastic tests in which a weak shock wave was reflected from one end of a propellant sample. In these tests the mean pressure under the propellant was low by the factor of .45. He then assumed this factor was also appropriate for the oscillating pressure as well and corrected his measured amplitudes accordingly. He attributed the low measurement to poor transducer contact. Unfortunately the transducer was not used to measure a mean as well as an oscillating pressure so that it is not known if the poor contact problem existed in his firings. It seems possible that Horton's correction may have been needless and that he was observing effects similar to those we are describing.

Let us now return to consideration of oscillatory pressure envelopes observed. In Figure 7, both oscillatory envelopes were seen to substantially drop in amplitude after the first one-third of the firing. The low-frequency firing was seen to exhibit a minimum in the oscillatory envelope. These observed amplitude reductions are presumed

to be manifestations of the supposed asymmetric reflection. If this reflection is due to the asymmetric flow as supposed, then a double-ended firing should not exhibit a reduction in amplitude. In Figure 12 is shown a reproduced oscillatory envelope from a double-ended firing whose frequency was somewhat less than the high-frequency trace shown in Figure 7. Clearly the envelope does not show an amplitude reduction.

In connection with these amplitude reductions, it was noted that, at least at times, there was a shift in frequency associated with the reduction. An example of this is shown in Figure 8 since these waveforms were sampled just before and just after the drop in amplitude. The postulated reflection, assuming its development to be coincident with the reduction in amplitude, would be expected to affect the frequency.

The phase-angle measurement may be in opposition to the supposed asymmetric reflection. In order to explain this we shall assume that the effect of the behavior in the vicinity of the nozzle is to decrease the pressure amplitude by an amount $e^{-\delta}$, i.e., for $x > x_1$

$$\tilde{p} = \left|\tilde{p}_g\right| e^{-\delta} e^{j\omega t} J_0 (k,r) \cosh j\gamma x \qquad (4.5)$$

where x_1 is the location of the boundary of the nozzle effects. If the pressure is given by an expression of this type, the expression for the phase angle remains unchanged, i.e.,

$$\tan \Phi = \tanh aL \tan bL \qquad (2.13)$$

Here it is noted that this equation requires the phase angle to approach π radians as bL approaches π radians in order that aL be finite. According to the reflection concept the value of bL would be expected to approximate

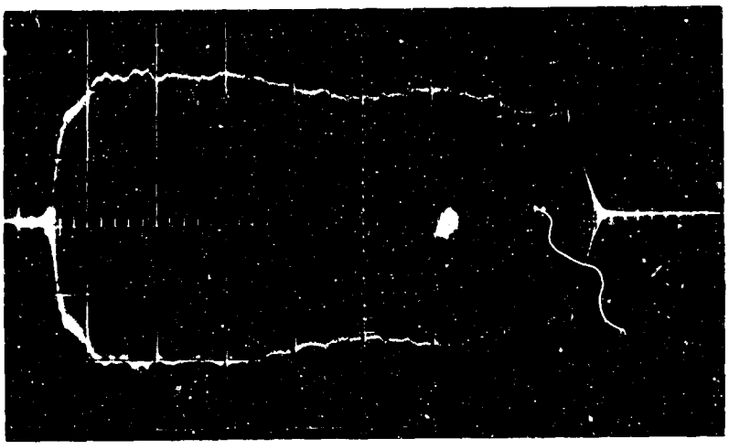

Run No. 0-264
Nominal frequency 3.0 kc.
Sweep from left.

Figure 12. Oscillatory envelope from a double-ended firing.

π radians. In which case the value of aL from Equation (2.13) would be unreasonably large. On the other hand, we must observe that $e^{-\delta}$ in Equation (4.5) may not sufficiently describe the effects of the reflection. In addition, the phase-angle measurement may be in error. The measurement was made with great care and attempts were made to compensate for electronic effects; however, in spite of this care, distortion of the waveform by the electronic systems may have caused a systematic error in the reading. The fact that the phase-angle trace from the reference signal was unstable suggests that distortion may have been occurring.

Real Part of Propagation Constant

We shall now examine the value of b as determined from the relative amplitude measurement and attempt to assess its implications in terms of the supposed asymmetric reflection.

It will be convenient to estimate the value in three ways. These are:

1. The [illegible]re-amplitude measurement in conjunction with Equation (2.12), advantage being taken of the smallness of a. This method will give the value of b necessary for the analysis of Chapter II to describe the end conditions. If the low-relative amplitude was due to the combustion, then this value should, in part, describe the actual accustic field.
2. From the theoretical propagation constant, Equation (2.7), b is expected to approximate $\frac{\omega}{c}$. The postulated effects of the nozzle are not expected to extend throughout the motor

so that this approximation should be valid near the propellant surface. The frequency is available and $\underline{c}$ will be estimated by assuming the mean flow through the nozzle to be isentropic and steady (see Appendix K).

3. Finally the value of $\underline{b}$ will be estimated as $\frac{\pi}{L}$. This is the value of $\underline{b}$ that would exist if the acoustic velocity was zero at the burning surface.

For brevity these methods of estimation will be called Method (1), (2), or (3), respectively. In Figure 13, the three estimates of $\underline{b}$ are shown. The plotted points were obtained by Method (1). Clearly this method predicts a much smaller value of $\underline{b}$ than the other two methods.

The low value of $\underline{b}$ predicted from Method (1) has two interesting implications, these being:

1. The wave propagates faster than the estimated velocity of sound. A wave propagates at a velocity of ω/b and with the indicated b values this velocity is about thirty per cent greater than the estimate for the isentropic velocity of sound. This situation seems highly unlikely even for a chemically reactive system.
2. Since $\underline{b}$ is not nearly equal to $\frac{\pi}{L}$, it is implied that the acoustic velocity is large at the transpiring boundary. The velocity amplitude is, in fact, estimated to be greater than the velocity of mean flow. Again, the situation seems unlikely.

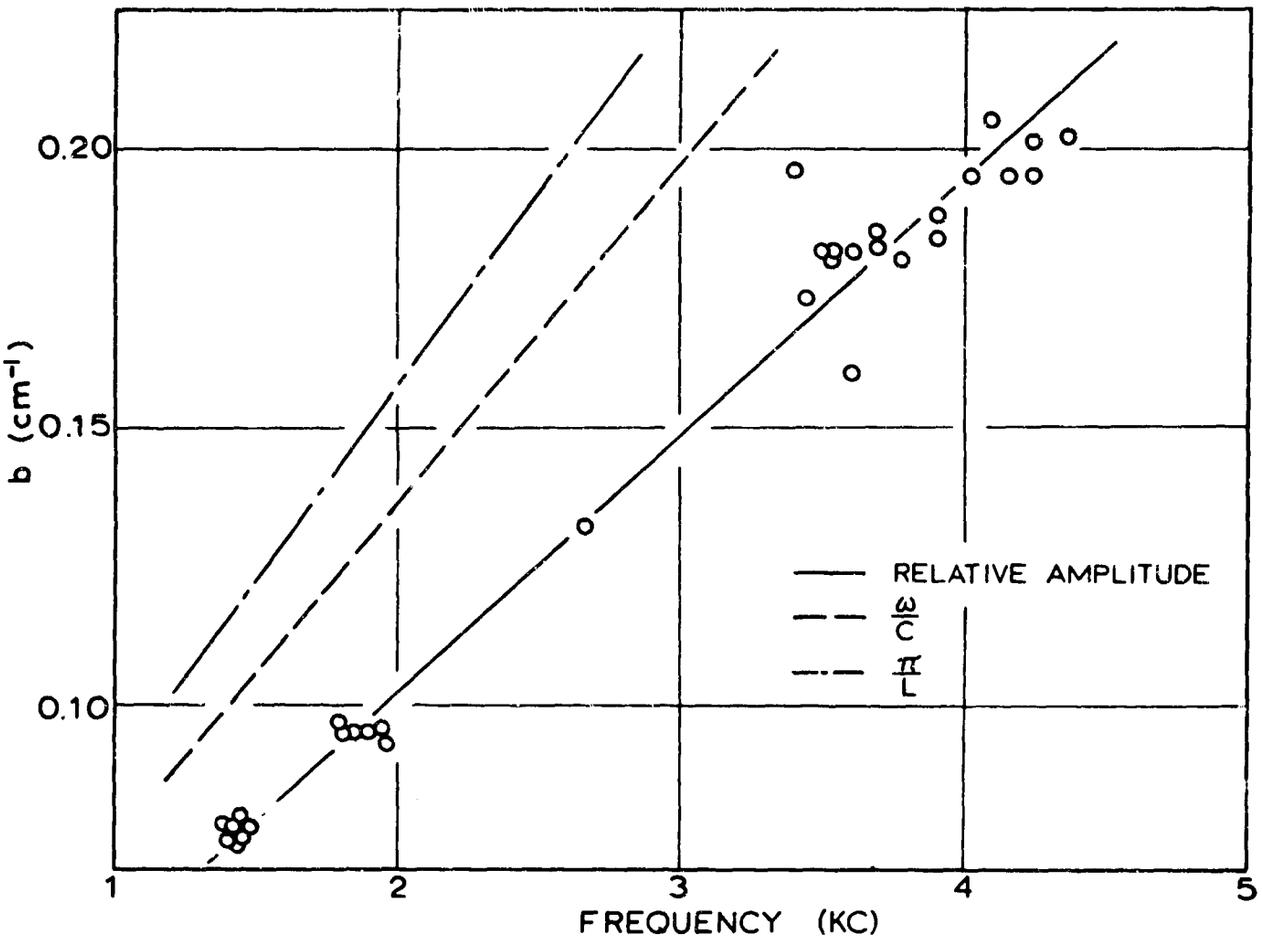

Figure 13. Frequency dependence of estimated b values.

The Estimated Response Function

In this section we shall show that the response function estimated with the developed analytical description of Chapter II and the experimental data, i.e., relative amplitudes and phase angles or decay rates, does not agree with an estimate obtained from growth-constant data. The value of b will then be re-estimated by Methods (2) and (3) and the corresponding response function estimate will then be shown to agree reasonably well with that obtained from growth-constant data. This situation provides additional support for the asymmetric-reflection concept. The response function as estimated from growth constant data will be developed initially.

Very early in this research work growth-constant data were obtained from double- and single-ended firings. After these early measurements were made it was necessary to purchase new ammonium perchlorate for making the propellant. Even though the new material was nominally the same and a size analysis showed nearly equivalent particle size distributions, the new propellant was found to burn at a rate about forty per cent higher than the old propellant (see Appendix H). The new propellant did have the same burning rate exponent, however. No explanation for the change in burning rate has been suggested.

Because the burning rates were different for the old and the new propellants, the acoustic admittance should be expected to be different. Therefore, in addition to other data, the growth constants were measured from later firings. The data from the old propellant are presented in Figure 14. In Figure 15 are presented the data on the

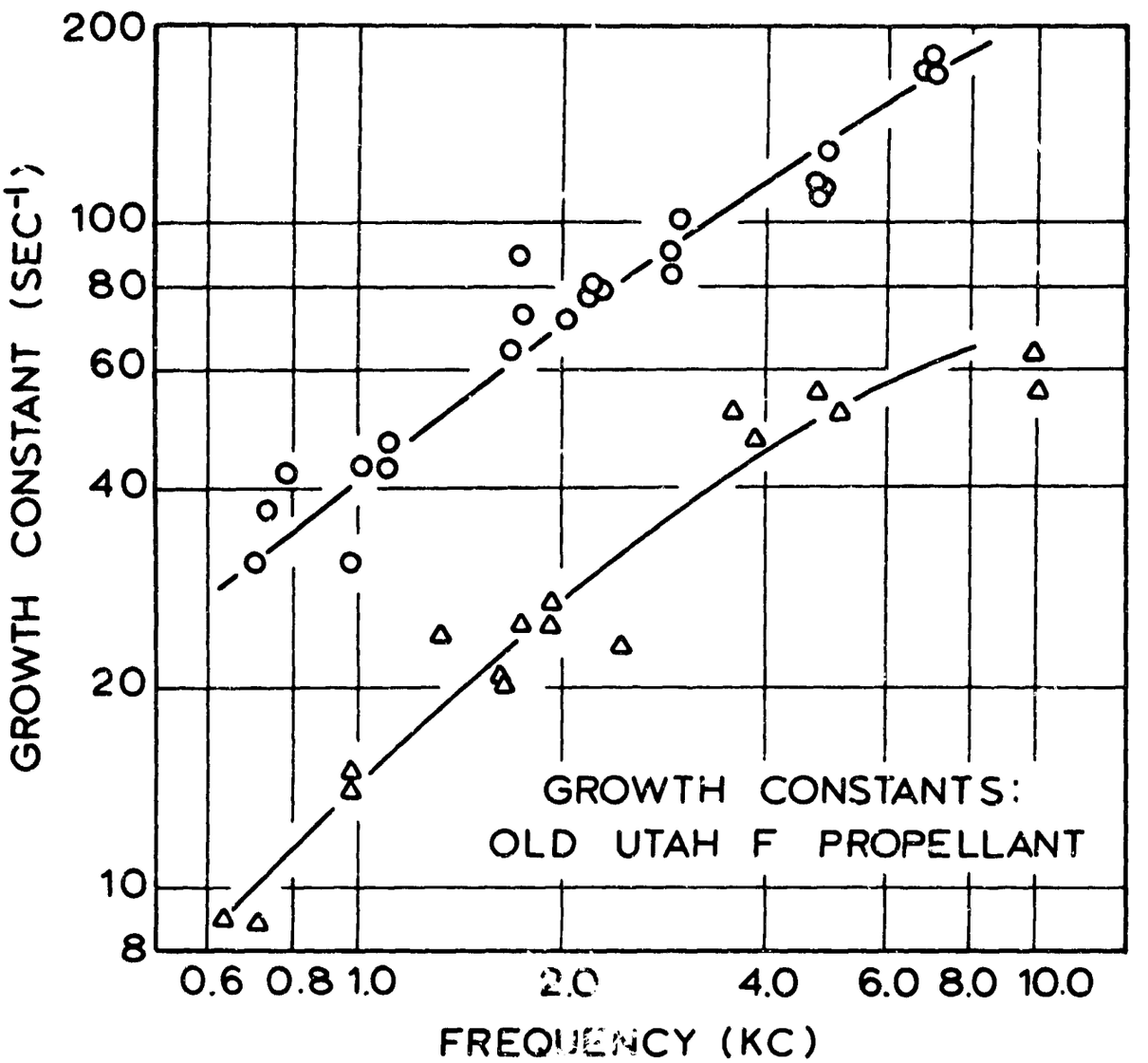

Figure 14. Growth constants for old Utah F-propellant. The upper curves are for double-ended firings. All points were obtained at a mean pressure of 14.5 atm (nominal).

new propellant; the dashed lines represent the older data and the solid lines are parallel to the dashed lines but through the new data. Only a few double-ended firings were made with the new propellant but these are adequate for the comparisons to be made.

The response function may be estimated from these growth-constant data in a manner suggested by Coates (Appendix E). He suggests that the damping be assumed equivalent for both double- and single-ended firings. The growth constant due to one burning surface is thereby approximated by the difference between the two kinds of growth constants. The response function may then be calculated from the result given by Cantrell (Equation (2.30)), with the assumption that the acoustic field is nearly that of the zero-order field being made. This result is consistent with that of Coates (Appendix E). However, it will be more consistent with this work to use Equation (2.15). Thus

$$aL = \frac{\alpha - \alpha_{DL}}{2f} \tag{4.6}$$

or through Coates' suggestion

$$aL = \frac{\alpha_2 - \alpha_1}{2f} \tag{4.7}$$

When $bL = \pi$ then Coates' result is obtained, i.e.,

$$\mathrm{Re}\left[\frac{\tilde{\mu}}{\tilde{\epsilon}}\right] = \frac{p_0}{\rho_s r_0} \frac{(\alpha_2 - \alpha_1)}{4Lf^2} \tag{4.8}$$

The response function estimates obtained from application of this equation are shown in Figure 16. The solid line and dashed line correspond to the old and new propellants, respectively. The dashed line has been drawn parallel to the solid line.

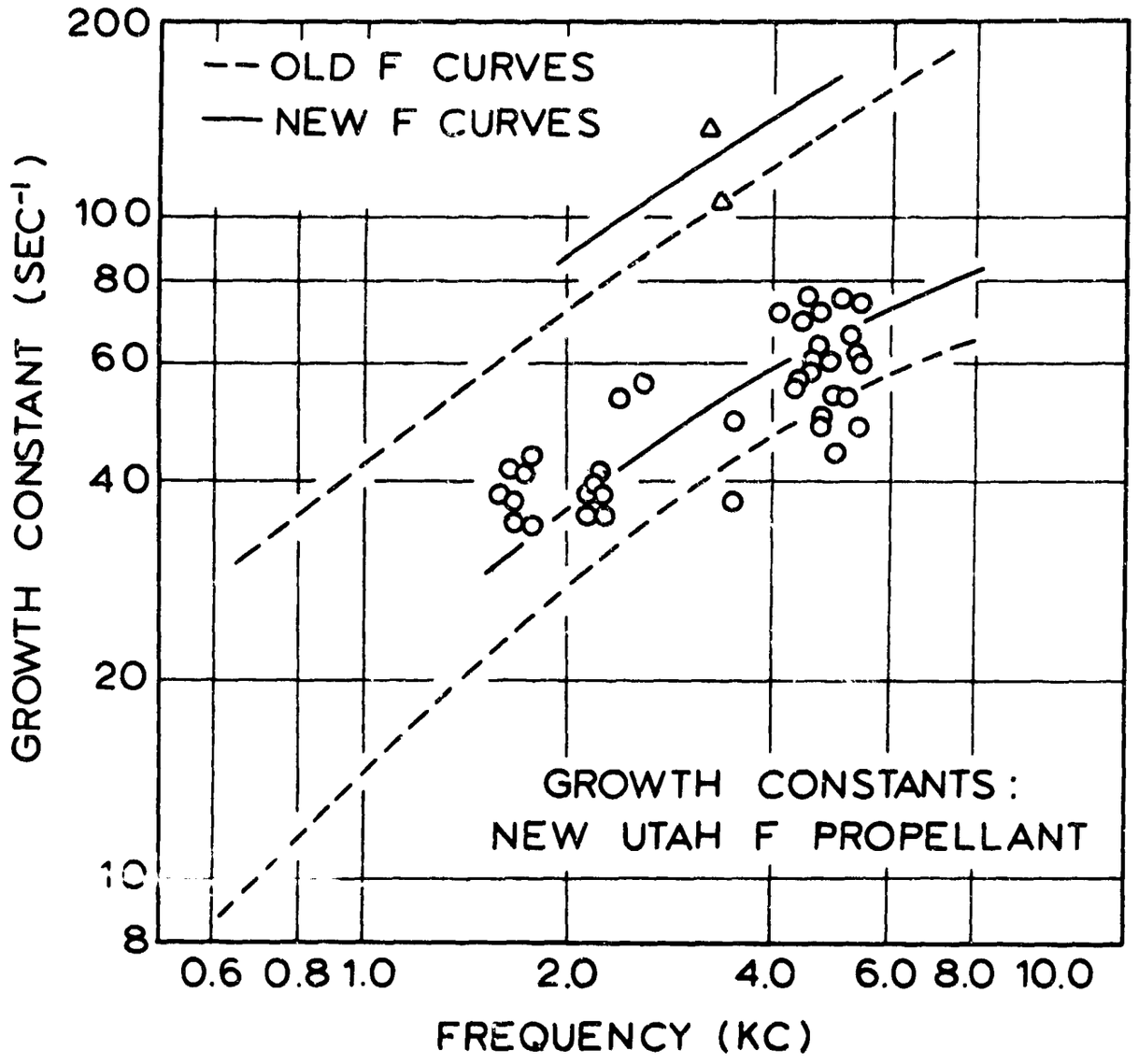

Figure 15. Growth constants for new Utah F-propellant. The upper curves are for double-ended firings. All points were obtained at a mean pressure of 14.5 atm (nominal).

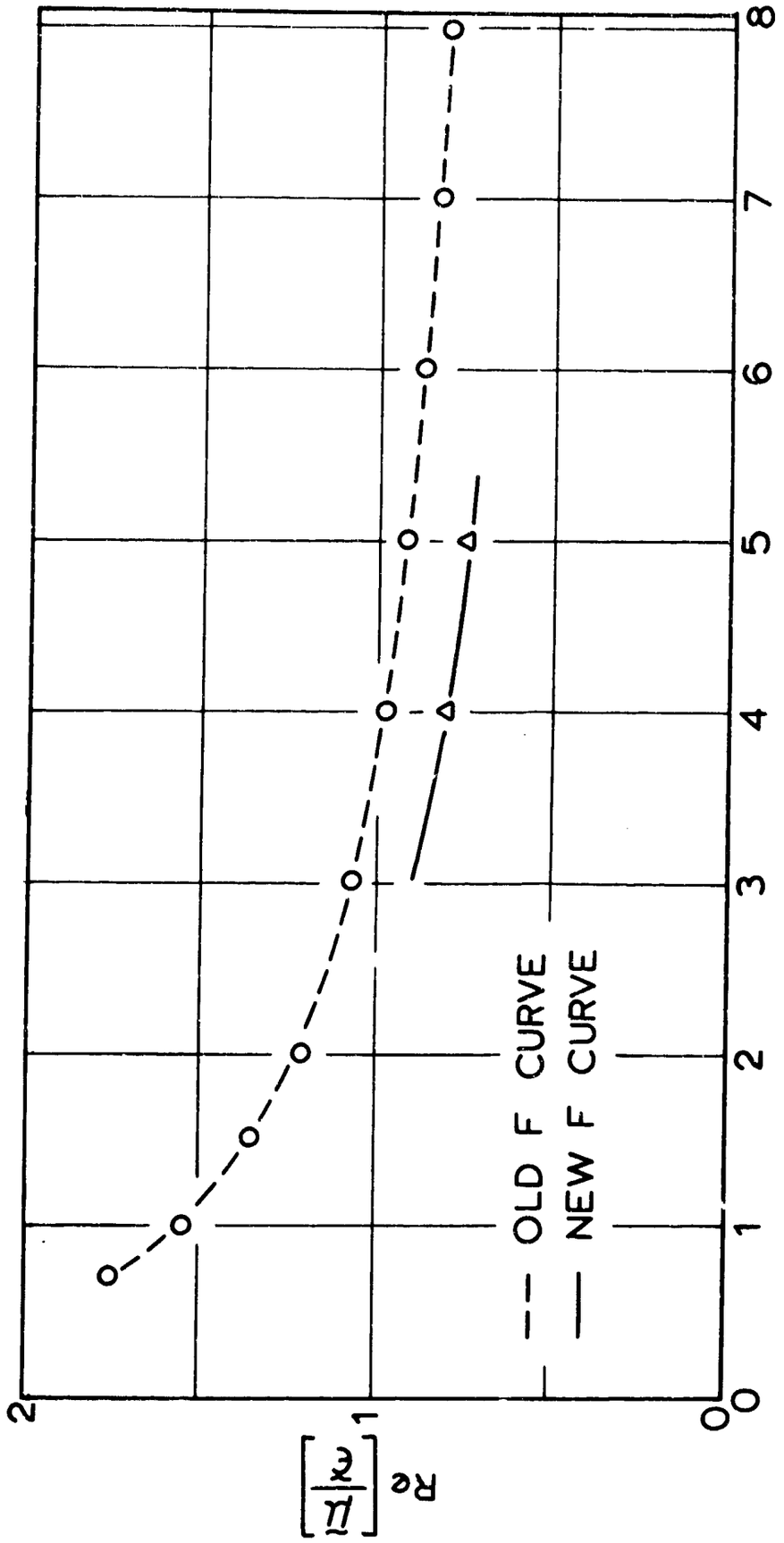

Figure 16. Calculated response function (real part) from growth constants. The points shown were calculated from the growth-constant curves.

It should be noted that Coates used the data shown in Figure 14, with a few of his own, in his comparison of growth-constant techniques (Appendix E). He was able to obtain good agreement between the double- and single-ended growth-constant estimate of the response function and estimates obtained from two strictly double-ended techniques. Thus the response-function estimates shown in Figure 16 should be reasonably good. These estimates may now be compared with those obtained from the relative amplitude measurement and phase-angle or decay-rate measurements.

The comparison is facilitated if the estimated values of $\underline{b}$ are smoothed. The calculated values of $\underline{b}$ obtained by the three methods of the last section are plotted on Figure 17 as a function of reciprocal chamber length. Straight lines fit the data adequately. These curves may be used to define a value of $\underline{b}$ at a particular chamber length for calculation purposes.

In order to estimate the response function we must estimate the value of $\underline{a}$ in addition to $\underline{b}$. The value of $\underline{a}$ may be obtained from the phase-angle (Equation (2.13)) or the initial decay rate (Equation (2.14)). The phase-angle data may only be used with the relative amplitude data.

The response function is related to the experimental information by the approximate equations (2.31) and (2.32)

$$\mathrm{Re}\left[\frac{\tilde{\mu}}{\tilde{\epsilon}}\right] = \frac{p_0}{\rho_s r_0}\left(\frac{a}{\omega}\right)\left[bL + \tan bL\,(1 + bL \tan bL)\right] \qquad (2.31)$$

$$\mathrm{Im}\left[\frac{\tilde{\mu}}{\tilde{\epsilon}}\right] = \frac{p_0}{\rho_s r_0}\left(\frac{b}{\omega}\right)\tan bL \qquad (2.32)$$

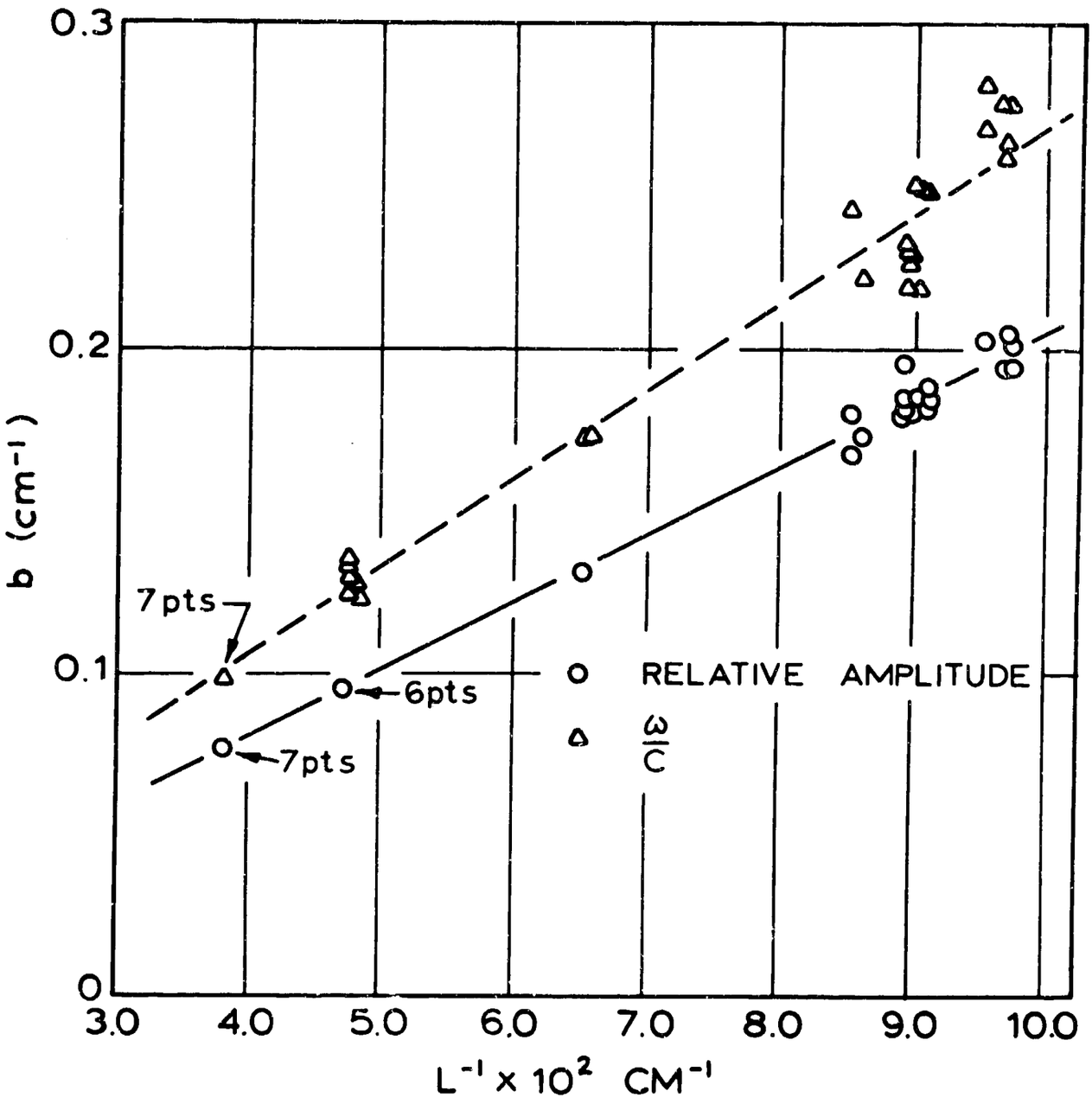

Figure 17. Inverse length dependence of b estimated by Methods (1) and (2).

The values of p_0, ω, and L to be used are readily obtained from the firing data. The values of r_0 and ρ_s are obtained from propellant data.

The response function was estimated for the case where the analytical description is assumed to hold, i.e., the value of $\underline{b}$ being obtained from the relative amplitude (Method (1)) and $\underline{a}$ from the phase angle and decay ate. The real part of response function as estimated in this manner, Equations (2.12), (2.31), and (2.13) or (2.14) being used, is shown in Figure 18 with the estimate obtained from the double- and single-ended growth constants. Clearly the former are larger by about a factor of two than the latter.

The response function was also estimated for the cases where $\underline{b}$ was approximated as $\frac{\omega}{c}$ and $\frac{\pi}{L}$ (Equations (2.14) and (2.31) being used). Because the value of $\underline{a}$ obtained from the decay rate is independent of $\underline{b}$, a very simple comparison may be made. By means of the curves for $\underline{b}$ shown in Figure 17, the estimates of Re $\left[\frac{\tilde{\mu}}{\tilde{\epsilon}}\right]$ are in the ratio 2.88: 1.00: 1.11 corresponding to $\underline{b}$ as estimated from Methods (1), (2), and (3), respectively. In Figure 19 the calculated estimates of Re $\left[\frac{\tilde{\mu}}{\tilde{\epsilon}}\right]$ corresponding to $b \simeq \frac{\omega}{c}$ are plotted. Also shown is the curve for the double- and single-ended growth-constant estimate. The agreement is seen to be reasonably good (note that the vertical scales are different on Figures 18 and 19).

These considerations indicate that (1) the acoustic behavior in the neighborhood of the burning surface is similar to a zero-order field, (2) the overall deviations from a zero-order field must be

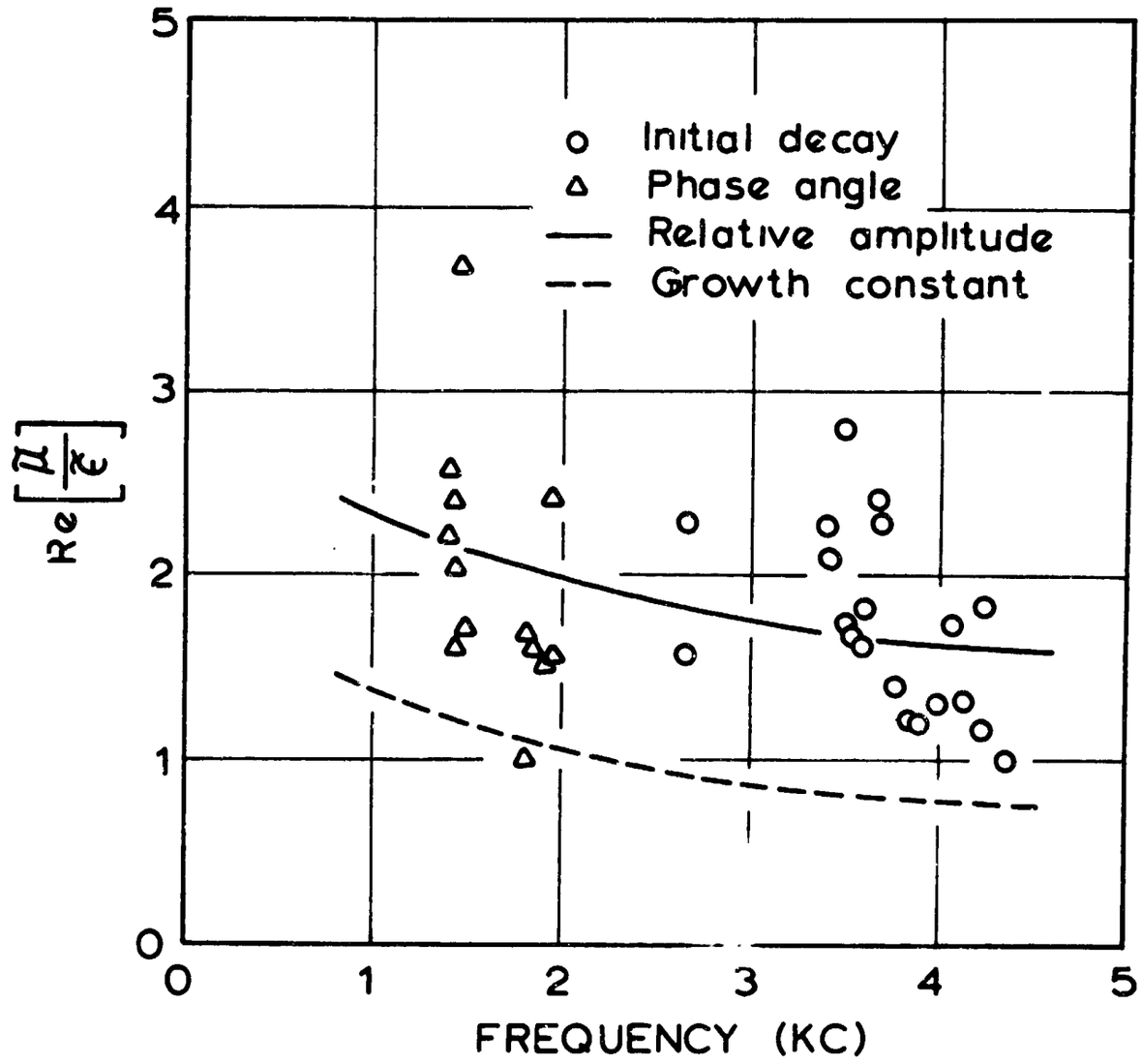

Figure 18. Calculated response function (real part) from relative-amplitude and phase-angle or decay rate data.

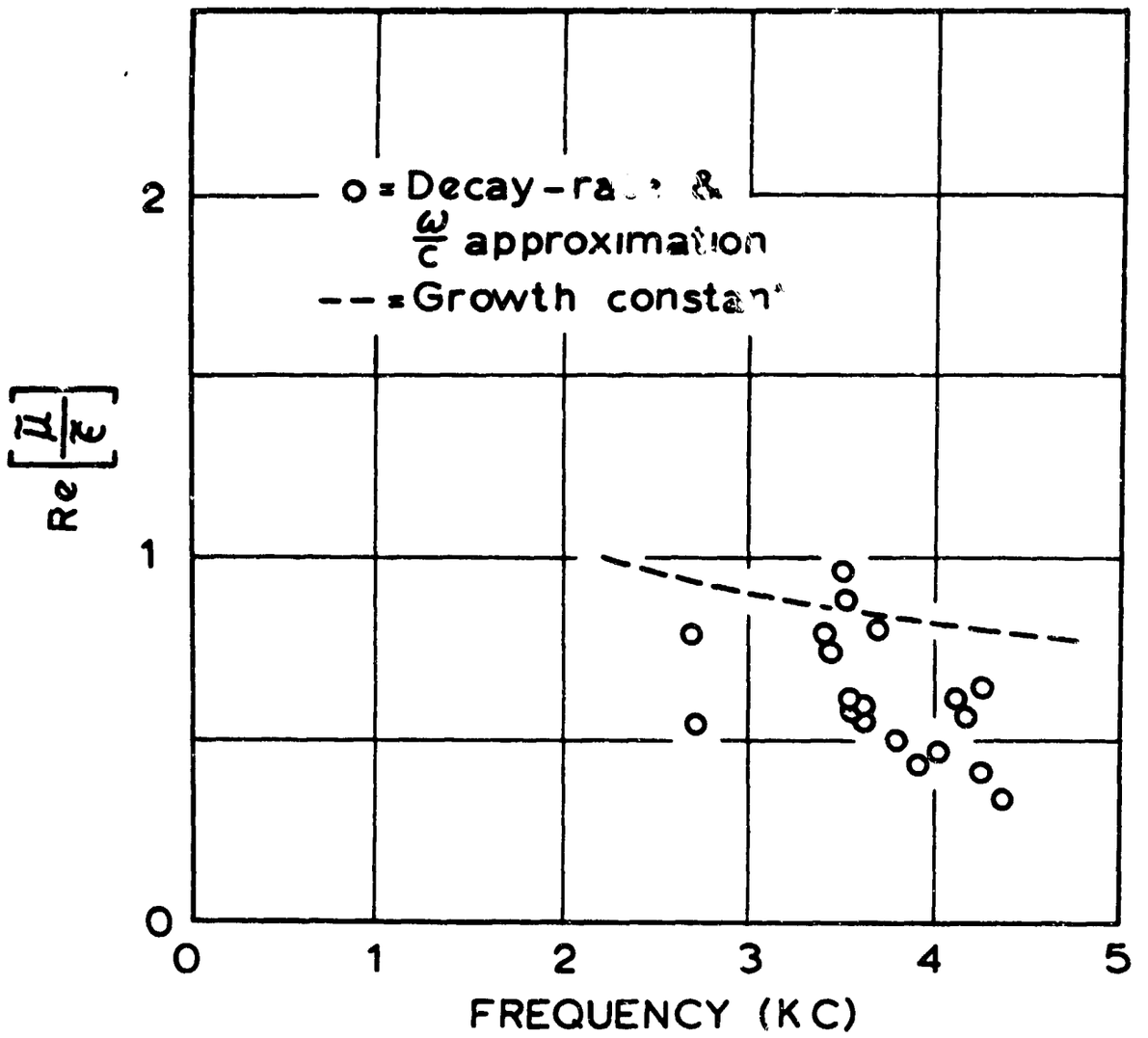

Figure 19. Calculated response function (real part) from decay-rate data and $b \simeq \frac{\omega}{c}$ approximation.

caused by effects other than the combustion. Thus they appear to support the concept of an asymmetric reflection.

Imaginary Part of the Response Function

The importance of Im $\left[\frac{\tilde{\mu}}{\tilde{\epsilon}}\right]$ has not been considered. Unless bL very nearly equals π radians, the numerical value of Im $\left[\frac{\tilde{\mu}}{\tilde{\epsilon}}\right]$ is much larger than Re $\left[\frac{\tilde{\mu}}{\tilde{\epsilon}}\right]$. In order to assess its importance we shall estimate the growth constant due to the burning surface by means of the Cantrell equation, i.e.,

$$\alpha_b = \frac{-\frac{1}{2}<\int_S \left\{ - p_1 u_1 + \frac{p_1^2}{\rho_0 c^2} + \rho_0 u_1 (\vec{u}_1 \cdot \vec{u}_0) \right\} dS >}{< \int_V \left\{ \frac{1}{2} \frac{p_1^2}{\rho_0 c^2} + \frac{1}{2} \rho_0 u_1^2 \right\} dV >} \qquad (4.9)$$

Equation (4.9) is obtained directly from Equation (2.22) by neglecting a small term in each integral. If bL is not nearly equal to π radians, then the third term in the surface integral may not be neglected. This term augments the growth constant, whereas, the contribution due to the first two terms in the surface integral is reduced by the relative amplitude squared. The growth constant corresponding to the various approximations for $\underline{b}$ was estimated from this equation, the integrals being evaluated for a frictionless acoustic field for simplicity. The growth constant corresponding to $b \simeq \frac{\omega}{c}$ was found to be about five per cent greater than that for the $b \simeq \frac{\pi}{L}$ case. The growth constant corresponding to the $\underline{b}$ obtained from Method (1) was about thirty-five per cent greater than that for the $b \simeq \frac{\pi}{L}$ case. Thus, as calculated by the several methods, the growth constant due to the burning surface is

not greatly changed even though the response function changes fairly drastically from one method to another.

Related Observations

In an effort to learn more about the behavior of the relative amplitude, this quantity was plotted through the firing for a run from each frequency range. The curves are shown in Figures 20 and 21. These figures clearly show that the relative amplitude was less than unity throughout each firing. However, early in the run the pressure at the burning end of the motor was measured through about 1.2 cm. of propellant and this may be the reason for the low measurement early in the run. These figures also clearly show that in the latter part of the run the measurement is not substantially dependent upon the propellant length. It is interesting to note the drop in relative amplitude at burn-out. This indicates that at the propellant end amplitude decreases in relation to the other end at burn-out. It may be associated with the decay in the flow field or mean-temperature field.

It was also found that the mean pressure was very strongly affected by the oscillatory amplitude. In Figure 22 are plotted the amplitude and mean pressure throughout a firing for a low-frequency range firing. The mean pressure is nearly a mirror image of the amplitude. This is attributed to the heat loss from the gas associated with the oscillatory behavior. The rate of heat transfer at the walls is apparently greatly enhanced by the oscillations. In Appendix K it is shown that the mean temperature is approximately proportional to the mean pressure

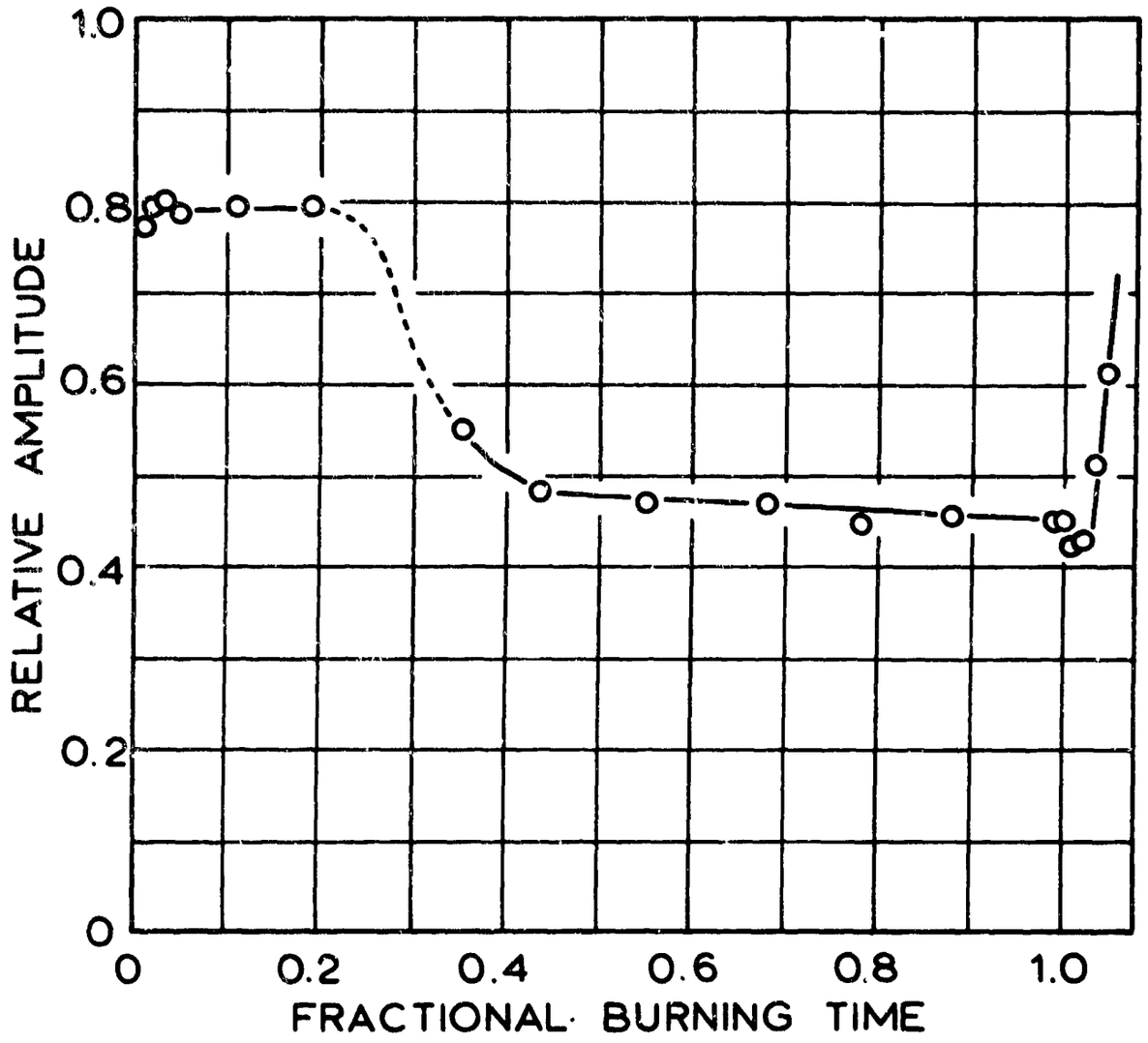

Figure 20. Measured relative amplitude throughout a firing. Burn-out occurs when the fractional time is 1.0. (Run No. 0-226, nominal frequency 3.9 kc).

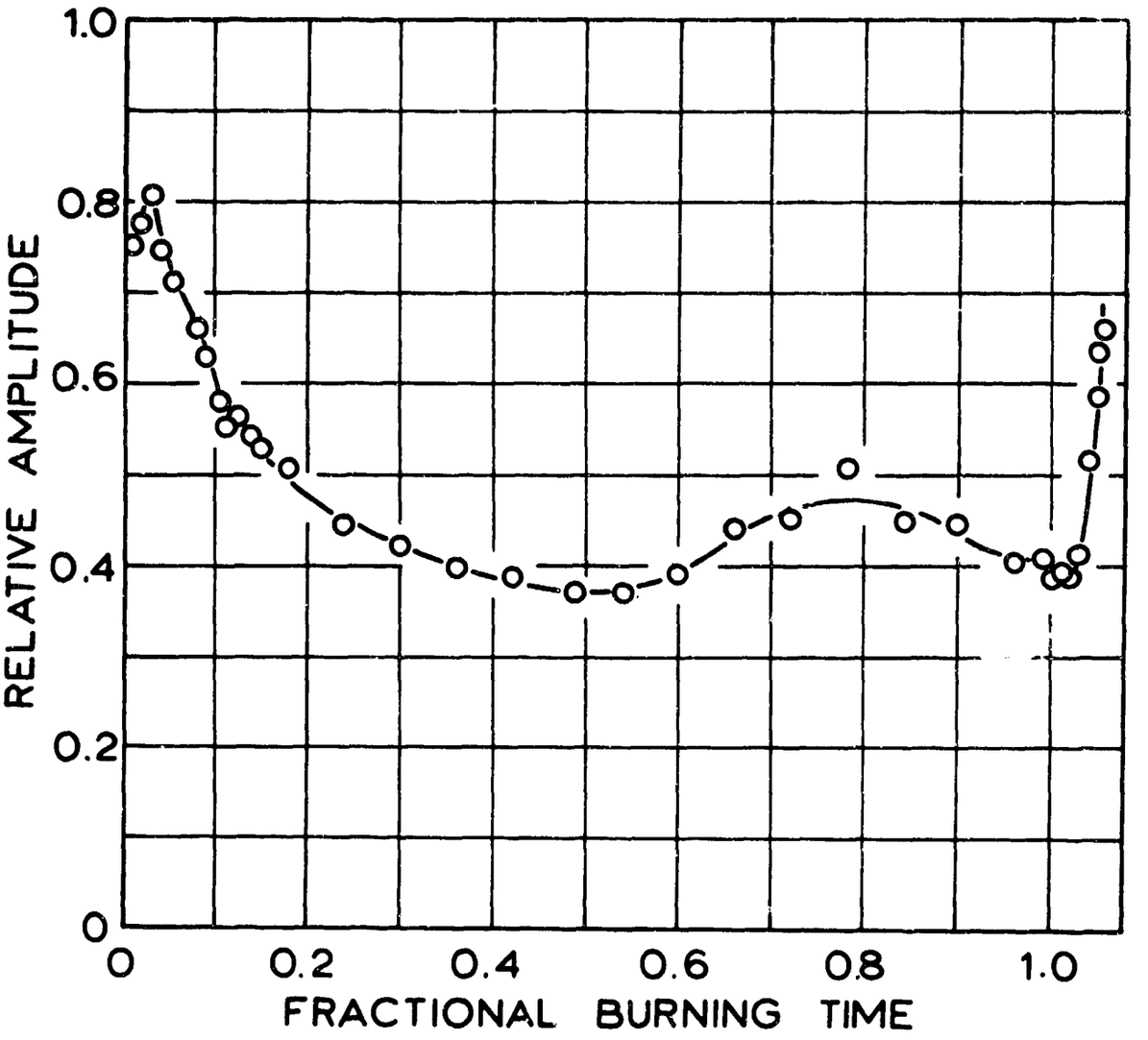

Figure 21. Measured relative amplitude throughout a firing. Burnout occurs when the fractional time is 1.0. (Run No. 0-227, nominal frequency 1.4 kc.).

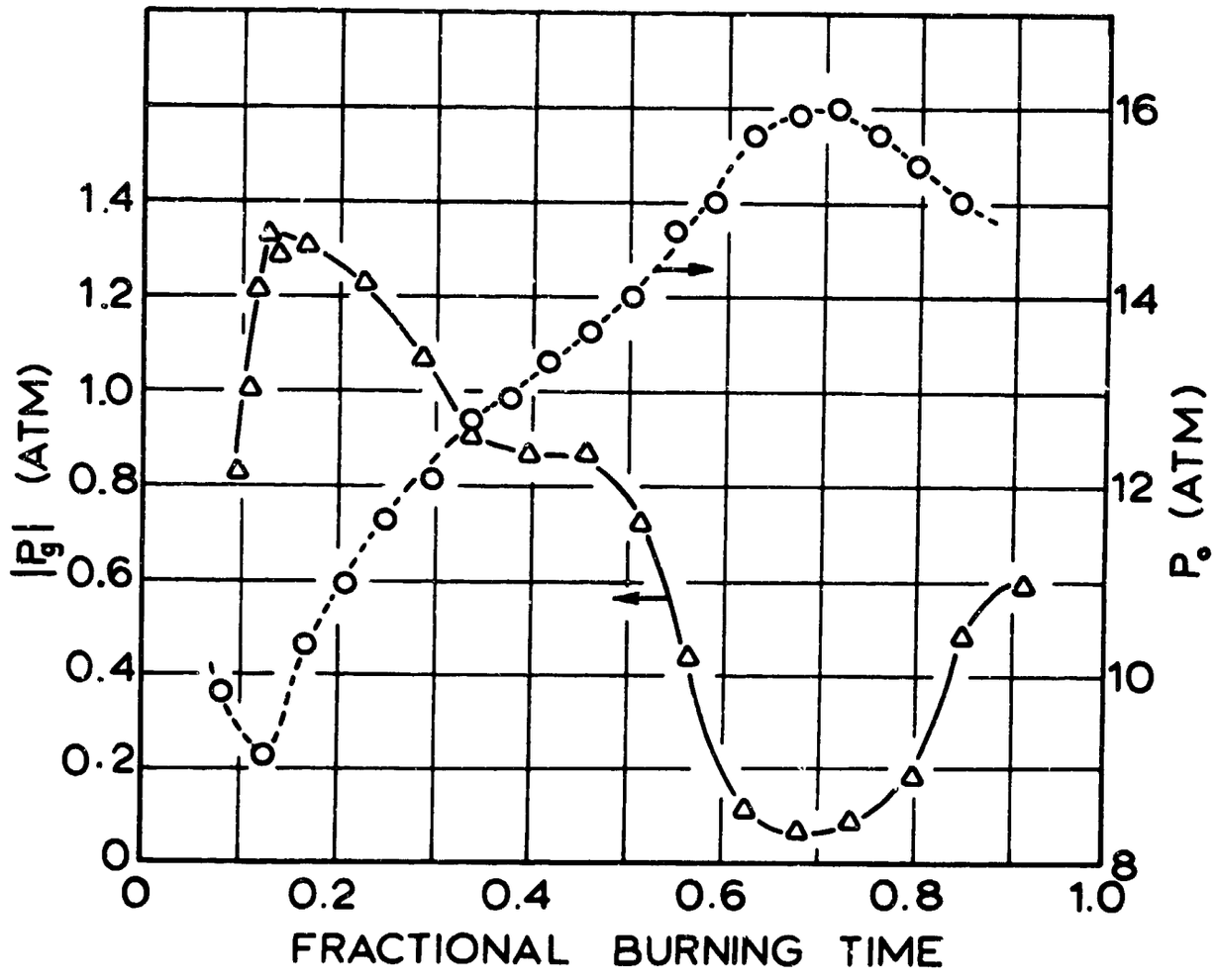

Figure 22. Comparison of the variation of pressure amplitude and mean pressure with burning time. Note the similarity in the two curves. (Run No. 0-227, nominal frequency 1.4 kc.).

if the flow through the nozzle is isentropic and at steady state. Therefore, the mean pressure drops when the rate of heat loss is increased.

The Asymmetric Reflection

It is difficult to suggest a plausible mechanism for the postulated reflection. The mean flow near the nozzle must be complex and, therefore, even an approximate analysis of the wave behavior is difficult. However, the flow does exhibit the asymmetry that apparently is needed. In addition, there may be vortices, or a vortex, generated by the mean flow and these could be significant in terms of a reflection.

There is a related, but small, convection of acoustic energy into the non-burning end of the motor. This is observed from consideration of the energy equation, when perturbed to first order, integrated over the volume, and time averaged (see Equation (B.4)). These considerations show that there are flux terms comparable to the energy flux at the burning surface. However, if attention is focused on either wave, rather than the composite behavior, it is found that there is an energy flux associated with each wave which is much larger than the convective effect, the latter being smaller by a factor of the Mach Number. Therefore, it is not likely to be important.

It should be possible to mathematically construct a mechanical or electrical analog of the acoustic system which would exhibit similar behavior to that observed. The construction of a realistic model is hampered by our poor understanding; however, such considerations could be fruitful. The mechanical system shown in Figure 23 was examined in

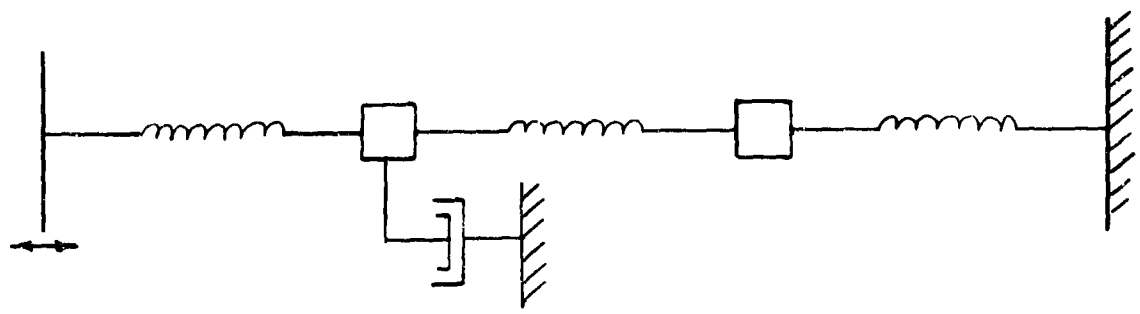

Figure 23. Mechanical analog.

this regard. The left side of the system shown is associated with the flame and the right side with the cold end. The relative amplitude (analog) obtained from an analysis of this system was found to be on the order of .5 for a suitable choice of parameters; however, it was necessary to choose an unduly large damping term in order to achieve this. The analysis indicates that other analogs could be analyzed which would exhibit the desired features and still retain realistic parameters. Such considerations, although tenuous, could lead to a better understanding of the behavior in the motor.

Thus, we find ourselves unable to suggest a satisfactory explanation of the postulated reflection and must, therefore, argue only that it must exist in order to explain our experimental observations.

Conclusions

In conclusion, we find that an asymmetric reflection must exist near the nozzle in order to explain a number of observations. This reflection is such that a portion of a wave traveling toward the

propellant surface is reflected so as to reinforce the wave traveling in the opposite direction. The justification for this conclusion is found primarily in the following observations:

1. The measured relative amplitude is consistently found to be much less than unity. A high level of confidence is placed in this measurement as representative of the ratio of amplitudes existing at the two ends of the gas cavity. The low value is thought to be due to the asymmetric reflection because (1) calculated values for $\mathrm{Re}\left[\frac{\tilde{\mu}}{\tilde{\epsilon}}\right]$ agree with the best available estimate when the reflection is assumed; (2) otherwise the calculated velocity of wave propagation is unduly large and the calculated velocity amplitude at the propellant surface is unduly large.
2. Analysis of possible mean temperature effects shows that these effects are in opposition to the low relative amplitude observed.
3. The low relative amplitude persists through most of the decay transient. This is expected to be possible only if there is an asymmetric reflection.
4. The low relative amplitude observed cannot be due to high attenuation effects because of the low α_D and persistence of the low relative amplitude in the decay transient.
5. Measurements made in the curved wall and near the propellant indicate that the asymmetric reflection occurs but not near the propellant surface.

6. The flow pattern near the nozzle is the only apparent source of the necessary asymmetry. Comparison of the oscillatory envelopes from double- and single-ended firings supports this concept.

CHAPTER V

LOW-FREQUENCY RESPONSE FUNCTION

In this chapter we shall discuss the measurement of the acoustic admittance under conditions where the gas-cavity-burning-surface system is actually stable. The manner in which these measurements were made is a rather simple extension of standard T-burner technique, but the approach has not been previously reported. The work was supported by Stanford Research Institute (SRI).*

SRI supplied two propellant formulations which were being used in their work and requested that the acoustic admittance of these propellants be measured at 35 atm. and in a motor 102 cm. in length.

The initial experimental approach was to measure double- and single-ended growth constants. Toward that goal the T-burner was lengthened to 102 cm. and several firings made. These firings showed that it would be impossible to attain the required mean pressure during the growth transient with a nozzled burner. The burner was, therefore, adapted for surge-tank operation so that the required mean pressure could be obtained by pre-pressurization. When the burner was operated in this manner it was found that the pressure pulse from the igniter excited the fundamental mode of oscillation. However, these oscillations

*Mr. Lionel A. Dickinson of SRI very kindly gave permission for the author to use the information reported here.

decayed out during the burning, the energy supplied by the flame being insufficient to maintain the oscillations. Therefore, the motor was actually a stable system.

The admittance calculation from growth constants does not require that the growth constants be positive. Thus double- and single-ended growth constants, even though they are negative, may still be used. In addition, the fact that the igniter excited the gas cavity made it possible to measure the damping in the motor by firing an igniter in an unloaded motor, i.e., with no propellant sample.

Experimental Work

The surge tank used for this work was too small to prevent a fairly significant rise in mean pressure; however, meaningful results were still obtained. The tank was pre-pressurized to 32 atm. with nitrogen and the subsequent ignition raised the pressure to 35 am. in the period when the negative growth constant was measured. The igniter was made up of F-propellant sawdust and Pyrofuse wire, the latter being electrically ignited. Several firings were made with each of the propellants supplied and with the igniter alone. In Figure 24 are shown pressure traces from a typical firing.

Calculated Results

The data obtained were sufficient to permit estimation of the response function for the propellants. The data are summarized in Table 1 and the calculated values in Table 2. The SRI-111 propellant burned rather fast so that when it was used in a double-ended firing

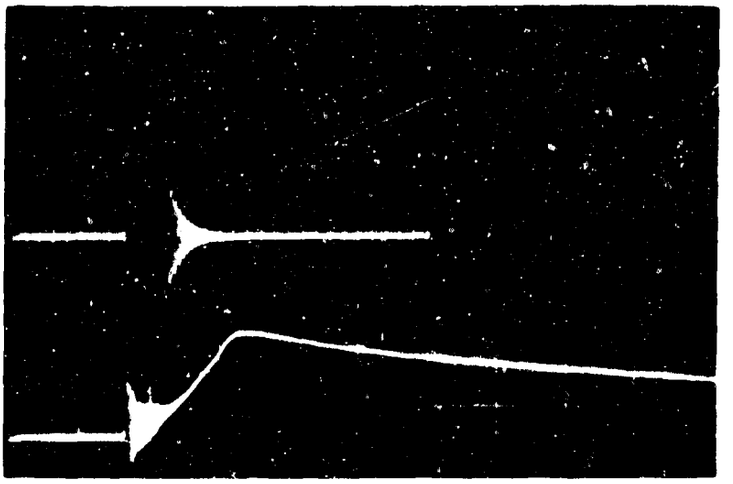

Figure 24. Typical pressure traces from 102-cm. T-burner firing. Top trace, oscillatory pressure followed by reference, .68 atm/cm. Lower trace, total pressure, 6.8 atm/cm., from 34.8 atm. initial level. Sweep rate was .5 sec/cm., from left.

TABLE 1

SUMMARIZED DATA

	Number of Firings	Frequency cps	α_{-1} Sec.
Igniter only	3	180	-19.8 ± 3
109 Propellant			
Single-ended	3	220	-11.8 ± 2.4
Double-ended	3	240	-3.8 ± 6
111 Propellant			
Single-ended	4	205	$-8.4 \pm .8$
Double-ended	1	---	0
F Propellant			
Single-ended	1	240	-8.9

TABLE 2

CALCULATED RESULTS

Propellant	109	111	F
$\alpha_1 - \alpha_{DL}$	8.0 ± 2.7	11.4 ± 1.1	10.9
$\frac{1}{2}(\alpha_2 - \alpha_{DL})$	$8.0 \pm .5$	9.9*	----
$\alpha_2 - \alpha_1$	8.3 ± 3.0	8.4*	----
$\mathrm{Re}\left[\frac{\tilde{\mu}}{\tilde{\epsilon}}\right]$ **	6.5	16	7.5

* $\alpha_2 = 0$ used

** $(\alpha_1 - \alpha_{DL})$ used

the mean pressure rose rapidly. This prevented obtaining a reliable value of the double-ended growth constant for this propellant. One double-ended firing was made and the growth constant measured in the early (and probably nonlinear) portion of the decay, the value being -3.6 sec.$^{-1}$. A better approximation is thought to be zero.

The response function may be calculated from Equations (2.15), (2.31), and the zero-order field approximation. Thus

$$\mathrm{Re}\left[\frac{\tilde{\mu}}{\tilde{\epsilon}}\right] = \frac{p_0}{\rho_s r_0}\left(\frac{\alpha_b}{4Lf^2}\right) \tag{5.1}$$

where

$$\alpha_b = \alpha_2 - \alpha_1 = \frac{1}{2}(\alpha_2 - \alpha_{DL}) = \alpha_1 - \alpha_{DL}$$

the density, ρ_s, was unknown for the SRI propellant and was approximated as 1.65 gm/cm^3.

Significance of Work

This work is particularly significant because it offers a new means of estimating the acoustic properties of relatively stable propellants. One of the greatest disadvantages of the T-burner method has been the inability to study propellants too stable to drive the burner. However, from this work, it appears that stable propellants can be studied by suitably pressure pulsing a T-burner. It is quite likely that suitable pulses could be generated to excite motors much shorter than 100 cm. so that the method could be used at higher frequencies. Horton observed oscillations being generated by his igniter at frequencies less than 600 cps. in a T-burner [29]. The

accuracy of this method is not great because of the necessity to subtract two kinds of growth constants. In this regard $\frac{1}{2}(\alpha_2 + \alpha_{DL})$ gives the highest accuracy. However, the simplicity of the method greatly compensates for the lack of accuracy. One may compare the simplicity of this appraoch to the work of Foner [15]. In order to apply the T-burner to relatively stable propellants, he has found it necessary to construct a very complex electronic and acoustic system. The method we have used at least will permit the ranking of the instability characteristics of various propellants which are too stable to maintain oscillations in a T-burner.

The magnitude of the calculated response function is also of significance. These values are as large or larger than any previously reported.

CHAPTER VI

SOLID-PHASE THEORY

As noted in Chapter I, the solid phase work developed as an extension of the work by Coates [11] and Ryan and Coates [49]. Coates constructed a T-burner in which a long grain of propellant was advanced as it burned so that the burning interface remained at a nearly fixed position. A sketch of the burner is shown in Figure 25. The propellant fit closely into the motor, the curved boundary being lubricated with grease, and was bonded to the face of the piston. Two pressure transducers were used; one measured the pressure at the face of the piston and the second measured the pressure at the non-burning end. Both transducers were located along the axis of the cylinder. Coates found that the solid participated strongly in the oscillatory behavior. At times he found the solid dissipated all of the acoustic energy supplied by the combustion and the oscillations ceased. The cessation apparently was associated with resonance phenomena in the solid. He was, however, encumbered in the analysis of his data by the inability to accurately measure phase angles.

More recently a theoretical description of the solid phase was developed by Ryan and Coates [49]. Coates' data, which had been recorded on magnetic tape, were re-evaluated by the author using the electronic phase meter. A reprint of the publication of this work may be found in Appendix L. These data, in terms of the analysis, suggested

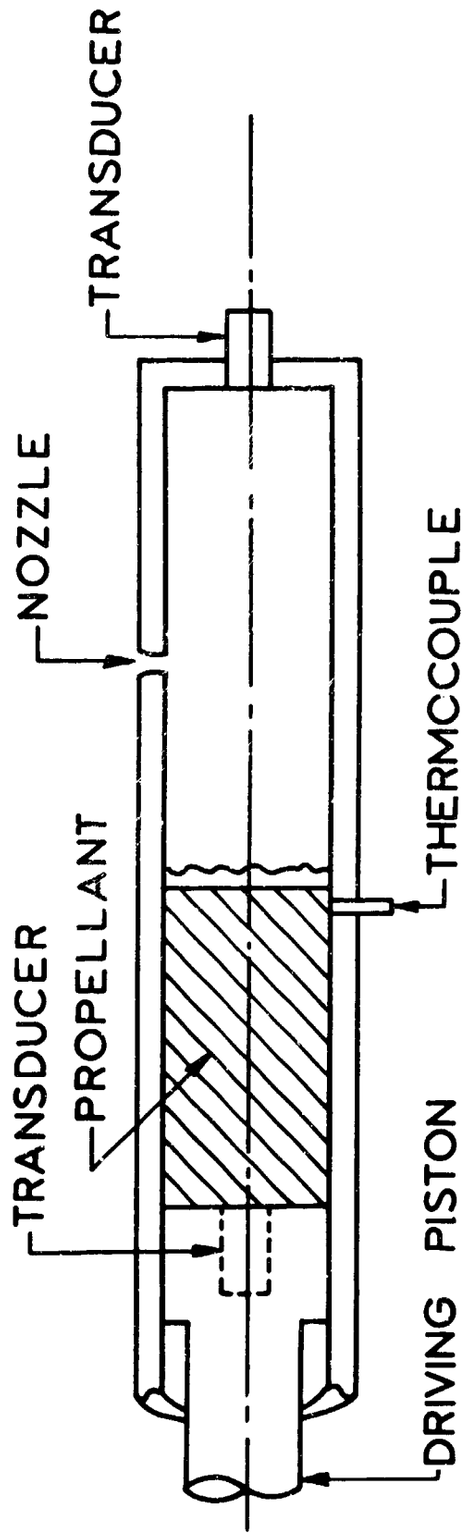

Figure 25. Sketch of T-burner configuration for solid-phase work.

a severe degradation in visco-elastic properties. In order to study this apparent degradation the author made a number of firings using Coates' burner.

The author's experimental data, though similar to Coates' data, led to some apprehension about the validity of the one-dimensional analysis used by Ryan. Therefore, a three-dimensional (cylindrically symmetric) analysis was developed. This analysis showed that the apparent change in properties could equally well be attributed to a change in conditions at the curved boundaries of the solid. The latter possibility is thought to be the more likely case. The low relative amplitude found in the gas-phase work must also be considered.

We shall proceed by developing a three-dimensional analysis of the wave behavior in the solid and then attempt to assess the implications of the experimental data.

Wave Behavior in the Solid

As in the gas-phase work, it will be necessary to infer the wave behavior from dynamic pressure measurements made in the motor. Also the dimensions and density of the propellant will be known. Unfortunately the visco-elastic moduli are not known for this propellant and these will have to be estimated.

In order to develop a theoretical description it will be necessary to make the following assumptions.

1. The propellant may be treated as homogeneous and isotropic. The assumption of homogeneity is justified because the scale of the heterogeneity is on the order of 100 microns. The

composition of the propellant is given in Appendix H.

2. Cylindrical symmetry will be assumed.
3. The frequency will be assumed to be constant.
4. Linear viscoelastic behavior will be assumed, i.e., the viscoelastic constants are only functions of the frequency. The viscoelastic constants will be treated as complex in accord with the usual technique [13,59].
5. The wave behavior is at steady state even though the length is changing slowly.

Under these restrictions the wave equations for the solid are [35]

$$\rho \frac{\partial^2 \xi_x}{\partial t^2} = (\lambda + 2\mu) \frac{\partial \Delta}{\partial r} + 2\mu \frac{\partial \omega_\theta}{\partial x} \tag{6.1}$$

$$\rho \frac{\partial^2 \xi_r}{\partial t^2} = (\lambda + 2\mu) \frac{\partial \Delta}{\partial x} - \frac{2\mu}{r} \frac{\partial (r\omega_\theta)}{\partial r} \tag{6.2}$$

where

$$\Delta = \frac{1}{r} \frac{\partial (r\xi_r)}{\partial r} + \frac{\partial \xi_x}{\partial x} \tag{6.3}$$

$$2\,\omega_\theta = \frac{\partial \xi_r}{\partial x} - \frac{\partial \xi_x}{\partial r} \tag{6.4}$$

The solutions to these equations are given by Love and are known as the Pochammer-Chree solutions [14,35]. Assume solutions of the form

$$\xi_r = U\, e^{j(\gamma x + \omega t)} \tag{6.5}$$

$$\xi_x = W\, e^{j(\gamma x + \omega t)} \tag{6.6}$$

where U and W are functions of r only. The γ used here is again a propagation constant. Through the use of Equations (6.5) and (6.6),

the wave equations may be separated into two equations of the Bessel type for Δ and ω_θ. Equations (6.3) and (6.4) may then be used to obtain

$$U = A \frac{\partial}{\partial r} J_0(hr) + B\gamma J_1 (kr) \tag{6.7}$$

$$W = Aj\gamma J_0 (hr) + \frac{jB}{r} \frac{\partial}{\partial r} [rJ_1 (kr)] \tag{6.8}$$

where

$$h^2 = \frac{\rho\omega^2}{\lambda+2\mu} - \gamma^2 \tag{6.9}$$

$$k^2 = \frac{\rho\omega^2}{\mu} - \gamma^2 \tag{6.10}$$

If γ is replaced by a negative γ, the solutions are the same except that the expression for W is replaced by the negative of that given in Equation (6.8). For this analysis we shall choose the origin at the face of the piston. The piston should be sufficiently rigid so that ξ_x will be zero at that surface. Therefore

$$\xi_x = W e^{j\omega t} \sinh j\gamma x \tag{6.11}$$

$$\xi_r = U e^{j\omega t} \cosh j\gamma x \tag{6.12}$$

The pressure measured at the origin is equal to the negative of the normal stress at this point. Similarly, the normal stress at the burning end of the propellant may be estimated from the pressure measured at the non-burning end of the motor. The normal stress is composed of

$$\tau_{xx} = \lambda\Delta + 2\mu \frac{\partial \xi_x}{\partial x} \tag{6.13}$$

$$\tau_{xr} = \mu \left(\frac{\partial \xi_r}{\partial x} + \frac{\partial \xi_x}{\partial r} \right) \tag{6.14}$$

from which it is found that

$$\tilde{p}_f = \left| \tilde{p}_s \right| e^{j\omega t} \cosh j\gamma \ell \tag{6.15}$$

Equation (6.15) forms the basis of the analysis as it provides the means for calculating γ from the experimental data. Ryan obtained an equivalent expression in his analysis. When his expression was applied to the experimental data, γ was found to vary with time. It was this variation that led Ryan and Coates to the conclusion that the propellant properties were changing.

Theoretically γ is obtained by applying the boundary conditions at the curved wall. The actual stress condition at this boundary is not known. Since the clearance is small ($\simeq$ .01 cm.) and the gap is filled with grease, one might expect a limited radial motion. However, when a radial displacement is estimated from the data and a Poisson's ratio of .5, the magnitude is found to be small compared to the gap. Thus we shall examine three limiting conditions: a free boundary, a freely-supported (no radial motion but free axial motion) boundary, and a fixed boundary.

A free boundary requires the stress to be zero at the wall. The stress components are given by Equation (6.14) and

$$\tau_{rr} = \lambda\Delta + 2\mu \frac{\partial \xi_r}{\partial r} \tag{6.16}$$

The free-boundary requirement leads to

$$\left\{ \left(\frac{\rho\omega^2}{\mu} - 2\gamma^2 \right) J_1(kr) \left[2\mu \frac{\partial^2 J_0(hr)}{\partial r^2} - \frac{\rho\omega^2\lambda}{\lambda+2\mu} J_0(hr) \right] - 2\gamma \frac{\partial J_0(hr)}{\partial r} \left[2\mu\gamma \frac{\partial J_1(kr)}{\partial r} \right] \right\}_{r=r_w} \tag{6.17}$$

Truncated series expressions may be used to approximate the Bessel functions. If r^2 is neglected, then

$$\gamma^2 = \frac{\rho\omega^2}{E} \tag{6.18}$$

where

$$E = \frac{\lambda + \mu}{\mu(3\lambda+2\mu)} \tag{6.19}$$

A freely supported boundary requires that ξ_r and τ_{rx} be n'l at the wall. In this case it is found that

$$\left\{ \frac{\partial J_0(hr)}{\partial r} \right\}_{r=r_w} = 0 \tag{6.20}$$

The lowest root gives

$$\gamma^2 = \frac{\rho\omega^2}{\lambda+2\mu} \tag{6.21}$$

All larger roots correspond to highly damped motions and should not occur. Equation (6.21) is precisely the result found if the wave equations are restricted to one-dimensional behavior.

Finally a fixed boundary requires that ξ_x and ξ_r be nil at the wall. Here it is found that

$$\left\{ \frac{\partial J_0(hr)}{\partial r} \; \frac{1}{r} \frac{\partial}{\partial r} \; [rJ_1(kr)] - J_1(kr) \; J_0(hr) \; \gamma^2 \right\}_{r=r_w} = 0 \qquad (6.22)$$

Again, series expansions may be used to approximate the Bessel functions. If r^2 is neglected, the frequency becomes zero. Therefore, no simple expression is obtained in this case.

Clearly the propagation constant, γ, can vary if the boundary condition changes during a firing. Later the magnitude of such changes will be estimated. In a one-dimensional analysis the propagation constant is only dependent upon the viscoelastic properties. Consequently the analysis requires the properties to change if the propagation constant changes.

Summary of Equations to be Used

The following equations will be important in later discussions:

$$\tilde{p}_f = \left|\tilde{p}_s\right| \; e^{j\omega t} \cosh j\gamma \ell \qquad (6.15)$$

$$\gamma^2 = \frac{\rho\omega^2}{E} \qquad \text{(free boundary)} \qquad (6.18)$$

$$\gamma^2 = \frac{\rho\omega^2}{\lambda+2\mu} \qquad \text{(freely supported boundary)} \qquad (6.21)$$

CHAPTER VII

SOLID-PHASE EXPERIMENTAL APPROACH

The experimental apparatus used in this work was that constructed by Coates. His motor was briefly described in Chapter VI. From that discussion the reader will recall (see Figure 25) that pressure measurements were made at both ends on the motor, i.e., under the propellant and at the cold end. The cold-end measurement is used to infer the pressure at the surface of the propellant. This inferred value and the second pressure measurement may then be used to calculate the propagation constant, γ, from Equation (6.15). The calculation was facilitated by a set of parametric curves which were developed from Equation (6.15). These curves allowed a direct calculation of the real and imaginary parts of γ from the phase angle and amplitude ratio between the two pressures. The curves may be found in Appendix M. Experimentally, therefore, it was necessary to measure the phase angle and amplitude ratio from the pressure data for suitable firings.

The experimental system differed from that used in the gas-phase study only by the inclusion of a system to position the propellant. The latter system was comprised of a hydraulically-driven piston and a driving-rate control. The sensing element for the control was a thermocouple mounted in the wall of the motor adjacent to the burning interface. The control varied the driving rate so as to maintain a fixed thermocouple temperature. The propellant was bonded to the face

of the piston and against the pressure transducer. When assembled, the curved wall of the propellant was coated with grease which provided lubrication, prevented burning along the side, and filled the thin gap between the propellant and the motor. A complete description of the apparatus and procedures may be found in Appendix G.

A number of firings were made in this mode of operation. Many of these did not provide usable data due to poor position control, poor mean pressures, or electronic difficulties. The control system was found to be adequate only for small corrections in the driving rate. It was, therefore, necessary to adjust the average driving rate until it was very close to the burning rate. Poor mean pressure occurred when the grease did not prevent burning along the walls of the motor. Electronic difficulties frequently arose because of the complexity of the system. However, in spite of these problems, usable data were acquired.

CHAPTER VIII

SOLID-PHASE RESULTS AND DISCUSSION

In this chapter the general nature of the experimental data will be discussed. An apparent variation in the propagation constant with burning time, reported by Ryan and Coates [49] and confirmed in this work, will be considered. Although the asymmetric reflection may be responsible, its effects cannot be assessed. In what follows, it will tentatively be assumed that the apparent variation occurs in the solid phase. The importance of the boundary conditions in determining the propagation constant will be examined. Finally it will be concluded that though little can be said with confidence, the apparant variation is more likely due to wall effects (or the asymmetric reflection) than to degradation of the propellant.

Character of the Data Obtained

In Figure 26 are shown the recorded data from two firings. These are typical of the kinds of data obtained. From such photographs the ratio of amplitudes and phase angle were measured throughout the firing. Note the irregularities in the phase-angle traces. These irregularities can frequently be asscciated with changes in amplitude so that it is unlikely that they are caused by distortion of the waveform. Observe also that neither does the amplitude ratio approach one at burn-out nor does the phase angle reach 180 degrees. These last two observations

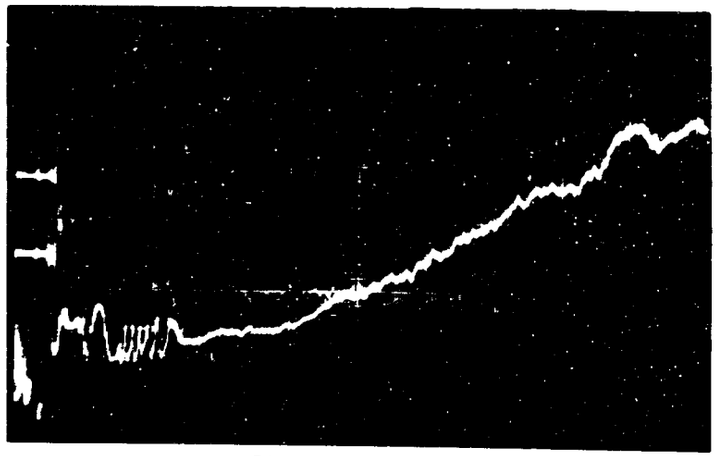

Run No. 184

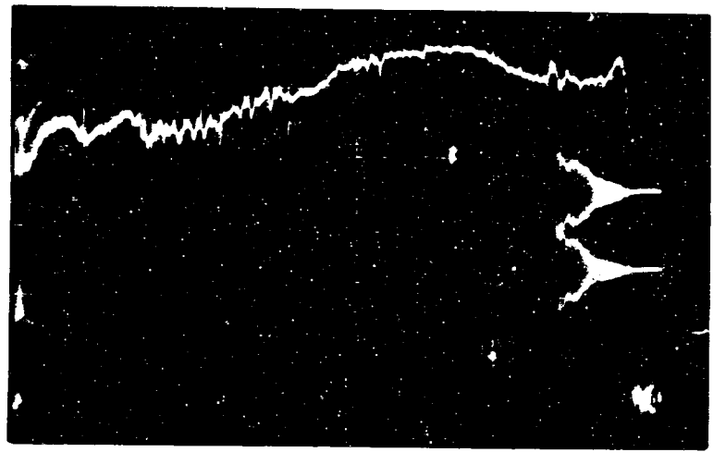

Time 5/8 sec/cm. from left.

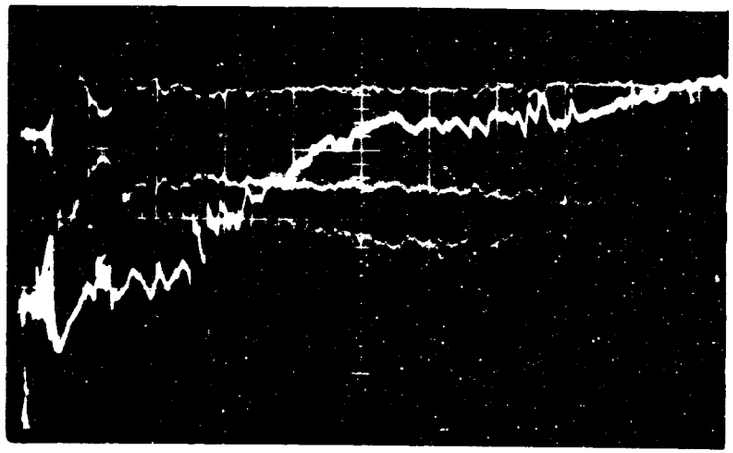

Run No. 0-177

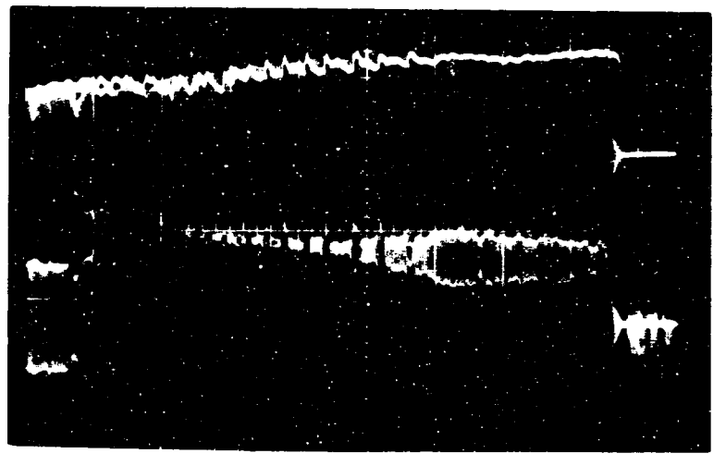

Time 5/8 sec/cm. from left.

Figure 26. Typical data from the solid-phase work. In each case, top and bottom oscillatory envelopes are from the cold and propellant ends, respectively. The third trace is the phase angle between signals reading upward at 30°/cm.

were frequently made and they motivated the gas-phase work described earlier.

The failure of the phase angle to approach 180 degrees is probably due to the instrumentation. Unfortunately no reference signal was recorded during this work. Instead the phase shift due to the instrumentation was measured and found to be less than five degrees for frequencies less than four kilocycles. An error this great at that time was considered acceptable. An examination of Figure 26 shows that the final phase angles are much less than 175 degrees. Phase angles on the order of 179 degrees were measured in the gas-phase work so that this phase angle should at least approach 175 degrees. We offer no explanation for the difference but recognize that it must be considered as a possible error.

It may also be observed in Figure 26 that the relative amplitudes at burn-out (about .65) are not as low as the .45 observed in the gas-phase work. The instrumentation was adjusted so that each signal would be amplified the same amount. Therefore, the instrumentation is not expected to have caused the entire discrepancy. It appears, then, that we must correct the ratio of amplitudes to be used in the calculations, but the amount of correction is uncertain.

We may observe that perhaps we should not expect the relative amplitude to reach .45 at burn-out. It is not unlikely that the amount of asymmetric reflection, which undoubtedly occurs, may vary during an extended firing. Conceivably the observed difference in relative amplitudes is an indication of such a variation. Thus, not only is the

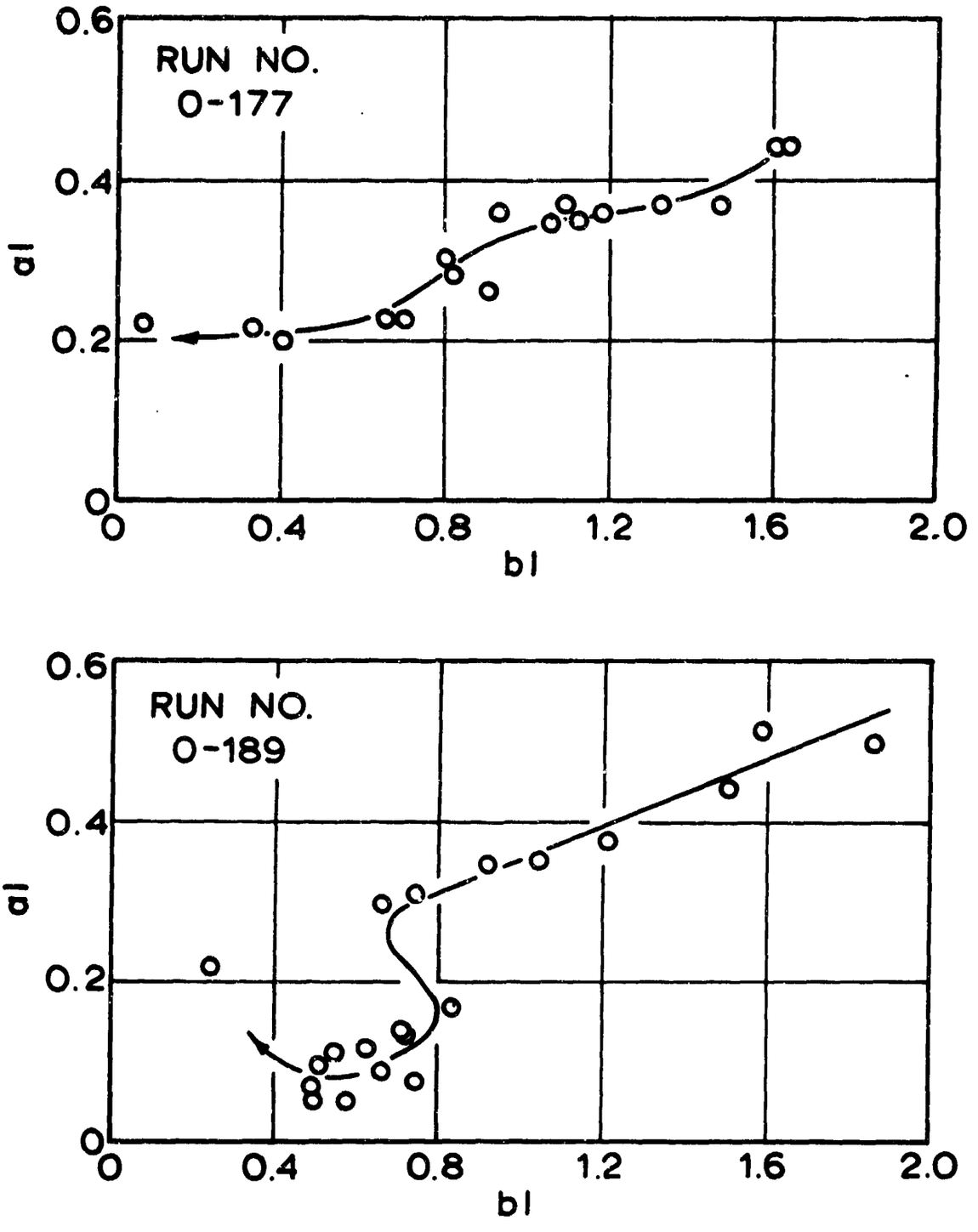

Figure 27. Calculated values of al and bl for two firings.

amplitude correction uncertain, but also the application of a constant correction is questionable.

The cessation of oscillations, which Coates [11] observed, never occurred in this work.

Calculated Propagation Constant

The propagation constant was calculated from the data by three methods, namely,

1. by neglecting the difference in amplitude at the two ends of the gas phase and assuming a phase shift in the gas of 180 degrees,
2. by assuming the relative amplitude in the gas phase to be .45 and the phase shift to be 180 degrees,
3. by assuming corrections for the amplitude and phase angle such that the amplitude ratio approached unity and the phase angle approached 180 degrees at burn-out.

The calculated propagation constant for each of these methods varied with the propellant length, the last method showing least variation. On Figure 27 are plotted the calculated values of $\underline{a}l$ and $\underline{b}l$ as calculated by Method (3) above. These are typical of the kinds of results obtained. The data and calculated values for a number of firings may be found in Appendix M. If the propagation constant were independent of length, the points would fall near a straight line through the origin. Clearly these calculated points are not well described by a non-length dependent propagation constant. Here we must recognize the possibility of an apparent variation arising from changes in the

ratio of amplitudes between the two ends of the gas column, i.e., changes in the amount of asymmetric reflection. In the gas-phase work the reflection was found to develop within .3 second from ignition; therefore, in these firings it is expected to have occurred essentially throughout. However, the separation of these gas-phase effects from the solid-phase effects is impossible without a better understanding of the asymmetric reflection. Therefore, lacking anything better, we shall tentatively assume that the propagation constant for the propellant is changing and attempt to learn what we can from the data obtained.

Importance of Boundary Conditions

In the theoretical discussion of the solid phase it was shown that the propagation constant is determined (1) by the viscoelastic properties and (2) by the conditions at the curved boundaries. In the analysis of Ryan and Coates [49] the second possibility was eliminated by the use of a one-dimensional analysis. They were, therefore, led to the conclusion that the properties must change. However, we shall shortly demonstrate that changes in the boundary condition are of great importance.

It may be noted that if Ryan and Coates [49] had used Method (3) rather than Method (1) in their calculations, they would have found the variation in the propagation constant to be significantly reduced.

The fact that the solid boundary condition may strongly affect the acoustic behavior has been noted by Angelus (1), Horton (26), and Coates (11) among others. Horton ran viscoelastic tests by reflecting

a weak shock wave from the end of a cylindrical grain of propellant. He found that the propellant behavior was strongly affected by the boundary conditions. In a similar experiment, Coates found that his propellant would not oscillate and attributed this to wall losses.

From Horton's data we may estimate the effect of changing the wall condition from a free to a fixed boundary. We estimate $\underline{b}$ for the free boundary to be about three times that for a fixed boundary. Horton reports an attenuation term only for the fixed-boundary case so that the difference in $\underline{a}$ may not be estimated. For the fixed boundary $a/b = .2$ is estimated.

If the viscoelastic constants were known for Utah F propellant, Equations (6.18) and (6.21) could be used to estimate the magnitude of possible wall effects. We shall, therefore, estimate these values. The value of μ will be estimated from shear data [46] for a propellant similar to Utah F. The value of λ will be estimated from compressibility data for a propellant somewhat less similar to Utah F. The compressibility at zero frequency will be used since we have found no other data in the literature; but in the frequency range of interest the compressibility should differ by no more than a factor of two [14,53,54]. By means of this approach, we estimate that

$$\mu = 2\ (1+j)(10^9) \quad \text{dyne/cm}^2 \qquad (8.1)$$

$$\lambda = 10\ (10^{10}) \quad \text{dyne/cm}^2 \qquad (8.2)$$

For comparison, we estimate from Horton's data that $\mu = 5\ (10^9)$ dyne/cm^2 for his propellant, Equation (6.18) and $\mu \ll \lambda$ being used. By means of Equations (6.18) and (6.21) it is found that

$$\gamma = .8 - j.3 \qquad \text{free boundary} \qquad (8.3)$$

$$\gamma = .09 - j.0009 \qquad \text{freely supported boundary} \qquad (8.4)$$

From these considerations it is clear that wall effects can be large enough to account for the observed changes in the propagation constant.

It seems likely that the thin grease film at the wall of the propellant could give rise to additional wall effects in the form of viscous losses. In this case the shear stress at the wall should be proportional to the rate of strain at the wall. An examination of the theory (Equations (6.11), (6.12), and (6.14)) shows that in this case the wall stress varies with x. Therefore, although the solutions of Chapter VI are invalid for this case, it appears that such wall effects could give rise to an apparently variable propagation constant.

Indications of Wall Effects

It appears that there is no way to separate the effects of the boundaries and the effects of the viscoelastic properties; however, there are a few experimental observations which seem to favor the former.

1. The data show some rapid fluctuations in phase and amplitude which are probably due to fluctuations in the boundary conditions.
2. The calculated values of $\underline{a}$ are larger than expected from those estimated for the various boundary conditions. This may well be an indication of strong viscous losses at the

wall. On the other hand, one successful firing with an increased clearance at the wall did not produce lower a values (Run 0-189, also see Figure 27.)

3. The calculated propagation constant frequently changes in the direction to indicate increased strength rather than weakening of the propellant. An example of this is shown in Figure 27 (the lower curve), where the curve drops substantially and indicates reduced values of a. Such changes are too large to be due to burning away of weaker material.

On the basis of this discussion it appears more likely that the apparent variation in the propagation constant, if it occurs in the solid phase, is due to wall effects.

Conclusions

In conclusion, we find that little can be said with confidence about the solid-phase behavior. It will be necessary to develop an understanding of the asymmetric reflection in order to gain much information from experiments similar to those described. Given this understanding, it will be necessary to separate wall effects from changes in properties; perhaps this could be achieved by independently evaluating the likelihood of changes in properties.

CHAPTER IX

SUMMARY OF CONCLUSIONS

During the gas-phase work, data were obtained which rather conclusively show the acoustic behavior in a single-ended T-burner to be greatly different from any previous description of the behavior. Most significantly, the acoustic-pressure amplitude was found to be lower at the burning end of the motor by a factor of .45 than the amplitude at the opposite end. High confidence is placed in this observation. Consideration of various observations has led to the conclusion that an asymmetric reflection is occurring in the vicinity of the nozzle, the reflection being such that a considerable portion of a wave traveling toward the propellant is reflected so as to reinforce the wave traveling in the opposite direction. There appears to be no other way of explaining the data. It is significant that the observed behavior appears to be associated with the acoustics of the cavity rather than the character of the burning surface.

In the low-frequency T-burner work, a method was devised to estimate the response function for a burning propellant when the system is actually stable, i.e., the growth constant is negative. The method made use of the pressure pulse from the igniter to excite oscillations in the cavity. It appears likely that the approach could be extended to much higher frequencies in order to study propellants under stable conditions.

The data from the solid-phase study proved to be intractable. It was found that changes were occurring in either the propellant properties, the boundary conditions at the wall of the propellant, or in the amount of asymmetric reflection. It was, however, impossible to determine which of these was actually changing.

LIST OF REFERENCES

1. Angelus, T. A., "Unstable Burning Phenomena in Double-Base Propellants," ARS Progress in Astronautics and Rocketry: Solid Propellant Rocket Research, edited by M. Summerfield (Academic Press, New York, 1960), Vol. I, pp. 527-559.

2. Berl, W. G., "Instability in Solid Rockets," Astronautics and Aeronautics 3, 54-62 (Feb. 1965). [Contains complete list of references for McClure-Hart-Bird Theory.]

3. Bird, R. B., Stewart, W. E., and Lightfoot, E. N., Transport Phenomena (John Wiley and Sons, Inc., New York, 1960), pp. 74-80. 313.

4. Calcote, H. F., "Acoustic Wave Burning Zone Interaction in Solid Propellants," Proceedings of the Third Meeting; Technical Panel on Solid Propellant Combustion Instability, Applied Physics Laboratory Report No. TG 371-5 (May 1963), pp. 59-62.

5. Cantrell, R. H., Hart, R. W., and McClure, F. T., "Linear Acoustic Gains and Losses in Solid Propellant Rocket Motors," AIAA J. 2, 1100-1106 (1964).

6. Cantrell, R. H., McClure, F. T., and Hart, R. W., "On Acoustical Damping in Cavities with Mean Velocity and Thermal Boundary Layers," J. Acoust. Soc. Am. 35, 500-509 (1963).

7. Cantrell, R. H., and Hart, R. W., "Interaction Between Sound and Flow in Acoustic Cavities: Mass, Momentum, and Energy Considerations," J. Acoust. Soc. Am. 36, 697-706 (1964).

8. Cheng, S. I., "High Frequency Combustion Instability in Solid Propellant Rockets," Jet Propulsion 24, 27-32 and 102-109 (1954).

9. Cheng, S. I., "Unstable Combustion in Solid Propellant Rocket Motors," Eighth Symposium (International) on Combustion (Williams and Wilkins Co., Baltimore, Md., 1962), p. 81.

10. Coates, R. L., Horton, M. D., and Ryan, N. W., "T-Burner Method of Determining the Acoustic Admittance of Burning Propellants," AIAA J. 2, 1119-1122 (1964).

11. Coates, R. L., "A Quantitative Experimental Study of the Oscillatory Combustion of Solid Rocket Propellants," unpublished Ph.D. Thesis, University of Utah, Dept. of Chemical Engineering (Salt Lake City, August, 1962).

12. Dobbins, R. A., and Temkin, S., "Measurements of Particulate Acoustic Attenuation," AIAA J. 2, 1106-1111 (1964).

13. Ferry, J. D., Viscoelastic Properties of Polymers (John Wiley and Sons, Inc., New York, 1961), pp. 11-14.

14. Ferry, J. D., Viscoelastic Properties of Polymers (John Wiley and Sons, Inc., New York, 1961), pp. 415-416.

15. Foner, S. N., Hudson, R. L., and Nall, B. H., "Admittance Measurements of Solid Propellants by an Acoustic Oscillator Technique," AIAA J. 2, 1123-1129 (1964).

16. Freudenthal, A. M., and Henry, L. A., "On 'Poisson's Ratio' in Linear Viscoelastic Propellants," ARS Progress in Astronautics and Rocketry: Solid Propellant Rocket Research, edited by M. Summerfield (Academic Press, New York, 1960), Vol. I, pp. 33-66.

17. Geckler, R. D., Selected Combustion Problems, Advisory Group for Aeronautical Research and Development, North Atlantic Treaty Organization (Butterworths Scientific Publications, London, 1954), pp. 289-339.

18. Gordon, C. G., and Smith, P. W., "Acoustic Losses in a Resonator with Steady Gas Flow," Bolt, Beranek, and Newman, Inc. Report No. 1142, Cambridge, Massachusetts (June 1964).

19. Grad, H., "Resonance Burning in Rocket Motors," Communs. Pure and Appl. Math. 2, 79-102 (1949).

20. Green, L. and Nachbar, W., "Analysis of a Simplified Model of Solid Propellant Resonant Burning," J. Aero/Space Sciences 28, 518-529 (1959).

21. Hart, R. W., and McClure, F. T., "Theory of Acoustic Instability in Solid Rocket Combustion," Tenth Symposium (International) on Combustion (to be published).

22. Hart, R. W., "Panel Discussion: Solid Propellant Combustion Instability," Eighth Symposium (International) on Combustion (Williams and Wilkins Co., Baltimore, 1962), pp. 900-918.

23. Hart, R. W., and Bird, J. F., "Scaling Problems Associated with Unstable Burning in Solid Propellant Rockets," Ninth Symposium (International) on Combustion (Academic Press, New York, 1963), p. 993.

24. Hart, R. W., and McClure, F. T., "Combustion Instability: Acoustic Interaction with a Burning Propellant Surface," J. Chem. Phys. 30, 1501 (1951).

25. Hart, R. W., and Cantrell, R. H., "Acoustic Radiation from Pressure-Antisymmetric Modes of a Centrally Vented Cylindrical Cavity," J. Acoustic Soc. Am. 35, 18-24 (1963).

26. Horton, M. D., "Oscillatory Burning of Solid Rocket Propellants," unpublished Ph.D. Thesis, University of Utah, Dept. of Chemical Engineering (Salt Lake City, June 1961).

27. Horton, M. D., "Use of the One-Dimensional T-Burner to Study Oscillatory Combustion," AIAA J. 2, 1112-1118 (1964).

28. Horton, M. D., and Price, E. W., "Dynamic Characteristics of Solid Propellant Combustion," Ninth Symposium (International) on Combustion (Academic Press, New York, 1963), p. 303.

29. Horton, M. D., "Testing the Dynamic Stability of Solid Propellants: Techniques and Data," U. S. Naval Ordnance Test Station Report NOTS TP 3610, NAVWEPS REPORT 8596 (August 1964).

30. Huggett, C., Bartley, C. E., and Mills, M. M., Solid Propellant Rockets, Princeton Aeronautical Paperbacks, Edited by C. Donaldson (Princeton University Press, Princeton, N. J., 1960), pp. 41-43 and 122-123.

31. Interagency Chemical Rocket Propulsion Group, Proceedings of the First Meeting, Combustion Instability Conference, CPIA Publication No. 68 (January, 1965).

32. Lawhead, R. B., and Carlson, L. W., "Physical Processes of Solid Propellant Combustion," Proceedings of the Third Meeting, Technical Panel on Solid Propellant Combustion Instability, Applied Physics Laboratory Report No. TG 371-5 (May, 1963), pp. 43-46.

33. Leader, G. R., "Experiments for the Measurement of the Acoustic Impedance of a Burning Solid Propellant," Proceedings of the Third Meeting, Technical Panel on Solid Propellant Combustion Instability, Applied Physics Laboratory Report No. TG 371-5 (May, 1963), pp. 51-56.

34. Leader, G. R., "Experiments for the Measurement of the Acoustic Impedance of a Burning Solid Propellant," Thiokol Chemical Corp., final report on contract no. Nonr 3473(00) under Office of Naval Research (June 1963).

35. Love, A. H. E., Mathematical Theory of Elasticity (Dover Publications, New York, 1944), 4th ed., p. 288.

36. McClure, F. T., Hart, R. W., and Bird, J. F., "Solid Propellant Rocket Motors as Acoustic Oscillators," ARS Progress in Astronautics and Rocketry: Solid Propellant Rocket Research, edited by M. Summerfield (Academic Press, New York, 1960), Vol. I, pp. 295-358.

37. McClure, F. T., "Panel Discussion: Solid Propellant Combustion Instability," Eighth Symposium (International) on Combustion (Williams and Wilkins Co., Baltimore, 1962), pp. 930-931.

38. McClure, F. T., Hart, R. W., and Bird, J. F., "Acoustic Resonance in Solid Propellant Rockets," J. Appl. Phys. 31, 884-896 (1960).

39. McClure, F. T., Hart, R. W., and Cantrell, R. H., "Interaction between Sound and Flow-Stability of T-Burners," AIAA J. 1, 586 (1963).

40. Muller, G. M., "Acoustic Admittance Measurements: Reflected-Pulse Method," Proceedings of the Third Meeting, Technical Panel on Solid Propellant Combustion Instability, Applied Physics Laboratory Report No. TG 371-5 (May 1963), pp. 47-50.

41. Muller, G. M., "The Study of the Origin and Propagation of Disturbances in the Burning of Solid Propellants, Phase I: The Measurement of Acoustic Admittance," Stanford Research Institute, final report, Contract No. AF 49 (638)-565 (May 1964).

42. Nall, B. H., "Acoustic Attenuation in a Solid Propellant," AIAA J. 1, 76 (1963).

43. Price, E. W., "Review of Experimental Research on Combustion Instability of Solid Propellants," ARS Progress in Astronautics and Rocketry: Solid Propellant Rocket Research, edited by M. Summerfield (Academic Press, New York, 1960), Vol. I, pp. 561-602.

44. Price, E. W., "Experimental Solid Rocket Combustion Instability," Tenth Symposium (International) on Combustion (to be published).

45. Rayleigh, J. W. S., The Theory of Sound (Dover Publications, New York, 1945), Vol. II, pp. 319-236.

46. Robinson, C. N., "Measurement of the Complex Dynamic Shear Compliance of Composite Solid Propellants," Proceedings of the Third Meeting, Technical Panel on Solid Propellant Combustion Instability, Applied Physics Laboratory Report No. TG 371-5 (May 1963), pp. 127-140.

47. Ryan, N. W., Coates, R. L., and Baer, A. D., "Participation of the Solid Phase in the Oscillatory Burning of Solid Rocket Propellants," Ninth Symposium (International) on Combustion (Academic Press, New York, 1963), p. 993.

48. Ryan, N. W., personal communication (University of Utah, Salt Lake City, Utah, April 1964).

49. Ryan, N. W., and Coates, R. L., "Acoustic Instability: Influence of and on the Solid Phase," AIAA J. 2, 1130-1134 (1964).

50. Shinnar, R., and Dishon, M., "Heat Transfer Stability Analysis of Solid Propellant Rocket Motors," ARS Progress in Astronautics and Rocketry: Solid Propellant Rocket Research, edited by M. Summerfield (Academic Press, New York, 1960), Vol. I, pp. 359-373.

51. Smith, A. G., "A Theory of Oscillatory Burning of Solid Propellants Assuming a Constant Surface Temperature," ARS Progress in Astronautics and Rocketry: Solid Propellant Rocket Research, edited by M. Summerfield (Academic Press, New York, 1960), Vol. I, pp. 375-391.

52. Smith, R. P., and Sprenger, D. F., "Combustion Instability in Solid-Propellant Rockets," Fourth Symposium (International) on Combustion (Williams and Wilkins, Baltimore, 1953), pp. 893-906.

53. Smith, T. L., Smith, J. R., and Hiam, L. E., "Viscoelastic Properties of Solid Propellants and Propellant Binders," Stanford Research Institute, Report No. 7, Contract No. Now 61-1057-d (April 1963).

54. Smith, T. L., "Response of Propellants to Different Types of Mechanical Excitation," Proceedings of the Third Meeting, Technical Panel on Solid Propellant Combustion Instability, Applied Physics Laboratory Report No. TG 371-5 (May 1963), pp. 121-126.

55. Strittmater, R., Watermeir, L., and Pfaff, S., "Virtual Specific Acoustic Admittance Measurements of Burning Solid Propellant Surfaces by a Resonant Tube Technique," Ninth Symposium (International) on Combustion (Academic Press, New York, 1963), p. 311.

56. Summerfield, M., et al., "Burning Mechanism of Ammonium Perchlorate Propellants," ARS Progress in Astronautics and Rocketry: Solid Propellant Rocket Research, edited by M. Summerfield (Academic Press, New York, 1960), Vol. I, pp. 141-182.

57. Technical Panel on Solid Propellant Combustion Instability: Proceedings of the Third Meeting, Applied Physics Laboratory Report No. TG 371-5 (May 1963).

58. Technical Panel on Solid Propellant Combustion Instability: Proceedings of the Fourth Meeting, Applied Physics Laboratory Report No. TG 371-5 (April 1964).

59. Tobolsky, A. V., Properties and Structure of Polymers (John Wiley, New York, 1960), pp. 99-117.

60. Williams, M. L., "Mechanical Properties and the Design of Solid Propellant Motors," ARS Progress in Astronautics and Rocketry: Solid Propellant Rocket Research, edited by M. Summerfield (Academic Press, New York, 1960), Vol. I, pp. 67-120.

61. Wylie, C. R., Advanced Engineering Mathematics (McGraw-Hill Book Co., New York, 1960), 2nd ed., p. 502.

APPENDIX A

ANALYTICAL EXPRESSIONS FOR THE PERTURBED PRESSURE AND VELOCITY IN A T-BURNER

Analytical expressions are desired for the oscillating pressure and velocity which may be used to infer the acoustic behavior at the burning surface from measurements made elsewhere in the motor. Rayleigh [45] gives an analysis of wave motion in a cylinder, for which he credits Kirchhoff. His treatment includes viscous and thermal effects for a cylindrically-symmetric cavity with no mean flow and assumes thermal equilibrium between the gas and the walls. His analysis will be applied to a T-burner with special consideration given to approximations necessary to obtain the final results.

It will be assumed that

1. the disturbing effect of the nozzle may be neglected,
2. the main body of the gas is approximated by a homogeneous and non-reactive ideal gas,
3. the effect of the steep temperature gradient at the walls may be accounted for in the parameters of the final solution,
4. the effect of turbulence is only to modify the effective viscosity and thermal conductivity,
5. the amplitude is sufficiently small to permit a linear perturbation analysis (see Appendix C for the limitations

of a linear analysis),

6. and, in accord with Rayleigh [45], the dissipation function will be neglected.

The effect of mean flow will be neglected initially and then approximated as a uniform flow (i.e., uniform throughout a cross section) in order to examine its effect.

Consequently, solutions are required for the following equations:

motion--x direction

$$\rho_0 \frac{D\tilde{u}}{Dt} + \frac{\partial \tilde{p}}{\partial x} = \mu \nabla^2 \tilde{u} + \frac{1}{3} \mu \frac{\partial}{\partial x} \nabla \cdot \vec{\tilde{u}} \qquad (A.1)$$

continuity

$$\frac{D\tilde{\rho}}{Dt} = - \rho_0 \nabla \cdot \vec{\tilde{u}} \qquad (A.2)$$

energy

$$\rho_0 C_v \frac{D\tilde{T}}{Dt} = k \nabla^2 \tilde{T} - p_0 \nabla \cdot \vec{\tilde{u}} \qquad (A.3)$$

Since the mean flow is being neglected, the substantial derivative is replaced by the partial derivative with respect to time. For convenience, define the following quantities:

$$\frac{\rho}{\rho_0} = s \qquad \left(\frac{\rho_0 C_v}{p_0}\right) T = \theta \qquad \frac{k}{\rho_0 C_v} = \upsilon \qquad (A.4a,b,c)$$

Assume an exponential time dependence, i.e., e^{ht} where h is a constant. Thus, Equations (4.2) and (A.3) may be rewritten as

$$hs = -\nabla \cdot \vec{\tilde{u}} \qquad (A.5)$$

$$h\theta = \upsilon \nabla^2 \theta + \nabla \cdot \vec{\tilde{u}} \qquad (A.6)$$

Now, with the aid of Equation (A.6) and the ideal gas law in perturbation form, Equation (A.1) becomes

$$h\tilde{u} - \mu'\nabla^2 \tilde{u} = \frac{\partial P}{\partial x} \tag{A.7}$$

where

$$P = \frac{p_0}{\rho_0}\left(s + \frac{R}{C_v}\theta\right) + \mu'' hs \tag{A.8}$$

Since the solution to these equations is lengthy and since the reader, with some persistence, may obtain the development from Rayleigh [45], it will only be very briefly outlined in this treatment.

Equations (A.5), (A.6), and (A.7) are combined to form a single equation in θ. The method of combination is not obvious. Roughly, the divergence of the vector equation, of which Equation (A.7) is the x component, is formed and Equations (A.5) and (A.6) are used to replace the divergence of velocity and s. The resulting equation is fourth order in θ. The solution to this equation is obtained by assuming, as a trial solution, the function Q' which satisfies the equation

$$\nabla^2 Q' = \lambda Q' \tag{A.9}$$

A characteristic equation is obtained, it being

$$\frac{\upsilon}{h}\left[\frac{p_0}{\rho_0} + h(\mu'+\mu'')\right]\lambda^2 - \left[\frac{\gamma_T p_0}{\rho_0} + h(\mu'+\mu''+\upsilon)\right]\lambda + h^2 = 0 \tag{A.10}$$

If λ_1 and λ_2 are taken as the roots of Equation (A.10), then

$$\theta = A_1 Q_1 + A_2 Q_2 \tag{A.11}$$

where Q_1 and Q_2 are the solutions to Equation (A.9) which correspond to λ_1 and λ_2, respectively. The constants A_1 and A_2 are to be determined by the boundary conditions. Equation (A.10) will be of interest later.

The reader is referred to Rayleigh for the remainder of the solution. Upon assuming an exponential dependence on x, i.e., $e^{j\gamma x}$, he obtains the following solutions:

$$\tilde{u} = AQ + \left(\frac{\upsilon\lambda_1 - h}{\lambda_1}\right) A_1 \frac{\partial Q_1}{\partial x} + \left(\frac{\upsilon\lambda_2 - h}{\lambda_2}\right) A_2 \frac{\partial Q_2}{\partial x} \tag{A.12}$$

$$\tilde{v} = \frac{-j\gamma A}{\frac{h}{\mu'} + \gamma^2} \frac{\partial Q}{\partial r} + A_1 \left(\frac{\upsilon\lambda_1 - h}{\lambda_1}\right) \frac{\partial Q_1}{\partial r} + A_2 \left(\frac{\upsilon\lambda_2 - h}{\lambda_2}\right) \frac{\partial Q_2}{\partial r} \tag{A.13}$$

$$\tilde{p} = p_0 \left(s + \frac{R}{C_v} \theta\right) \tag{A.14}$$

$$s = \theta - \frac{\upsilon}{h}^2 \theta \tag{A.15}$$

where

$$Q = J_0(k_0 r)\, e^{j\omega t} \sinh j\gamma x \tag{A.16}$$

$$Q_1 = J_0(k_1 r)\, e^{j\omega t} \cosh j\gamma x \tag{A.17}$$

$$Q_2 = J_0(k_2 r)\, e^{j\omega t} \cosh j\gamma x \tag{A.18}$$

$$k_0^2 = -\left(\frac{j\omega}{\mu'} + \gamma^2\right) \tag{A.19}$$

$$k_1^2 = -\left(\lambda_1 + \gamma^2\right) \tag{A.20}$$

$$k_2^2 = -\left(\lambda_2 + \gamma^2\right) \tag{A.21}$$

In order to obtain Equations (A.16), (A.17), and (A.18), an axial dependence of $e^{-j\gamma x}$ was incorporated, $\tilde{u}$ was set equal to zero at the origin, and a harmonic time dependence was assumed.

Consider now the roots of the characteristic equation, Equation (A.1C . If a harmonic time dependence is assumed, i.e., h=jω, the roots are given explicitly by

$$\lambda = \frac{-B_3 \pm \left(B_3^2 - 4A_3C_3\right)^{\frac{1}{2}}}{2A_3} \tag{A.22}$$

where

$$A_3 = \upsilon \left(\mu' + \mu'' + j \frac{p_0}{\rho_0 \omega}\right)$$

$$B_3 = - \frac{\gamma_T p_0}{\rho_0} + j\omega \left(\mu' + \mu'' + \upsilon\right)$$

$$C_3 = - \omega_2$$

Numerically it is found that μ', μ'', $\upsilon \ll \omega, c$ so that $B_3 \gg 4\, A_3C_3$ and

$$\lambda = \frac{-B_3 \pm \left(B_3 - \frac{2A_3C_3}{B_3}\right)}{2A_3} \tag{A.23}$$

to an excellent approximation. Thereby it is found that the two roots are

$$\lambda_1 = - \frac{\omega^2}{c^2} \tag{A.24}$$

$$\lambda_2 = j \frac{\gamma_T \omega}{\upsilon} \tag{A.25}$$

These are valid even for very turbulent behavior with effective viscosities on the order of 100 times the normal viscosity. It is highly unlikely that $4A_3C_3/B_3^2$ would ever be as large as 10^{-3} for a T-burner.

In the light of the results of Equations (A.24) and (A.25) and the fact that γ is on the order of unity, it is found that k_1 is very small and k_0 and k_2 are very large. Consequently in the vicinity of the curved boundary, $J_0(k_0 r)$ and $J_0(k_2 r)$ may be adequately approximated by asymptotic formulas and $J_0(k_1 r)$ may be adequately approximated by a truncated series. The approximations are again very good.

The propagation constant, γ, may be obtained by requiring that the perturbed velocities and temperature become zero at the curved boundary. Even though the result will not be expected to apply exactly, it is of interest to obtain an approximate expression. Through the use of the approximate representations for the Bessel functions the propagation constant is found to be

$$\gamma = \frac{\omega}{c}\left\{1 + \frac{(1-j)}{r_w 2^{1/2}\omega^{1/2}}\left[\upsilon^{1/2}\left(\gamma_T^{1/2} - \gamma_T^{-1/2}\right) + \left(\mu'^{1/2}\right)\right]\right\} \tag{2.7}$$

This result may be compared with an expression obtained by Cantrell et al. [6]. They have considered a somewhat similar problem but have included the effects of mean flow and the steep temperature gradient. By means of a variational approach they have obtained an approximate expression for γ as follows:

$$\gamma = \frac{\omega}{c}\left\{\frac{2\left\langle\frac{T_0}{T_c}\right\rangle}{1 + \left\langle\frac{T_0}{T_c}\right\rangle}\right\} + \frac{(1-j)}{c\, r_w}\left\{\frac{T_w}{T_c} + \frac{(\gamma_T - 1)}{(P_r)^{1/2}}\right\}\left(\frac{\omega\mu_w}{2\rho_{0w}}\right)^{1/2} \tag{A.26}$$

where $\langle\ \rangle$ here indicates a spatial average. Except for the temperature ratios the expressions are equivalent. There appears to be good

experimental agreement with Equation (A.27) for the case to which it really applies [12,45].

We shall examine the relative importance of each of the terms in the solution for $\tilde{u}$, Equation (A.12), because the complete solution is cumbersome. If it is required that the perturbed temperature and radial velocity be zero at the curved boundary, two equations are obtained which may be used to express A and A_2 in terms of A_1. When a particular numerical approximation was made, it was found that

$$A \simeq 10^{-176} A_1$$

$$A_2 \simeq 10^{-154} A_1$$

It is thereby concluded that, except very near the curved wall,

$$\tilde{u} = - \frac{\gamma c^2}{\omega} A_1 J_0(k_1 r) e^{j\omega t} \sinh j\gamma x \qquad (A.27)$$

where $\frac{\omega v}{c^2}$ has been neglected in comparison with one. The perturbed pressure, Equation (A.15), may be written as

$$\tilde{p} = \gamma_T p_0 A_1 J_0(k_1 r) e^{j\omega t} \cosh j\gamma x \qquad (2.5)$$

where again $\frac{\omega v}{c^2}$ has been neglected in comparison with one. The corresponding acoustic admittance at the burning boundary may then be written as

$$y = - \frac{\gamma}{\rho_0 \omega} \tanh j\gamma L \qquad (2.6)$$

It is also of considerable interest to investigate the effects of mean flow on the propagation constant. If the mean flow may be

represented as u_0 which is independent of position, then, in operator notation, the substantial derivative becomes

$$\frac{D}{Dt} = \frac{\partial}{\partial t} + u_0 \frac{\partial}{\partial x} \tag{A.28}$$

Now assume an exponential dependence, $e^{\pm j\gamma x}$, on axial position and a harmonic time dependence. Equation (A.28) thereby becomes

$$\frac{D}{Dt} = j(\omega \mp \gamma_{\pm} u_0) \tag{A.29}$$

Thus, effectively, the constant $\underline{h}$ in Equations (A.5), (A.6), (A.7), and (A.8) has a slightly changed significance but the solutions follow in the same manner. The propagation constant is, however, different for each wave. In the expression for the propagation constant, Equation (2.7), ω is replaced by $\omega \mp \gamma_{\pm} u_0$. Since $\gamma \simeq \frac{\omega}{c}$ then ω is approximately replaced by $\omega(1 \mp M)$. Thereby Equation (2.7) becomes

$$\gamma_{\pm} = \mp (1 \pm M) \gamma \tag{2.8}$$

Thus the velocity of a wave moving with the mean flow is increased by an amount approximately equal to the mean velocity. Since the Mach Number is small ($M \simeq .01$) in this work, the effect on the propagation constant should be correspondingly small and will be neglected. It is worthy of comment that Cantrell et al. have concluded from their work that the only effect of low Mach Number mean flow is to produce the steady-state boundary layer [6].

Finally, consider the transient periods during the growth or decay of oscillations. During these periods the angular frequency

becomes complex and the amplitude is modulated by an exponential time dependence, i.e., during the growth transient, ω is replaced by $\omega - j\alpha$. If we let β denote this complex frequency, then, for the transient periods, the expression for the propagation constant (Equation (2.7)) becomes

$$\gamma = \frac{\beta}{c}\left[1 + \frac{\eta}{\beta^{1/2}}(1 - j)\right] \tag{A.30}$$

where

$$\eta = \frac{1}{2^{1/2} r_w}\left[\upsilon^{1/2}\left(\gamma_T^{1/2} - \gamma_T^{-1/2}\right) + \mu'^{1/2}\right] \tag{A.31}$$

During stable oscillations, where $\gamma \equiv b - ja$, we find

$$b = \frac{\omega}{c}\left[1 + \frac{\eta}{\omega^{1/2}}\right] \qquad a = \frac{\omega^{1/2}\eta}{c} \tag{A.32}$$

however, the expression for a, at least, is not quite correct because non-linear effects have been omitted. Now during the growth transient we find from Equation (A.30)

$$b_G = \frac{\omega}{c}\left[1 + \frac{\eta}{\omega^{1/2}}\right] \quad a_G = \frac{\omega}{c}\left[\frac{\alpha}{\omega} + \frac{\eta}{\omega^{1/2}}\right] \tag{A.33}$$

If it may be presumed that the behavior of the flame is linear, the subscript G may be dropped from Equation (A.33) since b is expected to be essentially the same during the growth and stable periods. It will shortly be shown that $\alpha_{DL} = \eta\omega^{1/2}$ so that, from Equation (A.33).

$$a = \frac{\alpha + \alpha_{DL}}{c} \tag{2.15}$$

The decay transient is dealt with in a somewhat different fashion. After burn-out it is expected that the wave reflection at the (formerly) burning end will be nearly perfect because the wave then impinges upon a rigid steel flange. Consequently it is required that the acoustic velocity (axial direction) be nil at this point. This requirement leads to

$$\tanh a_d L + j \tan b_d L = 0 \tag{A.34}$$

Necessarily then

$$\gamma_d = \frac{n\pi}{L} \qquad n = 1,2,3, \ldots \tag{A.35}$$

the imaginary part being zero. With this result, Equation (A.30) may be used to obtain the real and imaginary parts of β_d, i.e.,

$$\omega_d = \frac{n\pi c}{L} \qquad \alpha_d = \eta \ \omega_d \tag{A.36}$$

where $\eta \ll (\frac{n\pi c}{L})^{1/2}$ has been used. In general, the fundamental frequencies before and after burn-out will not be the same. A Fourier series type of representation is required to meet the general initial conditions. However, if, during the decay, all frequencies higher than the fundamental are filtered out, then the decay rate that is measured is that of the fundamental. If the initial decay constant is listed, then η may be eliminated between Equations (A.32) and (A.36) to yield

$$aL = \frac{\alpha_D}{2f_D} \left(\frac{\omega}{\omega_D}\right)^{1/2} \tag{A.37}$$

Since the frequency dependence in this nonlinear region is questionable and since ω and ω_D should not differ greatly, we shall approximate

Equation (A.36) as

$$aL = \frac{\alpha_D}{2f} \qquad (2.14)$$

It may be noted that if the frequency dependence of a were some power other than .5, then the ratio of frequencies in Equation (A.37) would appear to that power. Therefore, the non-linearities should not affect the approximation in Equation (2.14) greatly.

The analysis given in this appendix provides most of the relationships used in the gas-phase work.

APPENDIX B

ANALYTICAL EXPRESSION FOR THE RATE OF OSCILLATORY GROWTH

There are several treatments available from which one may estimate the acoustic admittance of the burning boundary in a T-burner from growth and decay constants (e.g., [10] or Appendix E). Probably the most sound and most elegant treatment is that of Cantrell and Hart [7]. Their development will be outlined here.

The approach is to perturb the energy equation to second order, integrate over the volume, time average over harmonic terms, and then observe the consequences with respect to the growth constant. The perturbed equations of motion and continuity are used to eliminate the second-order terms from the final expression.

The energy equation for isentropic behavior of an ideal gas is

$$\frac{\partial}{\partial t}\left[\rho\left(C_v T + \frac{1}{2}u^2\right)\right] = -\nabla\cdot\rho\vec{u}\left(C_v T + \frac{p}{\rho} + \frac{1}{2}u^2\right) \qquad (B.1)^*$$

The equation of motion for irrotational and inviscid flow is

$$\rho\frac{\partial u}{\partial t} + \rho\nabla\left(\frac{u^2}{2}\right) + \nabla p = 0 \qquad (B.2)^*$$

The continuity equation is

$$\frac{\partial \rho}{\partial t} + \nabla\cdot(\rho\vec{u}) = 0 \qquad (B.3)^*$$

---

*These equations may be found in, e.g., Reference 3.

The energy equation when perturbed, integrated over the entire volume, and time averaged over harmonic terms becomes

$$< \frac{\partial}{\partial t} \int_V \left[\rho_0 \left(C_v T + \frac{u^2}{2}\right)_2 + \rho_1 \left(C_v T + \frac{u^2}{2}\right)_1 + \rho_2 \left(C_v T + \frac{u^2}{2}\right)_0 \right] dV >$$

$$= - < \int_S \vec{n} \cdot \left[\vec{m}_0 \left(h + \frac{u^2}{2}\right)_2 + \vec{m}_1 \left(h + \frac{u^2}{2}\right)_1 + \vec{m}_2 \left(h + \frac{u^2}{2}\right)_0 \right] dS > \tag{B.4}$$

where the definitions

$$C_v T + \frac{p}{\rho} = h \qquad \text{and} \quad \rho \vec{u} = \vec{m}$$

have been used. The divergence theorem (see, e.g., [61]). used in obtaining Equation (B.4). It is now necessary to eliminate the second-order terms from Equation (B.4) by means of the equations of continuity and motion.

One of the needed expressions is obtained by taking the dot product of $\vec{m}_0$ and the equation of motion, Equation (B.2), and subsequently integrating over the volume and time averaging. The corresponding result is

$$< \frac{\partial}{\partial t} \int_V \vec{m}_0 \cdot \vec{u}\, dV > = - < \int_S \vec{n} \cdot \left[\vec{m}_0 \left(h + \frac{u^2}{2}\right)_2 \right] dS > \tag{B.5}$$

The divergence theorem has again been used.

A second needed expression is obtained by multiplying the continuity equation by $\left(h + \frac{u^2}{2}\right)_0$. Upon integration and time averaging the result becomes

$$< \frac{\partial}{\partial t} \int_V \rho \left(h + \frac{u^2}{2}\right)_0 dV > = - < \int_S \vec{n} \cdot \vec{m}_2 \left(h + \frac{u^2}{2}\right) dS > \tag{B.6}$$

The final expression is obtained by re-expressing the integral

$$\int_V \rho\left(C_v T + \frac{u^2}{2}\right)\, dV$$

in terms of perturbed densities, pressures, and velocities, i.e.,

$$< \frac{\partial}{\partial t} \int_V \rho \left(C_v T + \frac{u^2}{2}\right) dV > =$$

$$< \frac{\partial}{\partial t} \int_V \left[\frac{p_0}{\rho_0} \left(\rho_2 + \frac{\gamma_T - 2}{2} \frac{\rho_1^2}{\rho_0}\right) + \vec{u}_2 \cdot \vec{u}_0 + \frac{u_1^2}{2}\right)\rho_0$$

$$+ \rho_1 \left(\frac{c^2}{\gamma_T \rho_0} \rho_1 + \vec{u}_1 \cdot \vec{u}_0\right) + \rho_2 \left(U_0 + \frac{u_0^2}{2}\right)\Bigg] dV > \qquad \text{(B.7)}$$

The substitutions

$$U_1 = \frac{c^2}{\gamma_T \rho_0} \rho_1 \qquad U_2 = \frac{c^2}{\gamma_T \rho_0} \left(\rho_2 + \frac{\gamma_T - 2}{2} \frac{\rho_1^2}{\rho_0}\right)$$

and

$$\left(\frac{u^2}{2}\right)_2 = \vec{u}_0 \cdot \vec{u}_2 + \frac{u_1^2}{2}$$

have been used in obtaining Equation (B.7).

Equations (B.4), (B.5), (B.6), and (B.7) are then combined to form

$$< \frac{\partial}{\partial t} \int_V \left[\frac{1}{2} \frac{p_1^2}{\rho_0 c^2} + \frac{1}{2} \rho_0 u_1^2 + \rho_1 \left(\vec{u}_1 \cdot \vec{u}_0\right)\right] dV > \quad =$$

$$< \int_S n \cdot \Bigg[p_1 \vec{u}_1 + \frac{p_1 \rho_1}{\rho_0} \vec{u}_0 + \rho_0 \vec{u}_1 \left(\vec{u}_1 \cdot \vec{u}_0\right)$$

$$+ \rho_1 \vec{u}_0 \left(\vec{u}_1 \cdot \vec{u}_0\right)\Bigg] dS > \qquad \text{(B.8)}$$

The substitutions

$$h_1 = \frac{p_1}{\rho_0} \qquad \text{and} \quad \vec{m}_1 = \rho_0 \vec{u}_1 + \rho_1 \vec{u}_0$$

have been used in obtaining Equation (B.8).

If the time dependence of the amplitude may be expressed as an exponential in time, i.e., $e^{\alpha t}$, and $\alpha \ll \omega$, then the differentiation with respect to time may be carried out explicitly. For example

$$< \frac{\partial}{\partial t} \int_V \frac{1}{2} \frac{p_1^2}{\rho_0 c^2} \, dV > = 2\alpha < \int_V \frac{1}{2} \frac{p_1^2}{\rho_0 c^2} \, dV > \qquad \text{(B.9)}$$

In this case Equation (B.8) may be rewritten as

$$2\alpha = \frac{- < \int_S \vec{n} \cdot \left[p_1 \vec{u}_1 + \frac{p_1^2}{\rho_0 c^2} \vec{u}_0 + \rho_0 \vec{u}_1 (\vec{u}_1 \cdot \vec{u}_0) + \rho_1 \vec{u}_0 (\vec{u}_1 \cdot \vec{u}_0) \right] dS >}{< \int_V \left[\frac{1}{2} \frac{p_1^2}{\rho_0 c^2} + \frac{1}{2} \rho_0 u_1^2 + \rho_1 (\vec{u}_1 \cdot \vec{u}_0) \right] dV >} \qquad \text{(2.22)}$$

which is equivalent to the result given by Cantrell and Hart. The neutral stability criterion, given by Cantrell and Hart, may be obtained directly by setting $\alpha = 0$, i.e.,

$$< \int_S \vec{n} \cdot \left[p_1 \vec{u}_1 + \frac{p_1^2}{\rho_0 c^2} \vec{u}_0 + \rho_0 \vec{u}_1 (\vec{u}_1 \cdot \vec{u}_0) + \rho_1 \vec{u}_0 (\vec{u}_1 \cdot \vec{u}_0) \right] dS > = 0 \qquad \text{(B.10)}$$

Equation (2.22) is too cumbersome in its present form to be very useful. However, if good approximations to the acoustic field can be made, the integrations can be carried out to obtain a more useful expression. For low-velocity mean flow, to which the equation applies, the last term in the integrands of both numerator and denominator may

be neglected. If the real part of the acoustic velocity at the burning boundary is not very small, then the third term in the integrand of the surface integral must be retained. Cantrell and Hart have assumed that the zero-order field is an adequate approximation and carried out the integrations. In this case the third term in the integrand of the surface integral is negligible. The result of this approximation is

$$\alpha - \alpha_{DL} = \alpha_b = - \frac{\gamma_T u_0}{L} \left(\frac{p_0}{u_0} y'\right) \qquad (B.12)$$

where $\omega = \frac{\pi c}{2L}$ and the definition of the virtual acoustic admittance have been used.

Equation (B.12) may be obtained much more simply, but with more restrictive assumptions. It is, however, reassuring that the same result is obtained, since this approach is reasonably general. Equation (2.22) applies to an acoustic field which does not approximate the zero-order field, as well as the simpler case, and, therefore, is of greater interest in this work.

APPENDIX C

LINEAR OR NONLINEAR BEHAVIOR

The assumptions have been made in the analysis of the gas phase that (1) the behavior of the flame is linear and (2) that the linearized conservation equations are an adequate description. Obviously these assumptions warrant scrutiny. Hart and McClure [21] have indicated that for amplitudes such that

$$\left|\frac{\tilde{p}}{p_o}\right| < .1$$

the gas may be treated as linear and the important nonlinear effects occur at the walls. A criterion such as this is necessarily rather arbitrary and requires a judgment as to how much error will be permitted. An estimate of this error will be made in this section. Also, the reasons for nonlinear effects at the wall will be considered.

It has been assumed that boundary condition at the flame zone was linear, i.e., the acoustic admittance was independent of amplitude. The justification for this assumption is that the oscillations grow exponentially, i.e., with the growth constant being a true constant, frequently to greater amplitudes than those occurring when our measurements were made. This is true of both single- and double-ended firings. An exponential growth is a strong indication of linear behavior [27]. Thus, this is the case in the amplitude region to which the analysis is applied, i.e., where the measurements were

made, then the linear assumption is thought to be valid. Because there is no reason to expect the behavior of the flame to change with burning time, changes in amplitudes during burning are thought to be due to other effects.

Now it is advantageous to examine the isentropic relationship. For first-order perturbations

$$\frac{\tilde{\rho}}{\rho_0} = \frac{1}{\gamma_T} \frac{\tilde{p}}{p_0} \tag{C.1}$$

but rigorously the relation should be written as

$$\frac{\tilde{\rho}}{\rho_0} = \left(1 + \frac{\tilde{p}}{p_0}\right)^{1/\gamma_T} - 1 \tag{C.2}$$

For the case where $\gamma_T = 1.25$ and $\tilde{p}/p_0 = .1$, the ratio of the calculated density variations from these two equations is 8.00:7.93. The error incurred by using the first-order perturbation approximation is less than one per cent at this amplitude level.

The error introduced by neglecting second-order terms in the equations of motion and continuity will be estimated by obtaining second-order approximate solutions and comparing these with the first-order approximations. The approach to be used for obtaining solutions to the nonlinear equations is given by Rayleigh [45]. The effects of viscosity and mean flow will be neglected. The motion will be assumed to be one-dimensional and isentropic. For this case the equations of motion and continuity are

$$\frac{\partial \tilde{u}}{\partial t} + \tilde{u} \frac{\partial \tilde{u}}{\partial x} + \frac{1}{\rho} \frac{\partial \tilde{p}}{\partial x} = \tag{C.3}$$

$$\frac{\partial \tilde{\rho}}{\partial t} + \tilde{u} \frac{\partial \tilde{\rho}}{\partial x} + \rho \frac{\partial \tilde{u}}{\partial x} = 0 \qquad (C.4)$$

where $\rho = \rho_0 + \rho$. The first-order approximations are obtained by neglecting the nonlinear terms as small. After application of the boundary conditions, these are found to be

$$\tilde{p}_1 = A\, e^{j\omega t} \cos \frac{\omega x}{c} \qquad (C.5)$$

$$\tilde{u}_1 = - \frac{jA}{\rho_0 c}\, e^{j\omega t} \sin \frac{\omega x}{c} \qquad (C.6)$$

The subscripts on p and u here indicate the order of approximation. These solutions are now substituted for the nonlinear terms in Equations (C.3) and (C.4) the result being

$$\frac{\partial \tilde{u}}{\partial t} + \frac{1}{\rho_0} \frac{\partial \tilde{p}}{\partial x} = 0 \qquad (C.7)$$

$$\frac{\partial \tilde{\rho}}{\partial t} + \rho_0 \frac{\partial \tilde{u}}{\partial x} = \frac{j\omega A^2}{\rho_0 c^4} \cos \frac{2\omega x}{c}\, e^{2j\omega t} \qquad (C.8)$$

The relationship for the cosine of the sum of two angles has been used to obtain Equation (C.8). Equations (C.7) and (C.8) may be combined to eliminate the perturbed velocity to yield

$$\frac{d^2 \tilde{p}}{dx^2} + \frac{\omega^2}{c^2} \tilde{p} = 2 \frac{\omega^2}{c^2} \frac{A^2}{\rho_0 c^2} \cos \frac{2\omega x}{c} \qquad (C.9)$$

where harmonic behavior has been assumed. The solutions to these equations are

$$\tilde{p}_2 = A\, e^{j\omega t} \cos \frac{\omega x}{c} + \frac{2}{3} \frac{A^2}{\rho_0 c^2}\, e^{2j\omega t} \cos \frac{2\omega x}{c} \qquad (C.10)$$

$$\tilde{u}_2 = - \frac{jA}{\rho_0 c}\, e^{j\omega t} \sin \frac{\omega x}{c} - j \frac{4}{3} \frac{A^2}{\rho_0^2 c^3}\, e^{2j\omega t} \sin \frac{2\omega x}{c} \qquad (C.11)$$

If $A = |\tilde{p}_g|$, $\gamma_T = 1.25$, and $|\tilde{p}_g|/p_0 = 1$, then the ratio of coefficients of the second to first terms is .053 for $\tilde{p}$ and .107 for $\tilde{u}$. Obviously the above procedure could be repeated to obtain higher order approximations; however, this should suffice.

The time-average energy density may be calculated from the second-order approximations as

$$< \frac{p_2^2}{2\rho_0 c^2} + \frac{\rho_0 u_2^2}{2} > = \frac{1}{2} \frac{A^2}{\rho_0 c^2} + \frac{A^2}{4\rho_0 c^2} \left[\left(\frac{2}{3} \frac{A}{\rho_0 c^2} \right)^2 + \left(\frac{4}{3} \frac{A}{\rho_0 c^2} \right)^2 \right] \tag{C.12}$$

Again for $A = |\tilde{p}_g|$, $\gamma_T = 1.25$, and $|\tilde{p}_g|/p_0 = .1$, the energy density due to the second term is about one per cent of the total.

On the basis of the above analysis it seems reasonable to assume that a linear description is adequate for amplitudes such that

$$\frac{|\tilde{p}|}{p_0} < .1$$

with an error of less than ten per cent. The greatest error appears to arise in the perturbed velocity; the error being about equivalent to $|\tilde{p}_g|/p_0$. It was found in the author's investigation that this ratio was about $\leq .05$ on the average for operation in the single-ended mode.

We shall now consider the kinds of nonlinear effects that might arise at the curved boundary. From the energy equation it is observed that energy will be lost at the wall through thermal conduction and work against viscous forces which will give rise to the terms of the type

$$\mathcal{E}_{loss} = \frac{\partial}{\partial y}\left(\tilde{u}\mu \frac{\partial \tilde{u}}{\partial y}\right) + \frac{\partial}{\partial y}\left(k \frac{\partial \tilde{T}}{\partial y}\right) + \ldots \qquad (C.13)$$

If the system behaves in a linear fashion, the energy loss terms depend upon the square of the amplitude [5]. Since both the viscosity and thermal conductivity depend upon temperature (absolute) to about the .6 to 1.0 power, they, too, depend upon the y coordinate. It is observed experimentally that the oscillations enhance the heat transfer to the walls and thus the mean temperature and temperature gradient must depend upon amplitude. Thus it is easily seen that the energy loss may become nonlinear. It also appears that variations in the mean temperature and velocity field may strongly affect the wall losses.

APPENDIX D

VIRTUAL ACOUSTIC ADMITTANCE

McClure [39] has pointed out that there is a convection of acoustic energy into the acoustic system at the burning boundary. Effectively the acoustic velocity is augmented over that which would exist in the absence of transpiration. In order to show how this arises we shall consider a one-dimension description for isentropic and inviscid behavior. The equations of motion and continuity are for this case,

$$\rho_0 \frac{\partial \tilde{u}}{\partial t} - \rho_0 u_0 \frac{\partial \tilde{u}}{\partial x} + \frac{\partial \tilde{p}}{\partial x} = 0 \qquad (D.1)$$

$$\frac{\partial \tilde{\rho}}{\partial t} - u_0 \frac{\partial \tilde{\rho}}{\partial x} + \rho_0 \frac{\partial \tilde{u}}{\partial x} = 0 \qquad (D.2)$$

Equations (D.1) and (D.2) may be combined to eliminate $\frac{\partial \tilde{u}}{\partial x}$; and terms involving u_0^2 may be neglected as small. The corresponding result is found to be

$$j\omega\rho_0 \left(\tilde{u} + u_0 \frac{\tilde{\rho}}{\rho_0}\right) + \frac{\partial \tilde{p}}{\partial x} = 0 \qquad (D.2)$$

where a harmonic time dependence has been assumed. In the absence of mean flow the quantity in parentheses in Equation (D.3) would be $\tilde{u}$. Thus the effective acoustic velocity is $\tilde{u} + u_0 \frac{\tilde{\rho}}{\rho_0}$. If one proceeds with obtaining a solution to Equations (D.1) and (D.2), the propogation constant is found to be

$$\gamma_{\pm} = \mp \frac{\omega}{c} (1 \pm M) \qquad (D.4)$$

By obtaining the solutions for $\underline{p}$ and $\underline{u}$ one can also find the effective velocity.

Since the corrections for mean flow have been neglected in this study, the acoustic admittance calculated from the pressure distribution is expected to be a virtual admittance. By assuming that the propagation constant was of the form of Equation (D.4) and estimating the Mach Number, it would be possible to obtain the actual admittance. However, in the latter case the pressure distribution is no longer of the cosine type and a much more elaborate calculation would be necessary. The small gain in information does not appear to be worth the additional work.

PAGES 124 THROUGH 128 OMITTED

APPENDIX F

THE EFFECTS OF A GRADIENT IN MEAN TEMPERATURE ON THE WAVE BEHAVIOR

The approach that will be used is to assume a mean temperature distribution and then examine the wave behavior. We shall assume that

1. the wave behavior is one-dimensional,
2. the gas is ideal and inviscid,
3. there is negligible mean flow,
4. and the wave behavior is isentropic.

Under these restrictions the equations of motion and continuity, Equations (2.2) and (2.3), may be differentiated and combined to give

$$\frac{\partial^2 \tilde{p}}{\partial t^2} = c^2 \frac{\partial^2 \tilde{p}}{\partial x^2} \tag{F.1}$$

where c is position dependent.

The mean temperature distribution should be obtained from an analysis of the heat transfer problem for the cavity; however, not enough is known about the heat loss at the walls to carry out the analysis. Therefore, it will be assumed that the temperature distribution can be represented as

$$T_0 = T_f \, e^{-\Gamma(L-x)} \tag{F.2}$$

where Γ is an arbitrary constant and x is taken as zero at the non-burning end of the motor. A second distribution will be assumed as

$$T_0 = \frac{T_f}{1 + K\, e^{\Gamma(L-x)}} \tag{F.3}$$

A solution to Equation (F.1) may be obtained, with Equation (F.2) and the isentropic assumption being used for c, as

$$\tilde{p} = e^{j\omega t}\, [A_1\, J_o(\zeta) + A_2\, Y_0\, (\zeta)] \tag{F.4}$$

where

$$\zeta = \frac{\omega}{c_f}\ \frac{2}{\Gamma}\ e^{\Gamma(L-x)/2}$$

The solution can be completed by application of the boundary conditions to this result; however, the behavior of the solution is more easily visualized if the temperature gradient is assumed to be small. For a small gradient, Γ is small and ζ is large; therefore, asymptotic formulas may be used for the Bessel functions. By means of these formulas, Equation (F.4) may be rearranged to give

$$\tilde{p} = \zeta^{-1/2}\ e^{j\omega t}\ A_3 \cos\ (\zeta + A_4) \tag{F.5}$$

The acoustic velocity must be nil at the origin; therefore,

$$\tan\ (\zeta_c + A_4) = -\frac{1}{2\zeta_c} \tag{F.6}$$

$$A_4 \simeq -\zeta - \frac{1}{2\zeta_c} \tag{F.7}$$

where $\zeta_c \doteq \zeta_{x=0}$ and advantage has been taken of the largeness of ζ. A second boundary condition is that pressure at the origin be equal

to the measured pressure at that point, i.e.,

$$\zeta_c^{-1/2} e^{j\omega t} A_3 \cos\left(\frac{1}{2\zeta_c}\right) = \left|\tilde{p}_g\right| e^{j\omega t} \qquad (F.8)$$

from which A_3 is obtained. Finally, since Γ is small, the exponential in the definition of ζ, Equation (F.4), may be approximated by a truncated expansion. The acoustic pressure may then be approximated as

$$\tilde{p} \simeq \left|\tilde{p}_g\right| e^{\Gamma x/4} e^{j\omega t} \cos\left[\frac{\omega}{c_c}\left(x - \frac{\Gamma x^2}{4}\right)\right] \qquad (F.9)$$

where

$$c_c = c_f e^{-\Gamma L/2}$$

From this result it is seen that the amplitude increases with mean temperature. Thus, if the mean temperature is higher at the burning end than at the non-burning end of the motor, the amplitude should be greatest at the propellant end. The same conclusion was reached when Equation (F.1) was solved with Equation (F.2) as the temperature distribution on an analog computer.

The second temperature distribution, Equation (F.3), also leads to an equation of the Bessel type. In this case, the solution is

$$\tilde{p} = e^{j\omega t}\left[C_1 J_\upsilon(\zeta') + C_2 J_{-\upsilon}(\zeta)\right] \qquad (F.10)$$

where

$$\upsilon = j\frac{2}{\Gamma}\frac{\omega}{c_f}$$

$$\zeta' = \frac{\omega}{c_f}\frac{2}{\Gamma} K^{1/2} e^{-\Gamma x/2}$$

If Γ is large, so that the temperature distribution approximates the thermal boundary layer at the cold end, the Bessel functions may be approximated by truncated series. In this case Equation (F.10) is approximated by

$$\tilde{p} = e^{j\omega t}\left\{ C_3\, e^{-j\frac{\omega x}{c_f}}\left[1 - \frac{\frac{\omega}{c_f}\frac{2}{\Gamma}K^{1/2}\, e^{-\Gamma x}}{4(1+\upsilon)}\right] + C_4\, e^{j\frac{\omega x}{c}}\left[1 - \frac{\frac{\omega}{c_f}\frac{2}{\Gamma}K^{1/2}\, e^{-\Gamma x}}{4(1-\upsilon)}\right]\right\} \qquad \text{(F.11)}$$

Here it is observed that as long as the wave length is large compared with the thickness of the boundary layer, the terms within [] in this equation are nearly unit. Therefore, for a thin boundary layer the solution is the same as that obtained if the layer is neglected and the layer has no effect.

If Γ is small and asymptotic formulas are used to approximate the Bessel functions in Equation (F.10), an equation of the same form as (F.9) is obtained. Therefore, this analysis also leads to the conclusion that a higher mean temperature at the burning end will cause a higher pressure amplitude. These last two conclusions were also verified by solving Equation (F.1), with (F.3) as the temperature distribution, on an analog computer.

APPENDIX G

APPARATUS AND PROCEDURES

In this appendix the details of the experimental system will be discussed.

T-Burner: Gas Phase Study

The T-burner used in the gas-phase work is shown in Figure 28. A sketch of the configuration is shown in Figure 1. The motor was constructed entirely from steel, except for a replaceable carbon nozzle. The central, or nozzle, section was coupled, and sealed by means of O-rings, to approximately equal lengths of tubing (1.27-cm. wall thickness, nominally), the ends of which in turn were sealed. The inside diameter was 3.96 cm. throughout. End closures accommodated the pressure transducers and were bonded firmly in place for each firing with an epoxy adhesive. Heavy steel flanges were used to rigidly clamp the motor together for a firing.

Propellant samples were cut to the desired length (1.27 cm., nominally) from cylindrical castings. Before cutting, these grains were prepared by scraping the sides to remove a parting agent acquired during casting and leaching to inhibit the sides and provide a clean surface for bonding purposes. The ends of the cut samples were scraped with a razor blade to remove irregularities. The curved wall of the sample was coated with epoxy, as was the top of the end closure except for the surface of the transducer. A small amount of epoxy was spread

Figure 28. Two views of the T-burner used in the gas-phase work.

around the inside of the end of the tube because of a tendency for the adhesive to be "wiped-off" the sample upon insertion. The sample was then placed on the end closure and inserted into the end of the motor. Firm transducer contact was obtained by placing a rubber stopper and weight on the free surface of the sample while the epoxy cured.

Converging nozzles were made from carbon rod stock, the throat diameter being determined by the mean pressure desired and length of motor to be used.

T-Burner: Solid-Phase Study

The motor used for the solid-phase work was constructed by and is described by Coates [11]. A sketch of the configuration is given in Figure 25. Except for the piston arrangement used to advance the propellant, the motor was the same as the motor for the gas-phase work. One end closure was replaced by the piston which advanced the propellant so that the burning interface remained at a nearly constant position. The piston was sealed by means of an O-ring. During burning the position of the interface was sensed by a thermocouple in the wall of the motor. The output of the thermocouple, in conjunction with a control unit, was used to control the rate of propellant movement. The piston was hydraulically driven, the rate being varied by an electrically operated control valve.

Propellant samples were cut to the desired length from castings which fit into the motor with a low wall clearance (.01 cm.). These samples were securely bonded to the face of the driving piston. Firm transducer contact was obtained by placing a weight on top of the sample

while the adhesive cured. The curved wall of the sample was liberally coated with hydrocarbon grease before assembling the motor.

Igniter System

The igniter system was composed of a short piece of Pyrofuze wire (3-5 cm.) and a small amount of F-propellant sawdust. Pyrofuze wire (Pyrofuze Corporation, Mount Vernon, New York) is a bi-metallic wire which reacts exothermically when heated. Short copper leads were attached to the Pyrofuze wire which was subsequently sprayed with an electrically insulating resin. The Pyrofuze wire and propellant sawdust were placed adjacent to the propellant in the motor and the copper leads passed through a rubber stopper inserted in the nozzle. Ignition was achieved by electrically heating the Pyrofuze. The function of the rubber stopper was to carry the igniter leads out of the motor as the pressure rose.

Instrumentation

The instrumentation is summarized by Figure 29 in which a block diagram of the electronic system is shown. The system shown is that most frequently used in the gas phase work but is little different from that used at other times. Switch (4) permitted a reference signal to be recorded following the firing data without stopping the tape recorder. The RC filters and voltage dividers (5) provided the necessary separation of the oscillating component from the total signal and permitted the adjustment of the recorded voltage to the proper level. During data acquisition the tape recorder (7) was operated at

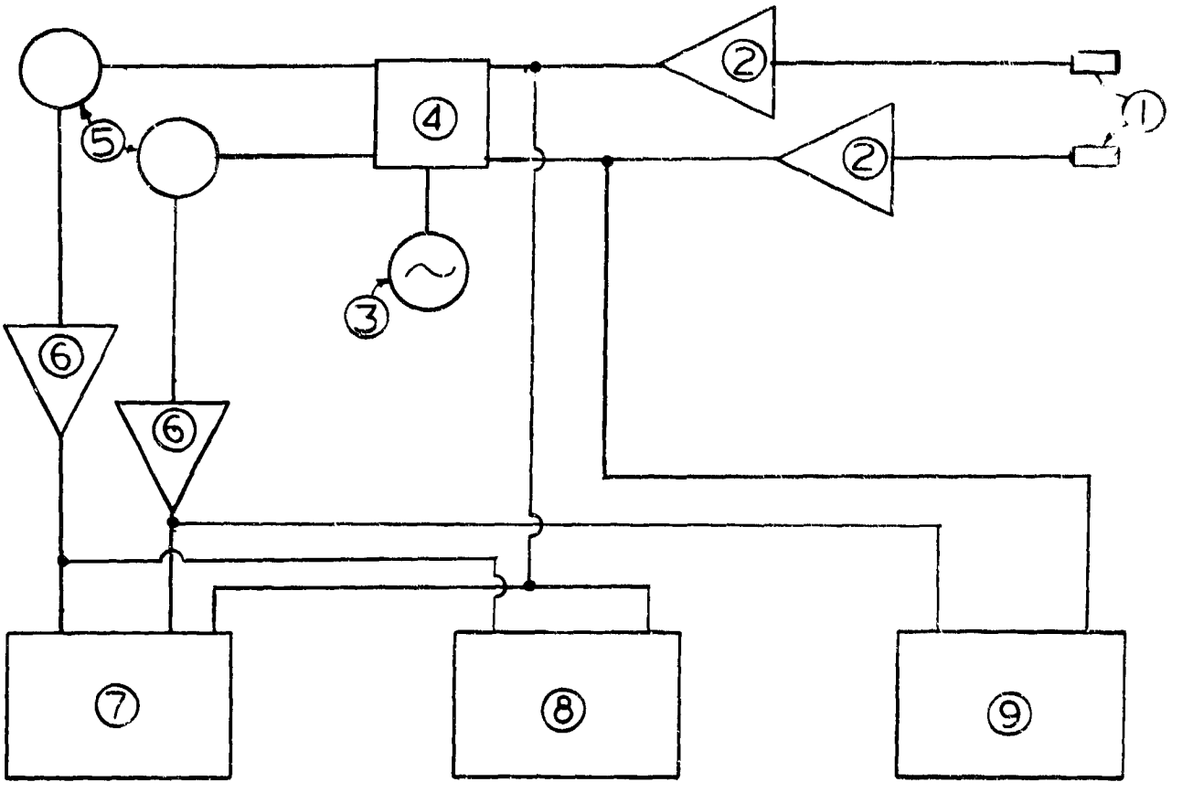

RECORDING SYSTEM (Reproduce System given on next page)

Figure 29. Block diagram of instrumentation.

1. Kistler Model 401 pressure transducers (or Model 616 water-cooled transducer)
2. Kistler Model 565 charge amplifier
3. Heath-kit Model AG-9A audio oscillator
4. Double-pole-double-throw switch
5. RC filters and voltage dividers
6. Tektronix Model 122 preamplifiers
7. Precision Instrument Model 207 tape recorder with two direct and one FM record-reproduce channels
8. Tektronix Model 535 oscilloscope with Type M plug-in unit
9. Hewlett-Packard Model 150A oscilloscope

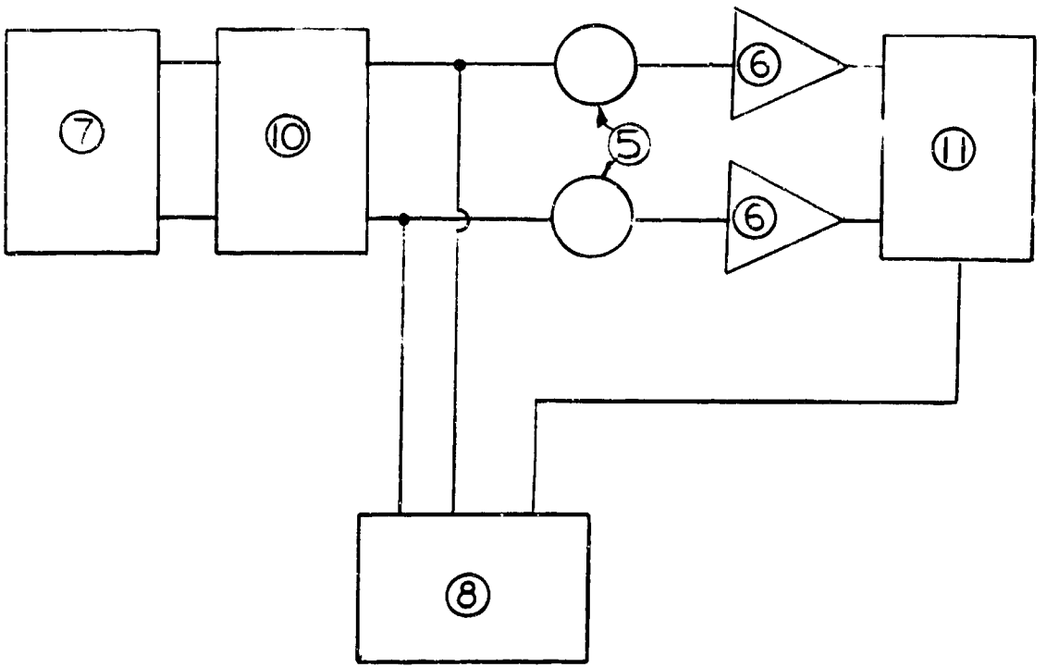

Figure 29 (continued)

5. RC filters and voltage dividers

6. Tektronix Model 122 preamplifiers

7. Precision Instrument Model 207 tape recorder

8. Tektronix Model 535 oscilloscope

10. Spencer-Kennedy Laboratories Model 302 variable electronic filter, dual channel

11. Ad-Yu Model 405 electronic phase meter

60 inches per second with two AC and one DC signal being recorded. The original data were also recorded photographically on the two oscilloscopes (8,9).

The data were reproduced from the tape recorder (7) at 7 1/2 inches per second (usually). The filter (10) reduced the distortion and noise levels. Oscillatory amplitudes and frequencies were measured by displaying the signals on the oscilloscope (8) and photographing the traces. The phase meter (11) was used to measure phase angles between the data signals, the meter output being displayed on the oscilloscope simultaneously with the oscillatory envelopes. The output of the tape recorder was amplifed (5,6) to the necessary input level for the phase meter.

The experimental system used was, for the most part, satisfactory. Most of the difficulties that arose were due to failures of the instruments or wiring, rather than any weakness of the overall system.

APPENDIX H

PROPELLANT

The propellant used in substantially all of the work reported here is known as Utah F. It was produced in small batches in this laboratory. The composition was:

1. 40 weight per cent coarse ammonium perchlorate (American Potash size: -48 +100),
2. 40 weight per cent fine ammonium perchlorate (American Potash size: 50 per cent less than 15 microns),
3. 2 weight per cent copper chromite (Harshaw Chemical, Cu-0202 P),
4. 15.3 weight per cent polybutadiene-acrylic acid copolymer (Thiokol),
5. 2.7 weight per cent epoxy resin (Shell, Epon 828).

The propellant was mixed for 60 minutes at a pressure of 7 to 8 mm. Hg absolute and a temperature of 65°C, nominally. It was cast, at the same pressure, into a cylindrical mold. It was cured for 7 days at 80°C, nominally.

F propellant has the following pertinent properties:

1. Linear burning rate, $r_o = .394\ (p_o)^{.425}$ cm/sec where p_o is in atmospheres (absolute).*

*The rate expression was determined from strand bomb data. These data may be found in: Beckstead, M. W., unpublished Ph.D. thesis, University of Utah, Dept. of Chemical Engineering (Salt Lake City, June, 1965).

2. Density, $\rho_s = 1.63$ gm/cm^3
3. Adabiatic flame temperature is 2600°K at 68 atm.
4. Calculated ratio of heat capacities, γ_T=1.24 at 68 atm. and 2600°K.
5. Calculated molecular weight is 23.5 gm/mole at 68 atm. and 2600°K.
6. Calculated isentropic velocity of sound is 1.07 (10^5) cm/sec at 68 atm. and 2600°K.
7. Heat capacity, C_p = .316 cal/gm K.
8. Thermal diffusivity is .001697 cm^2/sec.
9. Heat of combustion (old F propellant) is 2.563 Kcal/gm.

APPENDIX I

VALIDITY OF MEASUREMENTS

The experimental observation that the pressure amplitude at the burning surface was much less than that at the non-burning end was a source of concern. Consequently a rather thorough investigation was carried out in an effort to explain it.

It is felt that the low measurement was not due to the instrumentation for the following reasons:

1. The transducers and information channels were interchanged frequently and the observation was unaffected.
2. The transducer calibrations were frequently checked.
3. A reference signal was recorded immediately after each firing. The reference signal was switched into both information channels and passed through each complete system with the exception of the Kistler charge amplifiers and transducers. The signal came from a single audio oscillator which was set at a frequency close to that of the data. The reference was subsequently used to compensate for any differences in the gain of the two electronic systems.
4. The thermal effects on the transducers should be small. The output of the Kistler 401 transducer increases with temperature at the rate of .02 per cent per degree K. Thus, unless the temperature of the transducer increases enormously, the

effect will be insignificant. The DC level of the output drops with heating due to reduced stress on the crystal, the crystal being mounted under stress in the transducer. From the kinds of DC shifts encountered during operation, it is estimated that the temperature rose about 20°K.

5. The 401 transducer has a recess around the sensing diaphragm on the face of the transducer. Normally this recess was filled with silicone grease. It was thought that under pressure the propellant might be inadequately supported in this region and cause a slightly dome-like surface over the sensing diaphragm. In order to test for this problem the recess was filled with epoxy and a firing was made. The measured relative amplitude was .455.
6. As a check on the ability to accurately measure a pressure through the propellant, a thin sample of propellant (.35 cm.) was bonded into a short test section in the configuration used during a firing. The test section was then adapted to a dead-weight gauge tester and the transducer output was measured under these conditions. The mean pressure measured was about four per cent higher than that measured without the propellant. The small increase in output is attributed to an increased effective area for the sensing diaphragm, i.e., the recess causes more of the load to be supported by the sensing diaphragm than would occur if the measurement were made in a fluid.

7. Since no technique was available for dynamically calibrating the transducers, a crude dynamic comparison was devised. Two transducers were mounted in an assembled motor with no propellant. An igniter and a small amount of propellant sawdust were ignited near the midpoint of the motor. The outputs of the two transducers were then compared. A rate of pressure rise equivalent to 200 cps was obtained. No difference in output could be detected.
8. A great deal of care was exercised in assembly of the propellant sample and transducer to ensure proper contact with the sensing diaphragm. The transducer was mounted so that the sensing diaphragm protruded about .08 cm. above the end plate. This allowed for a reasonable glue line of epoxy. After assembly the propellant was held in firm contact by a small weight resting on a rubber stopper. It was felt that proper contact was thus obtained. If poor contact had been a problem, it should have appeared through distortion of the output signal. A comparison of the waveforms at the two ends of the motor was favorable.
9. Since Kistler transducers are acceleration sensitive, it was felt that this might be a problem. An output due to a vibrational acceleration could be in phase with the pressure and thus augment the amplitude of the total output. A test for such effects was devised. The cold end of the motor was closed by bonding a .3-cm. steel plate over the end.

The motor was assembled as usual except the transducer in the cold end was not mounted in contact with the .3-cm. plate. The transducer was thereby prevented from exposure to the gases but still exposed to any accelerations present. When a firing was carried out in this manner the output of this transducer showed no signal above the noise level even though strong oscillations were present in the motor.

10. Because the output of the Tektronix 122 preamplifiers used in each information channel is not flat in the frequency range of interest, a comparison of the relative output was made. A signal was passed through each amplifier-filter combination over the frequency range of 1.0 to 6.0 Kc. The variation in relative output was completely negligible.

On the basis of the above instrumentation evaluation it was concluded that the relative amplitude measured was that experienced by the transducers.

One area of obvious concern is the neglect of attenuation in the propellant, i.e , the assumption that the dynamic pressure measured under a thin slab of propellant is equivalent to that at the surface of the propellant. The validity of this assumption was checked by two routes. The first was to measure the pressure on the non-burning end of the motor through a .2-cm. slab of propellant whose surface was inhibited to prevent burning. The average relative amplitude for two runs made in this manner was .460. The second route was to examine the decay of oscillations after burn-out. It was found that the decay

occurred smoothly and that a non-unity relative amplitude persisted until the signals reached the noise level. It was thereby concluded that the pressure measured was equivalent to that at the propellant surface during burning.

The effects of the boundary layers at each end of the motor on the pressure measurement must be considered in order to complete the examination. At the non-burning end it is expected that there is a steep temperature gradient between the transducer and the main body of the gas. Because the mean flow is expected to be small, the effects of this thermal boundary layer can be approximated analytically without great difficulty. In Appendix F an analytical solution is obtained for a mean temperature distribution that is thought to approximate that due to the boundary layer. This solution (Equation (F.11)) indicates that the pressure amplitude is unaffected as long as the boundary layer is thin compared to the wave length. It is expected that the boundary layer may be neglected in the problem at hand.

The effect of the boundary layer associated with the flame is considerably more complicated to treat. It is usually argued that the amplitude must be unaffected in traversing the flame zone because the flame zone is much thinner than the wave length. However, because the flame zone is very complex, it is difficult to assure oneself that this argument is adequate. Consequently a rather extensive approximate analytical treatment of the wave behavior in the flame zone was developed. Because of its complexity it will be given in a separate appendix (Appendix J). The approach was to perturb the one-dimensional equations

of energy, motion, and continuity; with mean flow and mean temperature terms being retained. The resulting equations were combined and solved numerically. The solutions showed no indications of any serious reductions in amplitude in passing through the flame zone to the solid. It was concluded that pressure amplitude on the gas side of the flame zone was essentially the same as at the solid surface.

Consideration was also given to the effects of gradient in mean temperature along the motor. Analytical solutions were obtained for the wave behavior with assumed mean temperature distributions (see Appendix F). This analysis showed the pressure amplitude to be higher at the hottest end of the motor. Since the non-burning end cannot be hotter than the burning end, it was concluded that a gradient in mean temperature would oppose the low amplitude at the propellant end.

Several firings were made with a newly acquired water-cooled transducer mounted in the curved wall of the motor. The intent was to compare the amplitude measured by this transducer with the amplitude inferred from end measurements. The data obtained were rather erratic so that a good comparison could not be made; however, the amplitudes measured in the wall and near the propellant were compatible with the amplitudes measured under the propellant.

Two firings were made with the nozzle shifted toward the propellant from the midpoint. The damping effects of the nozzle should be minimized when the locations of the nozzle and the pressure node coincide. The data from these firings indicated that the amplitude was reduced when the nozzle was closer to the propellant than $x/L = .65$. When the

nozzle was located in the range $x/L = .55$ tc $.65$, the amplitude appeared to be normal. In both cases the relative amplitude was about the value observed before. The average relative amplitude was .475. Distortion seemed to be higher than usual. These measurements indicate that the pressure node is located near the midpoint of the motor.

The conclusions of importance may be summarized as follows:

1. The measured amplitude ratio exists within the motor. In particular, it is not introduced by the instrumentation; it is not introduced by either the thermal boundary layer at the cold end or the boundary layer associated with the flame; and it is not due to the propellant through which the low amplitude is measured.
2. Although the gas may be cooler at the non-burning end of the motor, the effect is in opposition to that measured.
3. Pressure measurements made in the curved wall of the motor and near the propellant were compatible with those made under the propellant.
4. Measurements made with the nozzle shifted toward the propellant from the midpoint of the motor indicate that the pressure node is in the vicinity of the midpoint.
5. The low relative amplitude persists through most of the decay transient.

APPENDIX J

ANALYSIS OF THE WAVE BEHAVIOR IN THE FLAME ZONE

At one point in the gas-phase work the data appeared to indicate that the pressure amplitude was significantly lower on the propellant side of the flame zone than on the gas side. Consequently, an elaborate analysis of the wave behavior in the flame zone was developed. Later consideration of the data showed that the observed amplitude behavior could not be due to the flame zone and, therefore, the analysis was really unnecessary. However, the analysis will be outlined.

The approach was to perturb the equations of motion, continuity, and energy for one-dimensional and inviscid behavior. The steady-state equations were subtracted from the perturbed equations and the resulting equations combined to form a differential equation in the perturbed pressure. Because of the inability to calculate the mean temperature distribution, various distributions were assumed. The differential equation was solved numerically. It was assumed that the analytical expression for the acoustic pressure, Equation (2.5), was sufficient outside the flame zone. The analytical solution was used to calculate initial values for the numerical integration. The numerical solution then gave the pressure amplitude at the propellant surface, i.e., under the flame zone.

The perturbed equations of motion and continuity, subject to the above conditions and after subtraction of the steady-state equations, are

motion - x direction

$$\rho_0 \frac{\partial \tilde{u}}{\partial t} + \rho_0 u_0 \frac{\partial \tilde{u}}{\partial x} + \tilde{\rho} u_0 \frac{\partial u_0}{\partial x} + \tilde{u} \rho_0 \frac{\partial u_0}{\partial x} + \frac{\partial \tilde{p}}{\partial x} = 0 \qquad (J.1)$$

continuity

$$\frac{\partial \tilde{\rho}}{\partial t} - \frac{\rho_0 \tilde{u}}{u_0} \frac{\partial u_0}{\partial x} + u_0 \frac{\partial \tilde{\rho}}{\partial x} + \tilde{\rho} \frac{\partial u_0}{\partial x} + \rho_0 \frac{\partial \tilde{u}}{\partial x} = 0 \qquad (J.2)$$

The quantity $\frac{\partial p_0}{\partial x}$ has been neglected since it can be shown to be small when $\rho_0 u_0^2 \ll p_0$ and the variation in molecular weight is neglected. A harmonic time dependence was assumed. Equations (J.1) and (J.2) may then be combined to solve for $\tilde{u}$. This expression is differentiated to obtain $\frac{\partial \tilde{u}}{\rho x}$. Both of these expressions may then be inserted into Equation (J.2) to obtain a differential equation in $\tilde{p}$ and $\tilde{\rho}$. It was then necessary to appeal to the energy equation to relate $\tilde{p}$ and $\tilde{\rho}$.

In perturbation from the energy equation is

$$\rho_0 C_p \frac{D\tilde{T}}{Dt} + \tilde{\rho} C_p \frac{DT_0}{Dt} = \frac{D\tilde{p}}{Dt} \qquad (J.3)$$

where the steady-state equation has been subtracted and the reaction terms and perturbed conduction terms neglected. A harmonic time dependence and a constant molecular weight are assumed. Equation (J.3) then yields an expression in terms of the zeroth and first derivatives of $\tilde{p}$ and $\tilde{\rho}$. This expression is then combined with the expression

obtained from the equations of motion and continuity to eliminate $\widetilde{\rho}$. A third-order equation is obtained with variable and complex coefficients. The coefficients are very complicated.

The third-order differential equation was solved with a Runga-Kutta-Gill integration technique. The mean temperature was assumed to be described by functions of the exponential, sine, parabolic, and cubic types. In addition, the effects of the chemical reactions were incorporated by making some very crude approximations.

A number of variations were tried and extensive computer time used in carrying out the analysis; however, in no case were we able to predict a pressure amplitude under the flame zone that was significantly less than that outside the flame.

APPENDIX K

ESTIMATION OF THE ISENTROPIC VELOCITY OF SOUND FROM THE NOZZLE CONDITIONS

The isentropic velocity of sound in the main body of the gas may be quite simply estimated from the nozzle conditions if it is assumed that

1. the flow through the nozzle is steady,
2. the conditions in the main body of the gas approximate the stagnation conditions for the gas,
3. the flow is isentropic,
4. and the contraction coefficient for the nozzle is unity.

All four assumptions should be quite good. Since the Mach Number at the throat of the nozzle must be unity, the gas temperature at the throat is related to the gas temperature in the main body of the gas as

$$\frac{T_{Ot}}{T_O} = \frac{2}{\gamma_T+1} \tag{K.1}$$

Now, if the mass generation rate at the propellant is equated to the mass flow rate through the nozzle, then

$$c = \left(\frac{D_t}{D_p}\right)^2 \frac{p_O}{r_c o_s} \gamma_T \left(\frac{2}{\gamma_T+1}\right)^{\frac{\gamma_T+1}{2(\gamma_T-1)}} \tag{K.2}$$

Everything on the right side of this equation is known, can be measured, or can be estimated reasonably well. The linear burning rate expression

(see Appendix H) may be substituted for r_c so that $\underline{c}$ may be expressed as a function p_o only, the function being a proportionality to $p_o^{.575}$.

Equation (K.2) was used to estimate the velocity of sound. For firings in the 2.5 to 4.5 kilocycle range, the throat diameter was .521 cm., whereas in the 1 to 2.5 kilocycle range the throat diameter was .510 cm. At 68 atm. and 2600°K, $\gamma_T = 1.24$. Since the pressure and temperature were actually somewhat lower than these values, $\gamma_T = 1.26$ was used. The calculations gave

$$c = .967\ (10^5)\ \text{cm/sec} \qquad D_t = .521\ \text{cm.}$$

$$c = .911\ (10^5)\ \text{cm/sec} \qquad D_t = .510\ \text{cm.}$$

If $\gamma_T = 1.24$ is used, $\underline{c}$ is lower by a factor of .985.

The above calculated values were used in Chapter IV.

PAGES 154 THROUGH 159 OMITTED

APPENDIX M

PARAMETRIC CURVES

This appendix contains the parametric curves developed from Equation (6.15) which were used in the solid-phase work. Use of the curves requires a knowledge of the ratio of amplitudes and the phase angle between the oscillating pressures at the ends of the propellant.

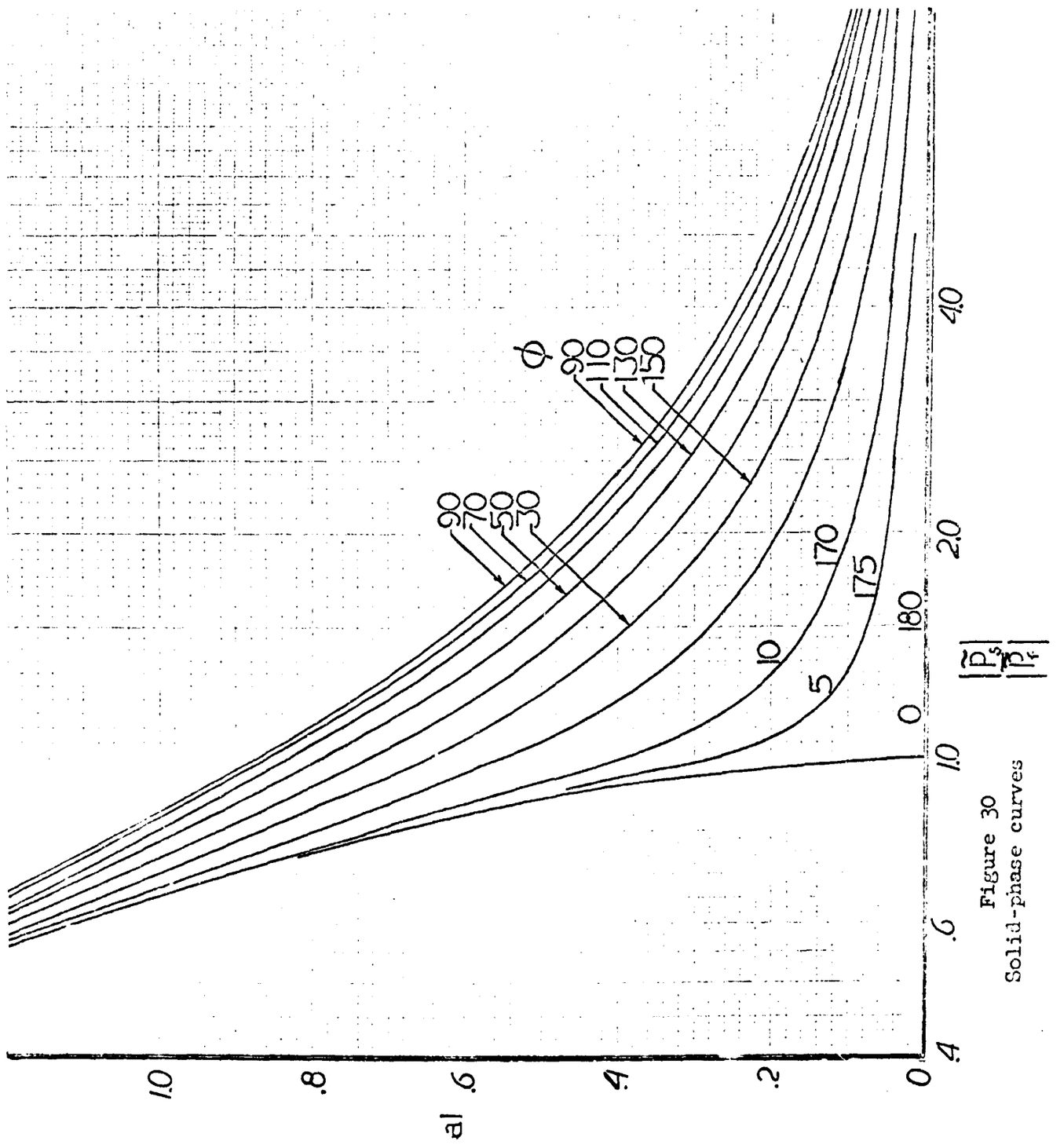

Figure 30
Solid-phase curves

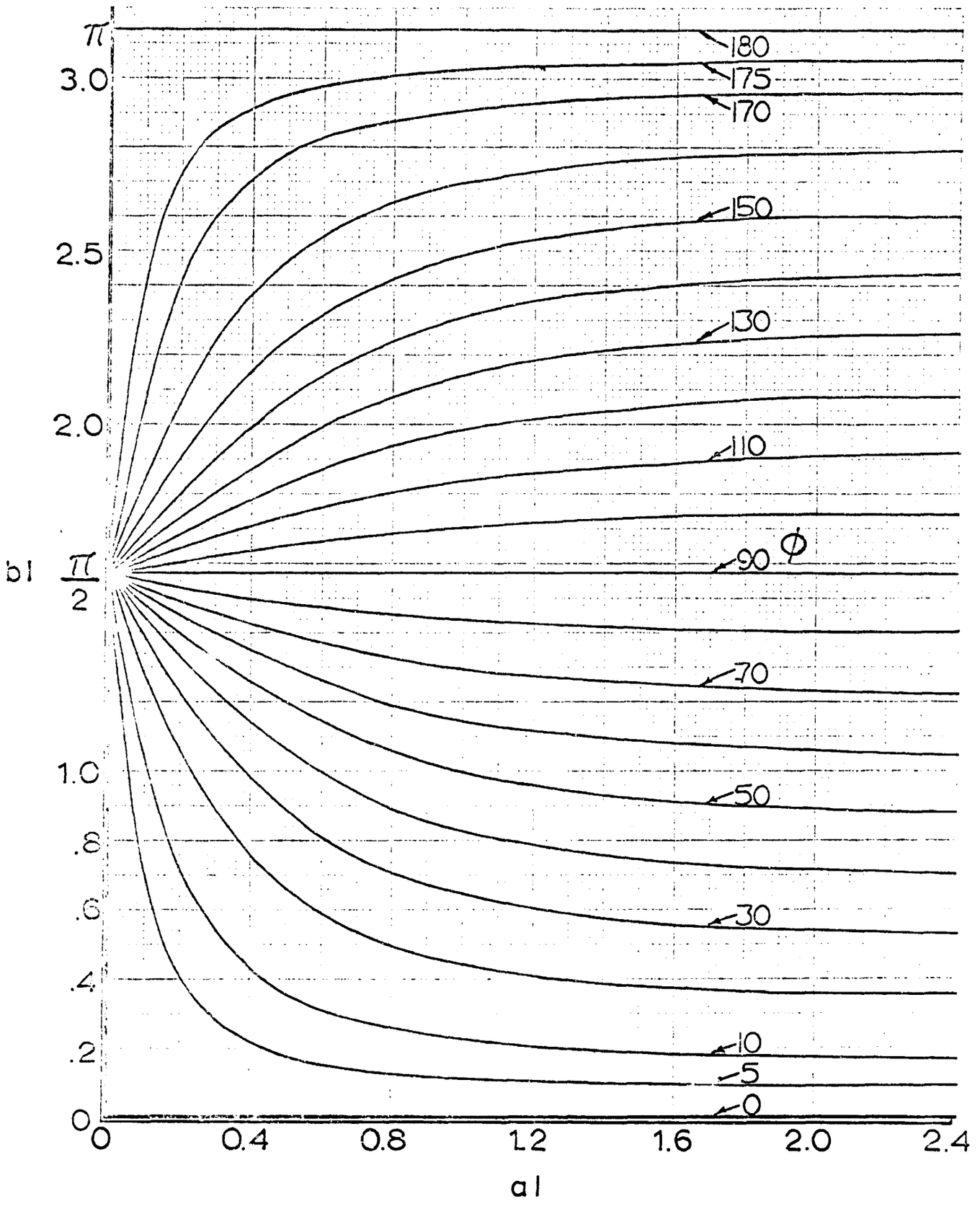

Figure 30 (continued). Solid-phase curves.

APPENDIX N

TABLES OF DATA

TABLE 3

GROWTH CONSTANT-FREQUENCY DATA FOR OLD UTAH-F PROPELLANT

Nominal mean pressure, 14.5 atm.

Nominal initial sample length, 1.3 cm.

	Run Number	α (sec^{-1})	f (kc.)	Notes
Double-ended firings	0-40	63	2.3	(a)
	0-44	72	2.0	
	0-45	169	6.7	
	0-53	167	6.9	
	0-57	43	1.0	(b,c)
	0-58	64	1.7	
	0-59	90	1.7	(c)
	0-64	73	1.7	(c)
	0-66	78	2.2	(c)
	0-67	91	2.9	(c)
	0-68	84	2.9	(a)
	0-69	81	2.2	
	0-70	79	2.3	(c)
	0-71	102	2.9	
	0-72	43	1.1	(b)
	0-73	31	.70	(b)
	0-74	37	.73	
	0-75	31	.98	
	0-76	183	7.0	
	0-77	117	4.7	(b,c)
	0-78	110	4.8	
	0-79	167	7.0	(b,c)
	0-82	42	.78	
	0-83	113	4.8	(c)
	0-101	64	1.7	
	0-102	47	1.1	(b)
Single-ended firings	0-103	14	.96	
	0-105	27	1.9	
	0-107	48	3.8	
	0-108	52	5.1	
	0-109	56	4.7	
	0-110	52	3.5	
	0-111	23	2.4	
	0-112	25	1.9	
	0-113	21	1.6	
	0-114	15	.99	
	0-115	9	.70	

TABLE 3 (continued)

Run Number	α (sec^{-1})	f (kc.)	Notes
0-124	25	1.7	
0-128	9	.63	(b)
0-131	20	1.7	
0-149	64	9.8	
0-151	56	10.2	

Notes:

(a) High mean pressure, the mean pressure exceeded the nominal value of 14.5 atm. by more than 3.5 atm.

(b) Low mean pressure, the mean pressure was less than the nominal value of 14.5 atm. by more than 3.5 atm.

(c) Marginal mean pressure, the mean pressure trace indicated a non-uniform burning area.

TABLE 4

GROWTH CONSTANT-FREQUENCY DATA FOR NEW UTAH-F PROPELLANT

Nominal mean pressure, 14.5 atm.

Nominal initial sample length, 1.3 cm.

	Run Number	α (sec^{-1})	f (kc.)	Notes
Double-ended firings	0-264	137	3.2	
	0-265	105	3.3	
Single-ended firings	0-208	49	4.9	
	0-209	48	5.0	
	0-210	73	4.3	(a)
	0-218	49	3.5	
	0-219	44	5.0	
	0-220	37	3.5	
	0-221	55	4.3	
	0-223	26	4.1	
	0-224	54	5.0	
	0-225	50	4.7	
	0-226	60	4.9	
	0-227	43	1.8	
	0-228	38	2.3	
	0-230	42	1.7	
	0-231	37	1.7	
	0-232	38	2.3	
	0-233	37	1.7	
	0-234	38	2.2	
	0-235	35	2.2	
	0-236	34	1.8	
	0-237	34	1.7	
	0-238	41	2.3	
	0-240	39	2.2	
	0-241	41	1.7	
	0-242	35	2.3	
	0-243	75	5.1	
	0-244	75	4.5	(a)
	0-246	70	4.5	
	0-248	61	4.6	(a)
	0-249	53	5.2	
	0-250	58	4.6	
	0-251	60	5.4	
	0-252	64	4.7	
	0-253	80	5.4	
	0-254	69	4.4	

TABLE 4 (continued)

Run Number	α (sec^{-1})	f (kc.)	Notes
0-255	66	5.2	
0-256	72	4.1	
0-257	66	5.3	
0-258	57	4.4	
0-260	61	5.3	
0-266	53	2.4	
0-267	56	2.6	

Notes:

(a) Marginal mean pressure, the mean pressure trace indicated a non-uniform burning area.

TABLE 5

RELATIVE-AMPLITUDE AND DAMPING DATA FOR GAS-PHASE STUDY

Nominal mean pressure, 14.5 atm.

Nominal initial sample length, 1.3 cm.

Run Number	f (kc.)	$\frac{\lvert\tilde{p}_s\rvert}{\lvert\tilde{p}_g\rvert}$	ϕ (degrees)	L (cm)	$-\alpha_D$ (sec^{-1})	Notes
0-195	-	-	-	-	-	(a,b)
0-200	3.78	.505	-	10.2	-	(c)
0-208	3.76	.481	-	11.8	-	
0-209	3.82	.540	-	11.0	-	
0-210	3.86	.555	-	11.8	-	(c)
0-211	4.01	.526	-	11.0	-	
0-212	3.70	.610	-	11.8	-	
0-214	3.70	.425	-	11.0	-	
0-217	3.69	.445	-	11.0	78	
0-218	2.66	.445	-	15.4	37	
0-219	3.69	.410	178.5	11.0	75	
0-220	2.66	.312	178.5	15.4	54	(c)
0-221	3.42	.424	177.5	11.6	63	
0-223	3.78	.518	177.0	11.8	47	
0-224	3.90	.453	178.8	11.1	42	
0-225	3.60	.403	177.7	11.8	59	
0-226	3.90	.465	178.3	11.0	42	
0-227	1.42	.398	178.6	26.2	-	(e)
0-228	1.80	.449	179.5	21.1	-	
0-230	1.44	.505	178.5	26.2	-	
0-231	1.39	.440	178.9	26.2	-	
0-232	1.81	.425	179.2	21.1	-	
0-233	1.48	.463	179.2	26.2	-	
0-234	1.85	.446	179.2	21.1	-	
0-235	1.96	.380	179.1	21.1	-	
0-236	1.45	.374	178.8	26.2	-	
0-237	1.46	.427	179.2	26.2	-	
0-238	1.94	.445	178.9	21.1	-	
0-241	1.43	.448	178.9	26.2	-	
0-242	1.90	.418	179.2	21.1	-	
0-243	4.36	.525	-	10.5	38	(d)
0-244	3.51	.474	-	11.4	-	(c)
0-248	3.51	.455	178.8	11.2	87	
0-249	4.25	.613	178.8	10.3	46	(c)
0-250	3.55	.427	179.0	11.2	52	

TABLE 5 (continued)

Run Number	f (kc.)	$\frac{\lvert\tilde{p}_s\rvert}{\lvert\tilde{p}_g\rvert}$	ϕ (degrees)	L (cm)	α_D (sec^{-1})	Notes
0-251	4.24	.479	179.0	10.3	69	
0-252	3.50	.455	177.4	11.2	79	
0-253	4.24	.425	177.9	10.3	43	
0-254	3.60	.467	178.9	11.2	51	
0-255	4.09	.518	178.2	10.3	63	
0-256	3.52	.465	178.6	11.2	54	
0-257	4.01	.425	178.4	10.3	46	
0-258	3.40	.585	179.1	11.2	68	
0-260	4.15	.455	-	10.5	48	

Notes:

(a) Omitted run numbers correspond, in general, to runs with very poor mean pressure behavior, including 0-195.

(b) No reference signal was used before 0-219 and, therefore, the phase angle could not be accurately measured for these early runs.

(c) Marginal mean pressure, the mean pressure trace indicated a non-uniform burning area.

(d) Unusually low amplitude.

(e) No α_D was measured in lower frequency range.

TABLE 6

DATA FROM MEASUREMENTS IN THE CURVED WALL OF THE MOTOR

Nominal mean pressure, 14.5 atm.

Nominal initial sample length, 1.3 cm.

Run Number	Position of Wall Transducer (a)	Ratio of Amplitudes (b)	f (kc.)	L (cm)	Notes
264	.75	1.0	3.2	16.5	(c)
265	.75	1.0	3.3	16.5	(c,f)
266	.94	1.1	2.4		(d)
	.92	1.2			
	.88	1.2			
267	.80	.60	2.6	16.5	(c)
	.78	.45			
	.77	.44			
	.76	.34			
270	.86	.19	1.7	21.6	(e)
	.85	.18			
	.84	.18			
271	.86	.22	1.8	21.6	(e,f)
	.85	.21			
	.82	.17			
272	.81	.18	2.50	16.5	(e)
	.80	.17			
	.78	.15			
	.76	.15			
296	.98	.97	2.7	16.0	(d)
	.96	.91			
	.95	.81			
	.94	.99			
	.93	.91			
299	.81	.15	2.5	16.5	(e,f)
	.79	.07			
	.76	.08			
300	.81	.07	2.5	16.5	(e,f)
	.79	.05			
	.76	.06			

Notes:

(a) Position of the wall transducer expressed as a fraction of the length of the gas cavity.

(b) Ratio of the amplitude measured at the wall to that measured at the end.

(c) Double-ended firing.

(d) Single-ended firing with end measurement under the propellant.

(e) Single-ended firing with end measurement at the non-burning end.

(f) Mean pressure trace indicated that the burning area was irregular.

TABLE 7

DATA FROM LOW-FREQUENCY FIRINGS

Nominal mean pressure, 35 atm.

Nominal initial sample length, 1.3 cm.

	Run Number	$-\alpha$ (sec^{-1})	f (cps)	Initial Pressure (atm)
Igniter only	0-285	20.0	180	33.4
	0-286	20.1	175	35.2
	0-287	19.4	184	40.3
Utah-F				
Single-ended	0-283	8.9	244	32.2
SRI-109	0-281	11.2	220	31.8
Single-ended	0-282	8.9	230	32.5
	0-290	15.4	210	32.2
double-ended	0-284	4.4	260	32.8
	0-288	4.2	222	31.5
	0-289	2.9	-	32.2
SRI-111				
Single-ended	0-291	8.3	202	32.2
	0-292	9.4	200	32.2
	0-294	8.7	214	32.5
	0-295	7.4	206	32.2
SRI-111				
Double-ended	0-293	3.6	358	32.5

TABLE 8

DATA FROM SOLID PHASE WORK

Nominal mean pressure, 14.5 atm.

Run Number	ℓ (cm)	$\lvert\tilde{p}_s\rvert / \lvert\tilde{p}_g\rvert$	ϕ (degrees)	f (kc)	Notes
159	4.0	.53	165	3.9	(a)
	3.2	.53	166	-	
	2.4	.54	168	-	
	1.6	.57	168	-	
	.8	.57	168	-	
162	5.6	1.0	160	3.9	(a)
	4.8	.94	161	-	
	4.0	.91	159	-	
	3.2	1.1	129	-	
	2.3	.84	129	-	
	1.7	.62	150	-	
	.9	.87	139	-	
168	9.8	1.0	142	3.9	(a)
	8.9	.87	149	-	
	8.1	.81	152	-	
	7.2	.84	153	-	
	6.4	.84	150	-	
	5.5	.70	156	-	
	4.7	.60	162	-	
	3.8	.50	162	-	
	3.0	.57	166	-	
	2.1	.58	166	-	
	1.3	.71	160	-	
	.4	.71	167	-	
169	15.3	1.2	38	3.81	(b)
	14.4	.83	60	3.66	
	13.5	.70	95	3.47	
	12.6	.63	126	3.42	
	11.7	.77	139	[illegible]52	
	10.8	.97	156	[illegible]1	
	9.9	1.3	169	[illegible]0	
	9.0	1.4	170	[illegible].43	
	8.2	1.5	176	3.44	
	7.3	1.5	180	3.45	
	6.4	1.7	178	3.46	
	5.5	1.7	176	3.56	
	4.6	1.8	174	3.62	
	3.7	1.8	175	3.61	
	2.8	1.8	174	3.55	

TABLE 8 (continued)

Run Number	ℓ (cm)	$\lvert\tilde{p}_s\rvert / \lvert\tilde{p}_g\rvert$	Φ (degrees)	f (kc)	Notes
0-177	13.3	1.4	60	3.80	(b)
	12.5	1.4	62	3.71	
	11.7	1.7	94	3.77	
	10.9	1.5	112	3.66	
	10.1	1.2	128	3.63	
	9.3	1.2	132	3.60	
	8.6	1.1	136	3.72	
	7.8	1.1	133	3.87	
	7.0	.93	143	3.90	
	6.2	.87	151	3.82	
	5.4	.98	150	3.89	
	4.6	.92	151	4.10	
	3.8	.83	157	4.07	
	3.1	.76	160	4.02	
	2.3	.69	163	4.03	
	1.5	.68	164	4.01	
	.7	.64	167	4.00	
0-179	14.6	1.3	43	3.47	(b)
	14.2	1.7	59	3.42	
	13.8	1.8	62	3.44	
	13.4	1.9	54	3.59	
	12.9	1.4	29	3.68	
	12.5	1.9	49	3.76	
	12.3	1.6	36	3.81	
	11.7	1.7	36	4.20	
	10.8	1.8	37	4.30	
	10.0	2.2	58	4.31	
	9.1	2.8	67	4.29	
	8.3	3.5	105	4.26	
	7.4	2.5	126	4.27	
	6.7	2.7	136	4.29	
	5.9	2.1	150	4.31	
	5.1	1.7	160	4.33	
	4.2	1.4	166	4.33	
	3.3	1.3	165	4.33	
0-182	10.7	.71	46	4.58	(b)
	9.8	1.1	31	4.52	
	9.0	1.6	41	4.46	
	8.2	1.6	53	4.46	
	7.4	2.7	90	4.45	
	6.6	2.4	126	4.38	
	5.7	1.9	143	4.37	

TABLE 8 (continued)

Run Number	ℓ (cm)	$\lvert\tilde{p}_s\rvert / \lvert\tilde{p}_g\rvert$	Φ (degrees)	f (kc)	Notes
	4.9	1.6	153	4.36	
	4.0	1.4	155	4.35	
	3.2	1.1	162	4.34	
	2.4	1.0	164	4.35	
	2.0	.97	164	4.36	
	1.5	.95	162	4.33	
	1.1	1.0	161	4.32	
	.7	1.0	166	4.30	
0-184	15.0	.96	44	4.10	(b)
	14.5	.77	30	4.05	
	13.5	.77	38	3.90	
	13.0	.88	43	3.95	
	12.1	.88	46	4.06	
	11.2	.76	58	4.11	
	10.2	.89	72	4.13	
	9.3	.92	90	4.11	
	8.4	1.0	104	4.05	
	7.5	1.2	138	3.97	
	7.1	1.1	127	3.98	
	6.5	1.1	136	4.04	
	6.2	1.1	128	4.09	
	5.2	.96	136	4.19	
	4.3	.92	146	4.22	
	3.4	.94	161	4.21	
	2.5	.77	168	4.20	
	1.5	.65	164	4.24	
0-187	12.7	1.4	44	4.0	(a)
	12.1	1.7	51		
	11.4	1.6	47		
	10.7	1.5	54		
	10.0	1.5	66		
	9.4	1.1	60		
0-189	14.1	1.2	41	3.9	(a)
	13.3	1.4	73		
	12.6	1.6	96		
	11.8	1.4	122		
	11.1	1.2	134		
	10.3	1.0	140		
	9.6	.92	148		
	8.8	.86	151		
	8.1	1.0	154		

TABLE 8 (continued)

Run Number	ℓ (cm)	$\lvert\tilde{p}_s\rvert / \lvert\tilde{p}_g\rvert$	ϕ (degrees)	f (kc)	Notes
	7.3	.95	157		
	6.6	.98	160		
	5.8	.92	160		
	5.1	.89	159		
	4.3	.82	161		
	3.6	.86	162		
	2.8	.81	162		
	2.1	.82	163		
	1.4	.83	160		
	.6	.73	161		
0-191	14.0	.82	21	4.0	(a)
	13.3	1.1	27		
	12.6	1.4	36		
	11.9	2.1	48		
	11.2	2.3	79		
	10.5	2.5	95		
	9.8	2.2	96		
	9.1	2.0	98		
	8.4	2.0	92		
	7.7	1.8	90		
	7.0	1.7	111		
	6.3	1.6	132		
	5.6	1.6	144		
	4.9	1.1	161		
	4.2	1.0	165		
	3.5	.93	166		
	2.8	.93	168		
	2.1	.93	169		
	1.4	.90	173		
	.7	.88	172		
0-194	3.7	.58	166	3.4	(a)
	2.9	.59	164		
	2.1	.58	166		
	1.3	.57	166		
	.5	.63	167		

Notes:

(a) Nominal frequency for entire run.

(b) Frequencies tabulated were obtained from a plot of frequency measurements. These measurements were made by sampling the recorded data at equal time increments. The tabulated values are accurate to two places only; however, a third place was retained to indicate the frequency control.

APPENDIX O

TABLE OF NOMENCLATURE

Roman

A, A_1, A_2, A_3, A_4	arbitrary constants in solutions to differential equations (except A_3 in Equation (A.22))	--
a	imaginary part of γ	cm^{-1}
a_D	$\underline{a}$ during initial decay	cm^{-1}
a_{DL}	$\underline{a}$ during linear decay	cm^{-1}
a_d	$\underline{a}$ during decay	cm^{-1}
a_G	$\underline{a}$ during growth	cm^{-1}
B, B_1, B_2	arbitrary constants in solutions to differential equations	--
b	real part of γ	cm^{-1}
b_D	b during initial decay	cm^{-1}
b_d	b during decay	cm^{-1}
b_G	b during growth	cm^{-1}
C_1, C_2, C_3, C_4	arbitrary constants in solutions to differential equations (except C_3 in Equation (A.22))	--
C_p	constant-pressure heat capacity	cal/gm K
C_v	constant-volume heat capacity	cal/gm K
c	$\left(\frac{\gamma_T p_0}{\rho_0}\right)^{1/2}$	cm/sec
D_t	diameter at the nozzle throat	cm
D_p	diameter at the burning surface	cm
E	Young's modulus	$dyne/cm^2$

Roman (cont'd)

$\mathcal{E}$	energy density	ergs/cm^3
f	frequency	cycles/sec
f(x,y,z)	unspecified function of position	--
h	solid-phase work, defined by Equation (6.9)	cm-1
h	Appendix A, constant	sec^{-1}
h	Appendix B, $C_V T + p/\rho$	ergs/gm
Im[ ]	imaginary part	--
i	indexing variable	--
J_υ	Bessel function of first kind and order υ	dimensionless
j	$(-1)^{1/2}$	dimensionless
K	arbitrary constant in Equation (F.3)	dimensionless
k	gas phase, thermal conductivity	cal/cm sec
k	solid phase, defined by Equation (6.9)	cm^{-1}
k_0, k_1, k_2	defined by Equations (A.19), (A.20), and (A.21)	cm^{-1}
L	length of gas cavity	cm
ℓ	length of propellant	cm
M	Mach Number	dimensionless
$\vec{m}$	mass-flux vector	gm/cm^{2}sec
$\dot{m}$	mass flux	gm/cm^{2}sec
n	integer	dimensionless
$\vec{n}$	unit-normal vector	dimensionless
P	defined by Equation (A.6)	cm^2/sec^2

Roman (cont'd)

P_r	Prandtl Number, $\mu C_p/k$	dimensionless
p	total pressure	atm
p_0	time-average pressure	atm
p_1	real part of first-order perturbation in pressure	atm
$\tilde{p}$	complex, first-order perturbation in pressure	atm
$\tilde{p}_g$	oscillating pressure at the cold end and at center line	atm
$\tilde{p}_s$	oscillating pressure under the propellant and at center line	atm
$\tilde{p}_f$	oscillating pressure at the burning interface and center line	atm
Q', Q, Q_1, Q_2	solutions to equations of the type of Equation (A.9)	dimensionless
$Re[\ ]$	real part	dimensionless
r	radial position	cm
r_0	unperturbed burning rate	cm/sec
r_w	r at the wall	cm
S	surface area	cm^2
s	condensation $\tilde{\rho}/\rho_0$	dimensionless
T	total temperature	K
$\tilde{T}$	perturbed temperature, first order and complex	K
T_0	time-average temperature	K
T_c	time-average temperature in main body of gas	K
T_w	wall temperature	K

Roman (cont'd)

T_{Ot}	mean temperature at throat of nozzle	K
t	time	sec
U	solid phase, defined by Equation (6.7)	cm
U	Appendix B, $C_V T$	erg/gm
U_1, U_2	Appendix B, first- and second-order perturbations of U	erg/gm
u	axial velocity, total	cm/sec
u_O	axial velocity, time average	cm/sec
$\tilde{u}$	axial velocity, perturbed and complex	cm/sec
$\vec{u}$	velocity vector, total	cm/sec
$\vec{u}_O$	velocity vector, time average	cm/sec
$\vec{u}_1$	velocity vector, real part of first-order perturbation	cm/sec
$\vec{u}_2$	velocity vector, real part of second-order perturbation	cm/sec
V	volume	cm^3
$\tilde{v}$	radial velocity, perturbed and complex	cm/sec
W	defined by Equation (6.7)	cm
x	position coordinate	cm
y	position coordinate	cm
y	acoustic admittance, complex	cm^3/dyne sec
y'	real part of admittance, y	cm^3/dune sec
y"	imaginary part of admittance, y	cm^3/dyne sec
z	position coordinate	

Greek

α	growth constant	sec^{-1}
α_1	single-ended α	sec^{-1}
α_2	double-ended α	sec^{-1}
α_b	α for burning surface	sec^{-1}
α_D	initial decay constant	sec^{-1}
α_{DL}	linear decay constant	sec^{-1}
$\alpha(A)$	amplitude dependent decay constant	sec^{-1}
α_d	decay constant	sec^{-1}
β	complex angular frequency, ω-jα	sec^{-1}
Γ	arbitrary constant, Equation (F.2)	cm^{-1}
γ	propagation constant, complex, b-ja	cm^{-1}
γ_T	ratio of heat capacities, C_p/C_v	dimensionless
Δ	defined by Equation (6.3)	dimensionless
δ	arbitrary constant, Equation (4.5)	dimensionless
ϵ	reduced pressure perturbation, $\tilde{p}/p_0$	dimensionless
ζ	defined by Equation (F.4)	dimensionless
ζ'	defined by Equation (F.10)	dimensionless
η	defined by Equation (A.31)	$sec^{-\frac{1}{2}}$
θ	$\left(\frac{\rho_0 C_v}{p_0}\right)\tilde{T}$, defined by Equation (A.4b)	dimensionless
$\theta(x,y,z)$	position-dependent phase angle	dimensionless
λ	solid phase, Lamé constant	$dyne/cm^2$
λ	Appendix A, eigen value	cm^{-2}
λ_1, λ_2	roots of Equation (A.10)	cm^{-2}

μ	solid phase, Lamé constant	$dyne/cm^2$
μ	gas phase, viscosity	gm/cm-sec
μ'	μ/ρ_0	cm^2/sec
μ''	$\frac{\mu'}{3}$	cm^2/sec
$\tilde{\mu}$	reduced mass-flux perturbation m/m_0	dimensionless
υ	$\frac{k}{\rho_0 C_v}$, defined by Equation (A.4c)	cm^2/sec
ξ_x	axial displacement	cm
ξ_r	radial displacement	cm
π	3.14159	dimensionless
ρ	total density	gm/cm^3
ρ_0	time average density	gm/cm^3
$\tilde{\rho}$	perturbed density, first order and complex	gm/cm^3
ρ_1	perturbed density, first order and real part	gm/cm^3
ρ_2	perturbed density, second order and real part	gm/cm^3
ρ_{0w}	ρ_0 at wall conditions	gm/cm^3
ρ_s	density of solid	gm/cm^3
$\tau_{xx}, \tau_{rx}, \tau_{rr}$	stress components	$dyne/cm^2$
ϕ	phase angle between $\tilde{p}_g$ and $\tilde{p}_s$	dimensionless
ω	angular frequency, real part of β	sec^{-1}
ω_θ	defined by Equation (6.4)	dimensionless

Security Classification

DOCUMENT CONTROL DATA - R&D

(Security classification of title, body of abstract and indexing annotation must be entered when the overall report is classified)

1. ORIGINATING ACTIVITY *(Corporate author)*

University of Utah
1400 East 2nd South
Salt Lake City, Utah 84112

2a. REPORT SECURITY CLASSIFICATION

UNCLASSIFIED

2b GROUP

3. REPORT TITLE

ACOUSTIC INSTABILITY IN COMBUSTION

4. DESCRIPTIVE NOTES *(Type of report and inclusive dates)*

Scientific Interim

5. AUTHOR(S) *(Last name, first name, initial)*

Carl L. Oberg
Norman W. Ryan
Alva D. Baer

6. REPORT DATE	7a. TOTAL NO. OF PAGES	7b. NO. OF REFS
August 1, 1966	194	61

8a. CONTRACT OR GRANT NO.	9a. ORIGINATOR'S REPORT NUMBER(S)
AF-AFOSR-446-63	
b. PROJECT NO. 9713-01	
c. 61445014	9b. OTHER REPORT NO(S) *(Any other numbers that may be assigned this report)* AFOSR 66-1764
d. 681308	

10. AVAILABILITY/LIMITATION NOTICES

1. Distribution of this document is unlimited

11. SUPPLEMENTARY NOTES	12. SPONSORING MILITARY ACTIVITY
	AF Office of Scientific Research (SREP) 1400 Wilson Boulevard Arlington, Virginia 22209

13. ABSTRACT

Acoustic instability in solid propellant rockets is observed as a high-amplitude oscillation in the acoustic modes of the gas cavity, the combustion processes providing the driving energy. In general, the solid phase, i.e., the propellant, participates in the wave behavior. In this work, the behavior of both the gas phase and the solid phase were experimentally studied in a side-vented end burner. When the burner was operated with a grain in only one end, a difference in acoustic pressure amplitudes not previously reported was observed. The phenomenon was confirmed and studied in some detail. It does not affect the data used to calculate acoustic admittance values.

DD FORM 1 JAN 64 1473

Security Classification

Security Classification

14. KEY WORDS	LINK A		LINK B		LINK C	
	ROLE	WT	ROLE	WT	ROLE	WT
Combustion **Combustion Instability** **Acoustic Instability** **Propellant** **Propellant Combustion**						

INSTRUCTIONS

1. ORIGINATING ACTIVITY: Enter the name and address of the contractor, subcontractor, grantee, Department of Defense activity or other organization *(corporate author)* issuing the report.

2a. REPORT SECURITY CLASSIFICATION: Enter the overall security classification of the report. Indicate whether "Restricted Data" is included. Marking is to be in accordance with appropriate security regulations.

2b. GROUP: Automatic downgrading is specified in DoD Directive 5200.10 and Armed Forces Industrial Manual. Enter the group number. Also, when applicable, show that optional markings have been used for Group 3 and Group 4 as authorized.

3. REPORT TITLE: Enter the complete report title in all capital letters. Titles in all cases should be unclassified. If a meaningful title cannot be selected without classification, show title classification in all capitals in parenthesis immediately following the title.

4. DESCRIPTIVE NOTES: If appropriate, enter the type of report, e.g., interim, progress, summary, annual, or final. Give the inclusive dates when a specific reporting period is covered.

5. AUTHOR(S): Enter the name(s) of author(s) as shown on or in the report. Enter last name, first name, middle initial. If military, show rank and branch of service. The name of the principal author is an absolute minimum requirement.

6. REPORT DATE: Enter the date of the report as day, month, year, or month, year. If more than one date appears on the report, use date of publication.

7a. TOTAL NUMBER OF PAGES: The total page count should follow normal pagination procedures, i.e., enter the number of pages containing information.

7b. NUMBER OF REFERENCES: Enter the total number of references cited in the report.

8a. CONTRACT OR GRANT NUMBER: If appropriate, enter the applicable number of the contract or grant under which the report was written.

8b, 8c, & 8d. PROJECT NUMBER: Enter the appropriate military department identification, such as project number, subproject number, system numbers, task number, etc.

9a. ORIGINATOR'S REPORT NUMBER(S): Enter the official report number by which the document will be identified and controlled by the originating activity. This number must be unique to this report.

9b. OTHER REPORT NUMBER(S): If the report has been assigned any other report numbers *(either by the originator or by the sponsor)*, also enter this number(s).

10. AVAILABILITY/LIMITATION NOTICES: Enter any limitations on further dissemination of the report, other than those imposed by security classification, using standard statements such as:

(1) "Qualified requesters may obtain copies of this report from DDC."

(2) "Foreign announcement and dissemination of this report by DDC is not authorized."

(3) "U. S. Government agencies may obtain copies of this report directly from DDC. Other qualified DDC users shall request through

_____."

(4) "U. S. military agencies may obtain copies of this report directly from DDC. Other qualified users shall request through

_____."

(5) "All distribution of this report is controlled. Qualified DDC users shall request through

_____."

If the report has been furnished to the Office of Technical Services, Department of Commerce, for sale to the public, indicate this fact and enter the price, if known.

11. SUPPLEMENTARY NOTES: Use for additional explanatory notes.

12. SPONSORING MILITARY ACTIVITY: Enter the name of the departmental project office or laboratory sponsoring *(paying for)* the research and development. Include address.

13. ABSTRACT: Enter an abstract giving a brief and factual summary of the document indicative of the report, even though it may also appear elsewhere in the body of the technical report. If additional space is required, a continuation sheet shall be attached.

It is highly desirable that the abstract of classified reports be unclassified. Each paragraph of the abstract shall end with an indication of the military security classification of the information in the paragraph, represented as *(TS), (S), (C), or (U)*.

There is no limitation on the length of the abstract. However, the suggested length is from 150 to 225 words.

14. KEY WORDS: Key words are technically meaningful terms or short phrases that characterize a report and may be used as index entries for cataloging the report. Key words must be selected so that no security classification is required. Identifiers, such as equipment model designation, trade name, military project code name, geographic location, may be used as key words but will be followed by an indication of technical context. The assignment of links, rules, and weights is optional.

Security Classification